REACTANT HAVING MULTILAYER FILM STRUCTURE FOR GENERATING HEAT FROM REACTION BETWEEN HYDROGEN AND METAL

Abstract

Reactor having a multilayer film structure for generating excess heat; methods for manufacturing the multilayer films; methods for manufacturing such reactors; and methods for controlling heat generation between hydrogen and metal.

Technical Field

This disclosure relates to a reactant having a multilayer film structure, a method for producing the same, a method for producing a reaction apparatus, and a method for controlling heat generation between hydrogen and metal. More specifically, this disclosure relates to a reactant having a multilayer film structure used in a “Condensed Matter Nuclear Science” reactor, a manufacturing method of reactant, a method of manufacturing a reaction apparatus (reactor/furnace), and a heat generation control method between hydrogen and metal.

Background

The discovery of “Cold Fusion” was first published in March 1989 by Professor Martin Fleischmann at the University of Southampton in the United Kingdom and Professor Stanley Pons in the University of Utah in the United States. At that time, it was widely thought their discovery would solve the global energy problems. Since then various efforts to verify and replicate such a discovery were made in the past 27 years around the world, but most of them were poor in reproducibility and credible excessive heat output data were rare if any.

The experiments reported by many researchers were poorly prepared, structured and studied, and there were many problems in experimental conditions, experimental contents, analysis methods, result analysis and the like. Since the name of “Cold Fusion” is not suitable for the reaction mechanism, today, it is

collectively referred as Less Energy Nuclear Reaction (“LENR”) or Condensed Matter Nuclear Science (“CMNS”).

Many CMNS researchers have experimented by designing and assembling various devices from experiences, and changing various factors. However, in many cases, the desired phenomenon did not occur. Even if rare abnormal phenomena occurred, reproducing such phenomena with a high degree of reproducibility has been extremely difficult, and thus remained as the subjects of CMNS research. Obviously, CMNS research results cannot be trusted unless these results have the accuracy and reproducibility with the reputable third party verifications. In addition, most reports that abnormal results were obtained have problems with equipment, measurement methods, and analysis. It has been nearly impossible to encounter reports of stable excess heat generation, large amounts of radiation, abnormal products formation from the CMNS experiments in the past from the researchers and scientists from around the world.

For nearly 30 years, various abnormal reactions have been observed when hydrogen is allowed to react with certain metals. However, the reported results lacked reproducibility and certainty. Therefore, the controlling factors could not be clarified, and the experiment results were not considered reliable. However, in recent years, precise and highly sensitive devices have been developed by researchers in this field. Heat generation, radiation emission, and the generation of other products, although rarely reported, are highly reproducible. We have been focusing on reproducing the aforementioned phenomenon for many years. When this phenomenon was first reported, the reaction was regarded as a type of nuclear reaction and investigations tended to focus on observing neutron emission during electrolysis in heavy water solutions. Focus later shifted to analyzing the isotopically changed products formed during the electrolysis experiments. Heat generation was a phenomenon that occurred suddenly and rarely in the process and was therefore difficult to reproduce. However, recently reports of heat-generating reactions in the nickel–hydrogen series have been increasing. Specifically, the occurrence of excessive heat exceeding the input energy in a reaction mainly involving nickel with other additive elements has been reported. The authors of these reports emphasized

the importance of an extremely clean system in the early electrolytic tests in which excess heat was generated. Therefore, we attempted to strictly detect excess heat by eliminating impurities in our test system. As a result, energy far exceeding the input was continuously obtained. According to the test results obtained thus far, the output thermal energy is double the input electrical energy of several hundred watts. The generated thermal energy follows an exponential temperature function. When the reactor temperature is 300°C, the generated energy is 1 kW. An increase of the temperature is expected to greatly increase the output energy.

Summary of Disclosure

This disclosure provides methods of generating excessive heat, which greatly exceeds the input energy, and methods to make such reactants, which cause such results. This disclosure also describes the methods to make reactors that utilize these reactants effectively to generate excess heat continuously and grouping arrangement for obtaining even greater excess heat effectively. For example with this disclosure, with several hundred watts of input electric energy, the output thermal energy reaches twice its input energy. It was found that the thermal energy generation by this reactor follows the exponential function of temperature and therefore this disclosure provides methods to control energy/heat generation.

Problem to be Solved

To provide a reactant having a multilayer film structure used in a “Condensed Matter Nuclear Science” reactor capable of generating a large amount of heat safely, reliably, inexpensively for a long time; Methods of manufacturing such reactors, and methods of controlling heat generation between hydrogen and metal in the reactor.

Solution

Using a reactant having a multilayer film structure used for a “Condensed Matter Nuclear Science” reactor. Such a reactor has a thin film of various metals such as (but not limited to) platinum, palladium, nickel, and palladium and/or platinum

deposited on a nickel and/or similar substrate. It is possible to solve the problems of making a reactor, which is safe, inexpensive, and capable of generating a large amount of heat and with effective heat generation control. This disclosure can help to solve the worldwide energy problem. This disclosure should help to reduce the use of fossil fuels for energy and thus reduce the emission of CO2 to prevent the further global warming.

Detailed Description of Disclosure

Reactant

The present disclosure provides a reactant having a multilayer film structure used in a “Condensed Matter Nuclear Science” reactor capable of causing heat generation between hydrogen and metal by “Condensed Matter Nuclear Science” reaction, etc. The present disclosure further provides methods for producing the reactors, methods for manufacturing reaction devices/systems, and heat control methods between hydrogen and metal.

For “Condensed Matter Nuclear Science” reactor, the main/key part is the reactant having a multilayer film structure. Figure 7 is used to further explain this reactant. In a reactant having a multilayered film structure used in a “Condensed Matter Nuclear Science” reactor which mainly contains hydrogen isotope and nickel in which the reactant is any one of a) plate, b) net/mesh, c) sprayed film, or d) electrodeposited film. A palladium layer, a nickel layer, a palladium and platinum layer are stacked in a certain order on the nickel base. Other materials / elements / metals / precious metals may be used for one or more of the layers. Some of these elements (at least one) must be in the form of nanoparticles. The thickness of the nickel base is several nm to 1000 nm. The reactant’s each layer on the nickel base has a thickness of 1 nm to 1000 nm. The thickness of each metal film to be laminated may be appropriately adjusted depending on the usage, conditions, purpose, etc., of the reactor as long as the thickness of each metal is within the above range. The reactant having the multilayer film structure of Figure 7 can be placed on any other base material format/ shape, for example, plate, net/mesh, sprayed film, electrodeposited film and the like.

In addition to the above explanation, here we will discuss reaction of the reactant described above in the reactor. Reactants that are reacting are: a) fine particle sized hydrogen active metal, b) hydrogen isotopes such as high purity hydrogen and deuterium. Hydrogen and deuterium molecules are broken down to atomic level, and the metal captures some of the atoms into its metal structure. Such a metal should have a high solubility and mobility of hydrogen and deuterium even at high temperature.

For the reactant having the multilayer film structure, instead of one of high purity nickel and palladium, it can be replaced by an alloy made out of LaNi5, YNi5, MmNi5, or TiFe. Further, it may be good to add an alloy in which at least one metal element selected from C, Al, B, Cu, Cr, Mn, Si, Ti, Zn, Co, V, Mo, Nb, and Zr is placed on the alloy surface.

In addition, for the reactant having a multilayer film structure shown in Figure 7, instead of one of high purity nickel and palladium, an alloy made out of one of the metals out of Mg, NiAl, and LiAl with any one of the followings C, Al, B, Cu, Cr, Mn, Si, Ti, Zn, Co, V, Mo, Nb, and Zr can be used.

Further, in addition to the reactant having the multilayer film structure according to any one of the above descriptions, on the surface of the reactant, a group of metals in alkali and alkaline earth atoms and with a hydrogen atom structure, for example, one containing at least one of Li, Na, K, and Ca having a hydrogen atom structure, may be added.

The method of controlling the heat generation between hydrogen and metal in the reactor is carried out by a) activating the surface of the reactant, b) atomizing the surface of the reactant, c) adding surface modification metal, d) eliminating impurities in the gas, e) gas pressure control, and f) controlling the input side heat/energy.

Furthermore, the method of controlling the heat generation between hydrogen and metal in the reactor is relying on the relation that the generated heat energy follows

the exponential function of the reciprocal of the absolute temperature with respect to the input electric energy.

The reason why the electrode has a multilayer structure is that the hydrogen molecule of the reactant is changed into a hydrogen atom ion state and introduced into the metal nanoparticle. When ionic hydrogen atoms are introduced into metal nanoparticles, the repulsive potential of the hydrogen nucleus is blocked by free electrons in the metal nanoparticles, the tunnelling probability between the hydrogen nuclei increases, and the nuclear reaction progresses further. The difference between the mass of helium and the combined masses of hydrogen & deuterium is converted into the energy.

The nuclear reaction finally produces helium through the production of intermediate products – carbon and nitrogen. This reaction is slow at a room temperature, but substantially increases as the temperature increases. The energy production appears to follow the following steps in the “Condensed Matter Nuclear Science” reactor.

$$^{12}C + {}^{1}H \rightarrow {}^{13}N + \gamma + 1.95\ \text{MeV}\ 1.3 \times 10^{7}\ \text{year}$$

$$^{13}N \rightarrow {}^{13}C + e+ + \nu_e + 1.37\ \text{MeV}\ 7\ \text{minute}$$

$$^{13}C + {}^{1}H \rightarrow {}^{14}N + \gamma + 7.54\ \text{MeV}\ 2.7 \times 10^{6}\ \text{year}$$

$$^{14}N + {}^{1}H \rightarrow {}^{15}O + \gamma + 7.35\ \text{MeV}\ 3.2 \times 10^{8}\ \text{year}$$

$$^{15}O \rightarrow {}^{15}N + e+ + \nu_e + 1.86\ \text{MeV}\ 82\ \text{second}$$

$$^{15}N + {}^{1}H \rightarrow {}^{12}C + {}^{4}He + 4.96\ \text{MeV}\ 1.12 \times 10^{5}\ \text{year}$$

For the overall reaction:

$$4\,p \rightarrow {}^{4}He + 2e^{+} + 3\gamma + 2\nu_e + 25.1\ \text{MeV}$$

In the CNO cycle via carbon and nitrogen, energy of about 25 MeV is generated per cycle. This reaction is a reaction occurring in a star having a mass larger than the sun. The time to complete one cycle of the CNO cycle is about 3.8×10^8 years, which is shorter than the time scale of the proton-proton chain reaction (about 10^9 years). For this reason, the energy generation rate per unit time is larger for large mass stars whose main energy source is the CNO cycle than for small mass stars, e.g. red dwarves. In addition, the CNO cycle is a very sensitive reaction to temperature. The energy production rate of the CNO cycle is proportional to the 15^{th} power of the temperature. Thus, as the temperature rises by 5%, the energy release will increase by 108%. Incidentally, if the reaction rate at room temperature is 1, the reaction rate will be doubled at 15°C rise. This energy generation method is based on this reaction. That is, it is a safe and efficient way that energy generation can be controlled easily by changing external temperature.

The tunnelling effect occurring in the CNO cycle seems to follow the following process:

1. Hydrogen is introduced into the metal nanoparticles.
2. The hydrogen concentration in the metal nanoparticles increases and the electric potential outside the hydrogen nucleus decreases due to shielding of electrons in the metal nanoparticles.
3. The extra-nucleus electrons are free electrons and exist in the Nano metal.
4. The Coulomb potential of the nucleus is shielded, and the orbit radius of the hydrogen atom becomes small.
5. The internuclear distance between hydrogen atoms becomes shorter.
6. As the internuclear distance decreases, the probability of nuclear fusion reaction between hydrogen nuclei increases due to the “tunnel” effect.
7. When the nuclear potential is shielded by 50%, the tunnel fusion reaction probability increases by order of 10X magnitude.
8. As the tunnel nuclear reaction increases, observable heat is generated.
9. Helium and the likes are generated by the nuclear reaction.

Note that electrons easily separate from the additional elements that promote the shielding effect of free electrons. Examples of the additive element include alkali and alkaline earth atoms (e.g., Li, Na, K, Ca, etc., having a hydrogen atom structure).

From the above, we narrowed down complex thermal events into three simple factors in order to confirm the abnormal heat generation of the hydrogen-metal system. Factors necessary for thermal analysis are precisely determined by the input power, the amount of air blown, and the temperature difference between inlet and outlet. Based on this thermal analysis and the result, it is presumed that the steps necessary for abnormal heat generation is as follows. 1: Activation of sample surface, atomization and addition of surface modification metal, 2: removal of impurities in the gas, 3: management of input temperature and gas pressure.

In particular, it is important to activate the metal surface, that is, to remove oxide, nitride, and carbide layers. As means for this, heating and discharge treatment in hydrogen gas is effective. It is also important that the gas used is low in impurities and thorough removal of released gas during the surface treatment.

After the reactant is produced, if it is kept at a high temperature hydrogen gas, the hydrogen molecule dissociates to atomic hydrogen on the metal surface, and its amount increases. The existence of this atomic hydrogen is considered a condition necessary for excessive heat generation. Amount of excess heat generation depends on temperature, and it is at least in the order of kW. Assuming the reactant is nickel, it can generate several X10 W per gram, and for area-wise is 1 to 10 W/ cm^2.

Manufactured Reactor / Device

An embodiment of this disclosure will be described by Figure 1 to Figure 20. Figure 1 is a schematic view of a “Condensed Matter Nuclear Science” reactor/furnace setup. In Figure 1, 1 is a reactant, 2 is a reaction reactor/furnace, 3 is a heater, 4 is a discharge nickel wire, 5 is a nickel net/mesh, 6 is nickel fine particles, 7 is an anode, and 8 is a cathode. Figure 2 is a cross section view of the reactor/furnace.

The reactants used are nanoised (made into nano-sized particles) hydrogen active metals, hydrogen and deuterium. Hydrogen and deuterium molecules are broken down to atomic level, and the metal captures some of the atoms into its metal structure. Such a metal should have a high solubility and mobility of hydrogen and deuterium even at a high temperature range.

1. In this case, Pd and Ni are used as reactant metals.
2. Hydrogen absorbing and hydrogen storable materials such as LaNi5, YNi5, MmNi5, TiFe, etc., can be used as other reactant alloys. Materials whose properties are changed by adding another metal element to the surface of this alloy are also candidates for the reaction material.
3. Candidate materials for high temperature (300°C or higher) reactants are alloys made of either Mg, NiAl, LiAl with a third metal.
4. Initially, surface refinement treatment of the reactant metal, impurity removal activation treatment, and surface modification treatment with other metals are necessary for heat generation.

Heating and discharge treatment or processing in hydrogen gas is effective to activate the metal surface, i.e. to remove oxide, nitride, and carbide layers.
Figure 3 shows the changes in voltage and current during discharge processing (described in more detail below with reference to Figure 8).
Figure 4 shows an inside view at the start of discharge processing.
Figure 5 shows an inside at the time of discharge treatment with D_2 gas introduction.
Figure 6 shows an inside view at the completion of discharge treatment.

Heat generation method from the activated reactant is described as follows:

The activated reactant is placed on a prearranged heater in the reactor/furnace, and:
—Impurity gases are removed by heating in vacuum.
—First, raise the temperature to 200°C and introduce deuterium (D_2) gas when the whole reactor/furnace inside temperature reaches a uniform temperature.
—Then if the reactant activation is good, excessive heat is generated.

Excess heat quantity is determined by gas pressure, reactant weight, input wattage. When excessive heat is generated, the temperature of the reactant goes up by several hundred degrees or more. As the reactant temperature rises, the amount of hydrogen in the reactant decreases. Thereafter, the exothermic reaction decreases and the reactant temperature decreases. As the temperature decreases, hydrogen enters the reactant again. As a result, excessive heat is generated again. By repeating this process, the reactants are stabilized at a constant temperature.

The calorific value of the Pd reactant is 1 to 10 watt per gram and the maximum temperature can reach 345°C. It is theoretically possible that the calorific value of the Ni reactant is 10 W/g and the maximum temperature can be 1000°C or more. In fact, the maximum operating temperature is determined by the heat resistance of the furnace/reactor, parts, etc., and therefore, it is fine to operate at a temperature of 850°C when right materials are used and the conditions are met. The calorific value depends on the amount of reactant and the removal rate of heat. In principle, a very large calorific value can be obtained by adjusting and arranging these factors.

In Figure 7It will be appreciated that the platinum layer and/or palladium layer may be replaced with another material, e.g. another precious metal. For each thickness, the Pt layer on the nickel substrate has a thickness of 1 nm to 100 nm, the Pd layer thereon also has the same as 1 nm to 100 nm, the Ni layer has a thickness of about several nm, and the Pd layer has a thickness of 1 to 100 nm. The uppermost Pt layer is 1 nm to 50 nm. The base layer of nickel requires a fine particle structure of 100 to 1000 nm.

Figure 8 is a schematic drawing of electrodes and their arrangement / locations for generating multilayer films or specific film formation. 16 is a high temperature heater, 17 is a deposition high voltage rod, 18 is a flange, 19 is a thermocouple, 20 is a Pt thin wire, and 21 is a Pd thin wire wound around a ceramic heater. This part also becomes the electrode mounting part on the top of the reactor/furnace. Three electrodes for heating and vapour deposition of the metal film base material are contained in the mounting part. Two electrodes are used for discharge at around

room temperature and the third one is an electrode for high temperature use (300°C to 650°C). For low temperature, a base metal (Pd, Pt thin wire as an example) is used directly at the tip of the electrode main body. For high temperature, a thin wire of such a material is wrapped around the base metal at the heater base. This heater's heating wire is covered and protected with a ceramic material such as alumina, and it is used at around 100°C. In a plasma film processing such as ordinary PVD (physical vapour deposition) method, the metal from the base metal is released from the plus electrode. In that case, the electrode surface area on the plus side is large both in direct current and in alternating current. However, in order to use less amount of precious metal for the reactor/furnace, the temperature of the base metal was raised to efficiently deposit it.

Figure 9 is an external view of the reactor/furnace. The main body of the reactor/ furnace 2 is made of stainless steel grade 316 (SUS 316), the volume is 2000 cm^3, and the weight is 16 kg and wrapped around by Heater 3. The Heater 3 can go up to 650°C with a stainless steel covering and a length of 200 cm and a capacity of 500 watts. The anode 7 in the reactor/furnace 2 is a discharge component in which a palladium wire having a thickness of 1 mm and a length of 200 mm (weight 2.82 g) is wounding around a 50 mm tip portion of a palladium tube having a thickness of 3 mm. The electrode is insulated from the main body, and the electrode polarity can be changed. The inner wall surface of the reactor is covered with a nickel mesh. The mesh is 500 mm × 500 mm in size, the wire has a diameter of 0.15 mm, the eye size is 50 mesh, and the weight is 40 g. The two meshes are attached to the center part of the reactor/furnace inner surface. The nickel mesh is pressed with a plate of nickel (thickness of 0.5 mm, width of 5 mm, length of 500 mm), to have a direct contact with the inner wall surface of the reactor/furnace for heat conduction.

First Measurement Experiment

Figure 10 is a schematic view of the reactor/furnace (photograph). The reactor comes with heater, discharge electrode, thermometer. In Figure 10, the right part of the reaction reactor/furnace has a peep window made of Kovar glass. A vacuum evacuation system is attached to the reactor/furnace body.

Figure 11 is a schematic diagram of the measurement system. 22 is computer for recording data, 21 is a data logger, 24 is an electric power input analyzer, 25 is a heater power supply, 23 is a DC fan power supply, 27 is a blower, 29 is an exhaust, 30 is an air intake hole. The reaction furnace 2 and the calibration heater 36 are installed in an acrylic insulation box 26. The acrylic insulation box 26 has a width of 400 mm, a depth of 750 mm and a height of 700 mm, and the air passage ports 34, 35 of 50 mm are opened near the bottom and the upper surface of the side surface. A DC fan of 15 V, 10 W is attached above the upper air passage opening 34. A platinum temperature-measuring element was installed at the center of the lower air passage port 30 and just under the fan at the center of the upper air passage port 29, respectively. The DC fan supplied a constant voltage of 15.5 V and a constant current of 0.42 A, that is, 6.51 W from the constant voltage power supply. This voltage current data was continuously accumulated in the data recording PC 20. The airflow rate of the DC fan was calibrated with a digital anemometer. This is a thermoelectric anemometer with a range of 0.2 to 20 m / s, a resolution of 0.1 m / s, and a measurement temperature range of 0 to 50°C. Figure 11 shows the reactor on the right side, the control system, the measuring system on the left side. From the lower left, there are an input power supply 25, a power input analyzer 24, a data logger 21, and a data accumulation personal computer 22. Baratron was used as reactor pressure measuring instrument. Data of reactor temperature in 6 places, current, voltage, and data of two inlets at air inlet and outlet were gathered in a data logger and accumulated in the data accumulation personal computer 22 every 5 seconds.

Figure 12 is a schematic diagram of heat measurement. In Figure 12, 29 denotes exhaust gas, 30 denotes intake air, 31 denotes a platinum temperature sensor, 32 denotes an input to a calibration heater, 33 denotes an input to the reactor, 34 denotes an upper air passage, 35 denotes a lower air passage, and 36 is a heater for calibration.

The reaction reactor/furnace 2 and the calibration heater 36 are installed at the same position in the heat-insulating box 28. A predetermined amount of air is allowed to

flow from the lower reactor/furnace passage port 35. The temperature of the intake port is measured by the platinum temperature sensor 31. A DC fan is provided in the upper air passage port 34, and a platinum temperature-measuring sensor 31 is attached to the opening portion and the lower portion of the fan. This is because the thermocouple 19 is not influenced by the heat generated from the fan motor because the location.

The calculation of the thermal measurement is as follows.

Input power:

$$\Delta W \times \Delta \mathrm{t} = \int_0^T Wtdt \quad (1)$$

Where ΔW is the time-to-time power and Δt is the data integration time interval.

Thermal output power:

$$V \times \mathrm{S} \times \rho \times \mathrm{Hc} = \int_0^T VdTdt \quad (2)$$

Where,

V = velocity measured by the wind speed measuring device in m/s; S = air-out port size (m^2) ：8.2×10^{-3}; ρ = air density (kg/m3) :1.293kg/m3; and Hc = Air heat capacity = 1.006kJ/kg/ °C

Equation (3) which is experimentally obtained:

$$\mathrm{V} = \mathrm{A} \times \exp(-\mathrm{W_b}/\mathrm{w}) + \mathrm{B} \quad (3)$$

Where A is a constant, -3.7, B is also a constant 4, w is also a constant 1.375, Wb is the blower input (watt), dT is the temperature difference between the air inlet and the outlet; ($dT = T_{out} – T_{in}$).

As for the airflow rate/amount measurement, the sensor portion of the digital anemometer was placed immediately below the fan, which is the outlet of the air in Figure 11.

Figure 13 shows the relationship between the input of the DC fan and the wind speed. The relationship between the input of the DC fan and the wind speed (central part) was experimentally obtained. In the figure, the black dots are the measured values and the dotted line is the approximation by the equation. This equation is the same as the equation (3). In the test, the input data of the DC fan was measured and compiled, but the input was always fixed at 4 W. Theoretically, the calorific value can be obtained from the airflow rate and the air temperature difference, and from the air heat capacity. However, to avoid errors, we calibrated the calorific value by changing the input using a reference heater for calibration. From this calibration, the true air volume at the air outlet was calibrated.

Figure 14 is a result by the reference & calibration heater. Power was supplied for 60 ks with the heater input set at 100 W. After the output became constant, the input was turned off and then the calorific value until the output became 0 was obtained. Then input becomes 100 (W) × 60 (ks) = 6.22 KJ, and the output obtained is 5.84 MJ. Then Out / In = 0.938. Then calibration seems correctly completed.

Next, the same electric power of 100 W was supplied to the reactor/furnace until the heat output became constant, and compared with the calibration data.

Figure 15 is a thermal output chart at input of 100 W. In this case, as shown in Figure 15, the heat output is not stabilized and increases with time. The input was stopped at 71 ks and the output calculation was done. For the input energy of 7.23 MJ, the output energy was 14.16 MJ. The Out/In ratio was 1.96, and thus a heat output exceeded the input by the factor of two and “excess heat” above the input was observed.

Figure 16 is a change in the output when a calibration test is performed with various input powers using the reference/calibration heater. The input of 80 to 248 W was given. The output is almost the same as the input.

Figure 17 is a chart of the output when the input to the reactor/furnace is changed. These tests behave differently than the calibration test. It turns out that the output

increases with time. For example, the 248 W input for 22ks, the thermal output reaches 480 W and thus the Out/In ratio becomes 1.94.

The results of the tests conducted in a vacuum, the tests performed by placing the reference/calibration heater in a testing chamber/box, and the results of the heat generation test are shown in Figure 18. Figure 18 is an example of a test conducted under various conditions. The horizontal axis is the input power, and the vertical axis is obtained by subtracting the input electric energy from the measured heating value. The black line is the result of the calibration heater. If the input is large, the temperature rises, the radiation heat loss increases and the excess heat swings to the minus side. In the case of a vacuum with no hydrogen gas in the reactor/furnace indicated by the blue line, the excess heat quantity is extremely small. In the excess heat generation test shown by the red line, when the input is large, the reactor/ furnace body is well heated and then the excessive heat generation is substantially increased.

Figure 19 is a graph showing the relationship between excess energy generation and reactor/furnace body temperature. The relationship shows that the excess heat generation increases as the temperature increases. For example, the excess energy Wex reaches 100 W at 100°C, 315 W at 200°C and 480 W at 250°C. It is also found that excess energy of 10 to 20 W is generated even at around room temperature.

Figure 20 is a graph showing the relationship between generation of excessive energy and absolute temperature. When the temperature in Figure 19 is expressed by the reciprocal of the absolute temperature, the relationship shown in Figure 20 is obtained. Excess energy is 1 / Tr = 0.001, that is, on the order of kW at about 700°C. The excess energy increases exponentially as the reactor/furnace body temperature increases. When the reaction activation energy is obtained from the linear part at 100 °C to 523°C in Figure 20, it becomes 0.165 eV / K / atom.

Second Measurement Experiment

We have been aiming at reproducing a long-standing curious phenomenon that occurs in metal–hydrogen systems.[1-5]) In particular, the reaction was considered a normal nuclear fusion reaction and confirmation experiments involving neutron generation during the electrolysis of heavy water were subsequently conducted.[6] Focus then shifted to analysis of the elements isotopically changed during the electrolysis tests. The generation of heat in the process, which had rarely been observed, suddenly became a recurring phenomenon.[7-10]). The heat-generating reaction of a nickel–hydrogen system, in particular, has been commonly reported[11-13]). This system, when compared to the initial Pd–D_2 system is regarded as a calibration test. The generation of excess heat in reactions involving nickel was observed with additive elements in these reports. However, the authors noted the importance of a very clean system in early electrolysis tests where excess heat was observed. Therefore, in the present work, we eliminated impurities in an attempt to precisely detect excess heat. Specifically, we developed a very simple heat estimation analysis method to confirm excess heat induced by the reaction between hydrogen and a metal. The factors considered are only the amount of air and the temperature difference between the air flowing into and out of the calorimetry system. These factors contribute mostly to heat analysis and can be used to easily estimate the excess heat. We describe the existence of excess heat in a simple metal–hydrogen system. When the reactive metal sample is activated at an elevated temperature in a hydrogen gas environment via an initial activation treatment, hydrogen molecules dissociate into atomic hydrogen on the metal surface, and the amount of dissociated hydrogen increases over time. The existence of this atomic hydrogen can be presumed to be a condition necessary for excess heat. The occurrence of excess heat depends on the temperature and the amount of reactant; the test data indicate that amount of excessive heat is on the order of at least 100 W. The excess heat calculated on the assumption that the reactant was nickel with several 10 W/g and 1–10 W/cm^2.

The experiment was performed on a reactor body for observation of excess heat by activated metal and hydrogen gas. The reactor body was a cruciform cylindrical shape and was connected to each part with a metal seal flange, as shown in schematics of the reactor in Figures 21A to 21F. The upper part of the reactor

comprises the heater power inlet, the high-voltage discharge electrode, and a thermocouple. Several platinum temperature-measuring elements were attached to the reactor. As shown in Figures 21A to 21F, a Kovar glass window was attached to the left side of the reactor and a pressure gage, mass spectrometer valve, and the gas inlet valve were connected to the reactor's right side. A vacuum evacuation system and a quadruple gas analysis system were connected to the body.

The reactor is made of SUS 316, its volume is 5,530 cm^3, and its weight is 50.5 kg. An aluminium ceramic heater with a maximum temperature of 1,000°C was positioned in the reactor's center. The heater was 30 x 30 mm^2, with a thickness of 2 mm. An R-type thermocouple was positioned near the heater. A palladium wire with a diameter and length of 0.3 mm and 200 mm, respectively, was wound around the heater. Two high-voltage electrodes were installed in the reactor. In Figures 21A to 21F, the electrode on the left inside the reactor, which was for discharge, was a 50 mm long, 3 mm diameter palladium tube wound with 200 mm of 1 mm diameter palladium wire (weight 2.82 g). This electrode was insulated from the reactor body. The polarity of both electrodes could be changed. The gas temperature around the electrode was measured with another thermocouple (indicated by vertical bars in the center), specifically, a stainless- steel-coated type-K thermocouple with a diameter of 1.6 mm and a length of 300 mm. This thermocouple was insulated in a 3 mm diameter, 100 mm long alumina tube so that it was not affected by the plasma discharge.

The inner wall surface of the reactor was covered with two pieces of Nickel mesh (e.g. 99.9%, Ni 200,180 mesh, from Inada Wire Mesh Co., Ltd.) the wire diameter is 0.055 mm, the total wire length is 896 m, and the surface area is 0.31 m^2. Each mesh was 300 × 300 mm^2 and composed of 0.15 mm diameter wire; the opening size was 50 mesh, and the total weight was 23 g. The two meshes were attached to the center part of the reactor inner surface. The nickel mesh was pressed with a nickel plate (thickness 0.5 mm, width 5 mm, length 500 mm) on the reactor inner surface to ensure contact with the inner wall of the reactor, which is necessary to maintain thermal conduction. A 2 m long heater tape was wrapped around the reactor body. Its purpose was to heat the nickel mesh in the middle of the reactor.

The heater tape was 100 V, 500 W, with a maximum temperature of 500°C. Six platinum temperature-measuring elements were attached to various parts of the reactor. The heater tape was wrapped several times with aluminium foil to make the temperature distribution of the reactor wall more uniform.

The reaction gas comprises deuterium (e.g. 99.9%, from Nippon Oxygen) for heat generation and hydrogen (99.99%) for the activation process; the feed rate composition is 99.8% D2. A ceramic heater is placed at the center of the reactor (square-shaped, 30 mm on each side and 2 mm in thickness) and wound with a fine Pd wire (0.3 mm in diameter and 0.3 m in length). The Ni mesh is activated by attaching it to the inner surface of the reactor; AC and DC discharge between the wire around the heater and the reactant mesh yield ions and electrons that irradiate the reactant. The activated mesh is sequentially cleaned: a neutral detergent is used, followed by alcohol and ultrasonic cleaning in acetone. This process covers the surface of the reactant mesh with fine metal particles.

The same type of heater used in
the reactor was installed as a heater for calibration of heat balance in the measuring box. The reactor body and the calibration heater were placed in an acrylic box with a width of 400 mm, a depth of 750 mm, and a height of 700 mm; a 50 mm diameter air-passage opening was open at the top and the bottom side of the box. A DC blower of 15 V, 10 W was installed on the top air-passage port. A platinum temperature sensor was positioned under the blower hole of the box top hole, and another sensor was positioned at the bottom hole of the box. The DC blower was supplied a constant voltage of 15.5 V and a constant current of 0.42 A (power of 6.51 W) from a DC power supply. The voltage and current data of the blower were continuously recorded by a PC. The airflow rate of the DC blower was calibrated with a digital anemometer (e.g. Custom Co., Ltd., CW-60). The thermoelectric anemometer ranged from 0.2 to 20 m/s, the resolution was 0.1 m/s, and the measurement temperature range was 0°C to 50°C.

In Figure 22, the box in the measurement reactor and calibration heater is shown on the right side, and the control and the measuring system is shown on the left side.

The rectangles in the lower left of the figure represent the input power supply, the power input analyzer (e.g. Yokogawa, PZ 4000), the data logger (e.g. Agilent, 34970A), and the PC for data acquisition. A capacitance diaphragm gauge (MKS Co. Ltd.) was used as the reactor's inner gas pressure gauge. Data corresponding to six reactor temperatures, two electric currents and voltages for the power supply in the reactor and the blower, and the temperatures of the inlet and the outlet airflows were collected by a data logger and recorded to a computer every 5 seconds.

The reactor and the calibration heater were installed in the same position in the insulation box. A certain volume of air was flowed into the bottom port of the reactor. The temperature of the inlet was continuously measured with platinum temperature sensor. A blower was installed at the upper air out port, and another temperature sensor was attached to the opening immediately below the blower. This sensor was installed at the bottom of the fan so that the thermocouple did not detect heat generated by the fan motor. The thermal calculations were carried out as follows.

The input power W_{total} was estimated as equation (4).

$$W_{total} = \sum_0^T \Delta W \times \Delta \mathrm{t} = \int_0^T W t dt, \tag{4}$$

Where ΔW is the power at each time and Δt is the data integration time interval. Thermal output power H_{out} was calculated as equation (5).

$$H_{out} = \sum_0^T \Delta V \times S \times \rho \times Hc \times \Delta t = \int_0^T V d T dt, \tag{5}$$

Where V is the wind velocity (m/s); S is the area of the air outlet, 8.2 x 10^{-3} m^3; ρ is the air density, 1.293 kg/m^3; and Hc is the heat capacity of air, 1.006 kJ/m^3.
The wind velocity at the flow meter was estimated by semi empirical equation (6).

$$V = \mathrm{A} \times exp\,(-W_b/w) + \mathrm{B}, \tag{6}$$

Where A is a constant, −3.7; B = 4; w = 1.375; Wb is the blower input (W); and dT is the temperature difference between the air inlet and the outlet ($dT = T_{out} – T_{in}$).

Figure 23 shows the relationship between the blower input and the airflow rate obtained from the air volume calibration results. In the figure, the black circle is the measured value, and the dotted line is the approximate expression value obtained using equation (6). Data corresponding to the input power for the blower were also collected during the test; however, the input power was approximately 4 W to 6 W. These results indicate that the heat can theoretically be calculated from the airflow rate, the difference between the temperatures of the air in and the air out, and the air heat capacity. However, we also calibrated the heat balance using another calibration heater.

The calibration test results are shown in Figure 24. An input power of 100 W was supplied for 60 ks to the control heater. After the output became constant, the input was ceased at 62.2 ks and the heat output decreased to 0 W at 80 ks. The input was 100 W × 62.2 ks = 6.22 MJ, and the output was estimated as 5.84 MJ; thus, the output/input ratio was 0.938. We estimated that the calibration of heat was reasonable and that the lost heat was due to heat escape and radiation from the box.

Figure 25 shows a change in heat output when input of 100 W to the reactor before the activation process. The D_2 gas pressure in the reactor is 760 Pa. The reason why the output power reaches at 100 W is slower than in Figure 24 is because the reactor body is heavy, and therefore the heat quantity for heating is necessary. After reaching at 100 W output, since excess heat does not come out, it is almost constant at 100 W.

Figure 26 shows the change in heat output when input of 100 W to the reactor during the activation process. The D_2 gas pressure in the reactor was 760 Pa as in Figure 25. Compared with Figure 25, the output reaches 100 W faster. It is because excess heat has already generating, which shows the output of almost 120 W. Excess heat is not stabilized with large fluctuations.

The same electric power of 100 W was supplied to the reactor until the heat output had stabilized, and the results were compared with the calibration data. In this case, as shown in Figure 27, the heat output stabilized at 20 ks. The heat input was ceased at 71 ks. The input energy was 7.23 MJ, and the output energy was estimated to be 14.16 MJ. The output/input ratio was 1.96; i.e., the heat output was almost twice the energy input.

We calibrated by Helium gas that once the deuterium gas in the activated reactor was evacuated, then introduced 760 Pa of Helium gas and tested at 100 W input and measured the output. Figure 28 shows the result for 100 W input power for 70 ks. From this, it can be understood that no excess heat is generated in case of just Helium gas. From the above experimental results, it became clear that in order to generate excess heat, the interior of the reactor was activated, deuterium gas was introduced, and the reactant had to be activated.

The calibration test by the control heater was performed by changing the input power. Figure 29 shows the output change for the input of 80 W, 120 W and 248 W. The outputs are almost the same as the inputs.

On the other hand, the results of various inputs to the reactor are shown in Figure 30. These tests behave differently than the calibration test. It turns out that the output increases with time. For example, if 200 W input is made for 65 ks, the thermal output reaches 380 W and the Out/In ratio reaches 1.882. The generated heat energy reaches about two times at any input energy.

The results of the calibration heater and the heat generation test in vacuum are shown in Figure 31. The horizontal axis represents the input power, and the vertical axis represents the value obtained by subtracting the input electrical energy from the measured heating value, that is, the excess heat quantity. The black line is the result of the calibration heater. As the input increases, the amount of radiation loss due to the temperature rise increases, and the output heat amount becomes lower than the input. As a result, this excess thermal graph display is negative. When there is no hydrogen gas (vacuum) in the reactor indicated by the blue line, excessive heat

quantity is extremely low. The excess heat in this case is presumed to have been generated by hydrogen gas remaining in the reactant. In the excess heat generation test indicated by the red line, the furnace body temperature rises as input increases, and as a result, the excess heat generation amount increases. In this test, excess heat of 150 W at 200 W input and 480 W at 500 W input occurs.

The relationship between excess heat and the reactor temperature is shown in Figure 32. The excess heat increases with increasing temperature of the reactor. For example, the excess heat is 100 W at 100°C, 315 W at 200°C, and 480 W at 250°C. Excess heat of 10 W to 20 W was generated even near the room temperature.

When the temperature of the reactor (Tr), as shown in Figure 32, is expressed as the reciprocal of the absolute temperature, the excess heat relationship is linear (Figure 33). We speculate that the excess heat would reach the order of kilowatts at 1/Tr = 0.001, i.e. approximately 700°C. We confirmed that the excess heat increases exponentially with the reactor temperature. The reaction activation energy E_a was calculated on the basis of the linear region between 100°C and 523°C in Figure 29 to be 0.165 eV/K/atom.

To precisely confirm the abnormal heat generation of the hydrogen–metal system, complex thermal factors were narrowed down to two simple factors and analyzed. As a result, we confirmed the occurrence of an abnormal heat-generating reaction. Factors for thermal analysis are required to precisely change the amount of heat depending on the input power, the amount of flowing air, and the air inlet and outlet temperatures. On the basis of this thermal analysis and the results presented in this work, we presume that the method necessary for abnormal heat generation is as follows.

1: Activation of the sample surface and atomization and addition of surface modification metal;
2: Removal of impurities in the gas; and
3: Control of the reactor temperature and the hydrogen gas pressure.

Activation of the metal surface, that is, removal of the oxide, nitride, and carbide layers, is particularly important. Heating and discharge treatments in hydrogen gas was effective for activating the metal surface. The use of highly pure gas and thorough removal of released gas during the surface treatment are also important. After a reaction metal sample has been produced by the activation treatment, where the sample is maintained under a hydrogen gas atmosphere at high temperatures, dissociates hydrogen molecules into atomic hydrogen on the metal surface, and the amount of dissociated hydrogen increases with increasing treatment time. The presence of this atomic hydrogen can be presumed to be a condition necessary for excess heat. The occurrence of excess heat depends on the temperature, and it is at least on the order of kilowatts. The excess heat calculated on the basis of the assumption that the reactant was nickel with several 10 W/g and 1 to 10 W/cm^2.

It will be appreciated that various aspects of the second experiment apply similarly / analogously to the first experiment and vice versa.

Third Measurement Experiment

Figure 34 to Figure 54 are various illustrations of a vertical reactor as well as graphs of measurement experiments relating to heat generation from the vertical reactor.

Figure 34 and Figure 35 are external views of a vertical reactor.
Figure 36 is an inner view of the vertical reactor, showing all material surfaces covered by reaction material after the long test.
Figure 37 is an inner view of the vertical reactor before test, showing the Ni mesh contacted on the inner wall.
Figure 38 is an internal view of the vertical reactor, showing the arrangement of the reactor device / reactants.

Figure 39 and 40 are graphs for a first run of the experiment.
Figure 39 is a graph showing change of temperature difference between air out and air in and gas pressure of the vertical reactor for 100W.

Figure 40 is a graph showing changes of input and output heat of the vertical reactor during 100W input power.

Figure 41 and 42 are graphs for a second run of the experiment.
Figure 41 is a graph showing change of temperature difference between air out and air in and gas pressure of the vertical reactor during excess heat test.
Figure 42 is a graph showing changes of input and output heat of the vertical reactor at 100W input power.

Figure 43 and 44 are graphs for a third run of the experiment.
Figure 43 is a graph showing change of temperature difference between air out and air in and gas pressure of the vertical reactor during excess heat test.
Figure 44 is a graph showing changes of input and output heat of the vertical reactor for input power of 300W.

Figure 45 and 46 are graphs for a fourth run of the experiment.
Figure 45 is a graph showing change of temperature difference between air out and air in and gas pressure of the vertical reactor during excess heat test of 300W.
Figure 46 is a graph showing changes of input and output heat of the vertical reactor for input power of 300W.

Figure 47 and 48 are graphs for a fifth run of the experiment.
Figure 47 is a graph showing change of temperature difference between air out and air in and gas pressure of the vertical reactor during control test of 100W.
Figure 48 is a graph showing changes of input and output heat of the vertical reactor system power of 100W to the control heater.

Figure 49 and 50 are graphs for a sixth run of the experiment.
Figure 49 is a graph showing change of temperature difference between air out and air in and gas pressure of the vertical reactor during excess heat test of 100W.
Figure 50 is a graph showing changes of input and output heat of the vertical reactor for input power of 100W.

Figure 51 and 52 are graphs for a seventh run of the experiment.
Figure 51 is a graph showing change of temperature difference between air out and air in and gas pressure of the vertical reactor during excess heat test of 100W.
Figure 52 is a graph showing changes of input and output heat of the vertical reactor for input power of 100W.

Figure 53 and 54 are graphs for an eighth run of the experiment.
Figure 53 is a graph showing change of temperature difference between air out and air in and gas pressure of the vertical reactor during excess heat test of 100W.
Figure 54 is a graph showing changes of input and output heat of the vertical reactor for input power of 100W.

It will be appreciated that various aspects of the third experiment apply similarly / analogously to the first and second experiments and vice versa.

Broad Statements of Disclosure

Statement 1:

In a reactant having a multilayered film structure used in a “Condensed Matter Nuclear Science” reactor which mainly contains hydrogen isotope and nickel in which the reactant is any one of a) plate, b) net/mesh, c) sprayed film, or d) electrodeposited film. A palladium layer, a nickel layer, a palladium and platinum layer are stacked in a certain order on the nickel base/substrate. Some of these elements (at least one) must be in the form of nanoparticle. The thickness of the nickel base/substrate is several nm to 1000 nm. The reactant’s each layer on the nickel base/substrate is 1 nm to 1000 nm.

Statement 2:

A reactant having a multilayer film structure described in Statement 1, wherein at least one of high purity nickel and palladium is replaced by at least one alloy selected from the group consisting of LaNi5, YNi5, MmNi5, and TiFe.

Statement 3:

For the reactant having the multilayer film structure according to Statement 2, on the surface of the alloy described by Statement 2 shall be covered by at least one of the following high purity elements – C, Al, B, Cu, Cr, Mn, Si, Ti, Zn, Co, V, Mo, Nb, and Zr.

Statement 4:

A reactant having a multilayer film structure according to Statement 1, wherein at least one of high purity nickel and palladium is replaced by an alloy that contains at least one metal selected from Mg, NiAl, LiAl, with one or more high purity elements such as C, Al, B, Cu, Cr, Mn, Si, Ti, Zn, Co, V, Mo, Nb, and Zr.

Statement 5:

In addition to the reactant having the multilayer film structure according to any one of the Statements 1 to 4, it is preferable that on the surface of the reactant shall be

covered by a metal with hydrogen atom structure that is in the alkali and alkaline earth family.

Statement 6:
For a reactant having the multilayer film structure according to Statement 5, it is preferable that the metal element having the hydrogen atom structure is composed of at least one selected from the group consisting of high purity Li, Na, K, and Ca.

Statement 7:
Manufacturing processes for a reactant having a multilayered film structure used in a “Condensed Matter Nuclear Science” reactor, which mainly contains high purity hydrogen isotope and high purity nickel in which the reactant is any one of a) plate, b) net/mesh, c) sprayed film, or d) electrodeposited film. A palladium layer, a nickel layer, a palladium and platinum layer are stacked in a certain order on the nickel base. Some of these elements (at least one) must be in the form of nanoparticle. The thickness of the nickel base/substrate is 1nm to 1000 nm. The reactant’s each layer on the nickel base/substrate is 1 nm to 1000 nm.

Statement 8:
The methods for producing a reactant having the multilayer film structure according to Statement 7, wherein the film forming is to laminate with metals of platinum, palladium, nickel, palladium, platinum in the order as above on a high purity nickel substrate. Arranging the order of these metal atoms also arranges the distribution of the microparticles in order to improve the reactivity of the product.
Arranging is done with the following steps:
(1) Deuterium gas inside the reaction reactor/furnace is set to several thousand Pa or less
(2) While maintaining such a gas pressure, depositing the metal atoms that are released by plasma discharge from the center electrode onto the surface of the reactant.

Statement 9:

The methods for producing a reactant having the multilayer film structure according to Statements 7 or 8, wherein at least one of high purity nickel and palladium is replaced by at least one alloy selected from the group consisting of LaNi5, YNi5, MmNi5, and TiFe.

Statement 10:
A method for producing a reactant having a multilayer film structure according to Statement 9, the surface of the selected alloy is covered by one of the following high purity elements such as C, Al, B, Cu, Cr, Mn, Si, Ti, Zn, Co, V, Mo, Nb, and Zr.

Statement 11:
A method for producing a reactant having the multilayer film structure according to Statements 7 or 8, wherein at least one of high purity nickel and palladium is replaced by an alloy that has a) at least one element selected from Mg, NiAl, LiAl, and b) at least one more element added from the group consisting of high purity C, Al, B, Cu, Cr, Mn, Si, Ti, Zn, Co, V, Mo, Nb, and Zr.

Statement 12:
A method for producing a reactant having a multilayer film structure according to any one of Statements 7 to 11, with the following processes:
In the reaction reactor/furnace Pd and Pt electrodes are provided at the center of the reactor filled with high purity hydrogen and/or deuterium, and discharge treatment is performed by applying an alternating high voltage discharge between the Pd and Pt electrodes and the reactant until the surface of the reactant becomes rough.

Statement 13:
In addition to the methods for producing a reactant having the multilayer film structure according to Statement 12, a Pd or Pt electrode is formed by winding Pd or Pt thin wire around the center anode rod material with its surface to be coved by one element selected from the group of metals having an atom contained in alkali and alkaline earth atoms and having a hydrogen atom structure. The covering or surface making is done by electric discharge.

Statement 14:

The methods for producing a reactant having a multilayer film structure according to Statements 12 or 13, wherein an element having the hydrogen atom structure is selected from the group consisting of high purity Li, Na, K, and Ca.

Statement 15:

The processes for producing a reactant having a multilayer film structure for a “Condensed Matter Nuclear Science” reactor, thin films of platinum, palladium, nickel, palladium and platinum are stacked in this order on a nickel substrate.
Under a high temperature and high voltage and then rolling it during the annealing of the reactant to produce a reactant described above.

Statement 16:

In the process for producing a reactant having a multilayer film structure for a “Condensed Matter Nuclear Science” reactor, thin films of platinum, palladium, nickel, palladium and platinum are stacked in this order on a nickel substrate by plating.

Statement 17:

A method for producing a reactant having a multilayer film structure for a “Condensed Matter Nuclear Science” reactor according to Statements 15 or 16, characterized in that the temperature of the reactant is rapidly lowered after the high temperature treatment to make the reactant structure “amorphous”.

Statement 18:

A power generation method using a reactant having a multilayer film structure used in the “Condensed Matter Nuclear Science” reactor according to any one of Statements 1 to 6, wherein placing a wire onto the base metal of the reactant and another wire on the surface metal of the reactant to cause a voltage difference between the both wires to generate electricity.

Statement 19:

A method for producing a reactant having a multilayer film structure for use in a “Condensed Matter Nuclear Science” reactor according to Statements 1 or 2, characterized in that the temperature is rapidly lowered to make the amorphous after the high temperature treatment.

Statement 20:
More than one “Condensed Matter Nuclear Science” reactor according to Statements 1 or 2 are combined together to utilize each other’s heat effectively to accelerate and enhance heat generation.

Statement 21:
The direct electricity generation method from a reactor having the reactant described in Statements 1 or 2.

Statement 22:
A method of manufacturing a reactor used in a “Condensed Matter Nuclear Science” reactor, wherein the reactor is provided with a heater around the reactor of high purity stainless steel, and palladium/platinum anode and a cathode described by any one of Statements 1 to 6 on the inner wall surface of the reactor, thus the reactant is in close contact with the inner wall of the reactor. The electrodes are both assumed to have variable polarity. A vacuum pump, an intake / exhaust port, a thermocouple, a thermal measurement device, a thermal control device and a hydrogen isotope injection device are used in the reactor making process.

Statement 23:
A method for controlling heat generation between hydrogen and metal in a “Condensed Matter Nuclear Science” reactor described by any one of Statements 1 to 22. Controlling heat generation requires during the reactor making controlling/ managing of a) reaction temperature, b) gas pressure, c) multilayered surface creation, d) gas impurity elimination, e) reactant activation, f) microparticle processing.

Statement 24:

The method of controlling heat generation between hydrogen and metal according to Statement 23, wherein the activation of the surface of the reactant and the micro-articulation treatment step are carried out in such a manner that in either hydrogen or deuterium filled reactor with a Pd or Pt electrode in the center of the reactor and discharge treatment is performed by applying an alternating high voltage between the electrode and the reactant so that the surface of the reactant is roughened.

Statement 25:
The hydrogen-metal heat generation control method according to Statements 23 or 24, wherein the Pd electrode is modified by winding a Pd thin wire around the electrode and applying by electric discharge one element as the surface of reactant selected from the group of metals having an atom contained in alkali and alkaline earth atoms and also having a hydrogen atom structure.

References

1. M. Fleischmann, S. Pons, and M. Hawkins: J. Electroanal. Chem., 261, (1989) 301.

2. S. Pons and M. Fleischmann, J. Electroanal. Chem., 287, (1990) 293.

3. M. Fleischmann and S. Pons, J. Electroanal. Chem., 332, (1992) 33.

4. M. Fleischmann and S. Pons, Phys. Lett., A 176, (1993) 118.

5. M. Fleischmann M and S. Pons, Phys. Lett., A 187, (1994) 276.

6. J. E. Jones, E. P. Palmer, J. B. Czirr, D. L. Decker, G. L. Jensen, J. M. Thorne, S. F. Taylor and L. Rafelski, Nature, 338, (1989) 737.

7. T. Mizuno, T. Akimoto, K. Azumi, M. Kitaichi and K. Kurokawa, Fusion Technol. 29, (1996) 385.

8. T. Mizuno, T. Ohmori, T. Akimoto and A. Takahashi, Jpn. J. Appl. Phys. 39, (2001) 6055.

9. T. Mizuno, T. Akimoto, T. Ohmori, A. Takahashi, H. Yamada and H. Numata, Jpn. J. Appl. Phys. 40, (2001) L989.

10. T. Mizuno, T. Ohmori, K. Kurokawa, T. Akimoto, M. Kitaichi, K. Inoda, K, Azumi, S. Shimokawa and M. Enyo, Denki Kagaku Oyobi Kogyo Butsuri Kagaku 64, (1996) 1160 [in Japanese].

11. S. Forcardi, R, Habel and F. Piantelli, Il Nuovo Cimento, 107A, N.1, (1994) 163-167. 12. S. Forcardi, R, Habel and F. Piantelli, Il Nuovo Cimento, 111A, N.11, (1998) 1233-1242.

13. E. Cerron-Zeballos, I. Crotty, D. Hatzifotiadou, J. Lamas Valverde, M. C. S. Williams and A. Zichichi, Nuovo Cimento, 109A, (1996) 1645-1655.

14. Japan Patent Publication: TokuKaiHei 5-27062

15. Japan Patent Publication: TokuKaiHei 7-104080

16. Japan Patent Publication: TokuKaiHei 11-271484

17. Japan Patent Publication: TokuKai 2014-37996

Drawings

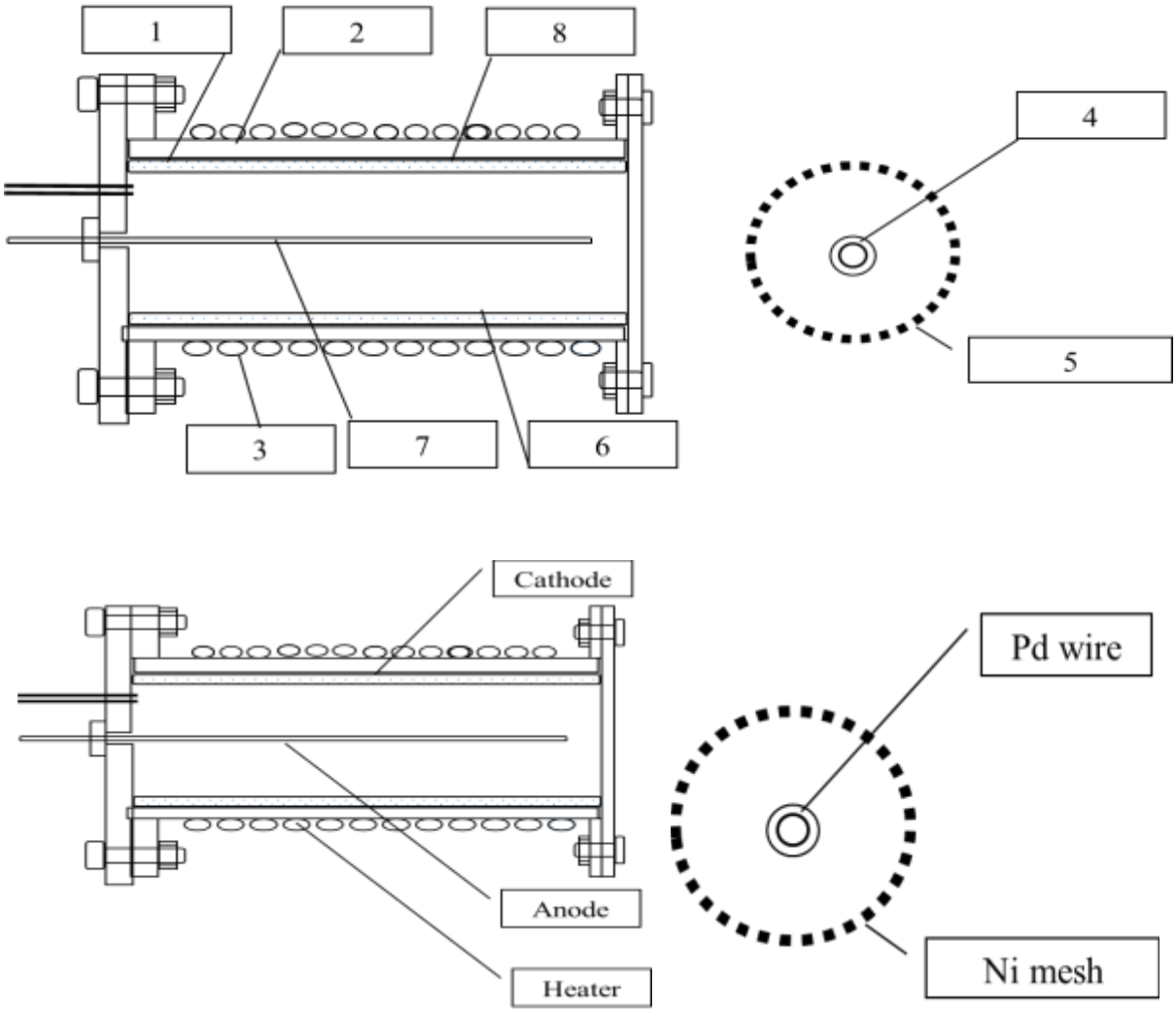

1 Reactant ; 2 Reactor ; 3 Heater ; 4 Discharge Nickel wire ; 5 Nickel mesh ; 6 Nickel fine particles ; 7 Anode ; 8 Cathode

Cross section of the reactor/furnace with multilayer reactant ;

Center rod is the discharge electrode covered by Pt, Pd thin wire ;

The reactor/furnace/reactor main body is cylindrical, and is connected to each part by way of ICF flanges

Figure 1

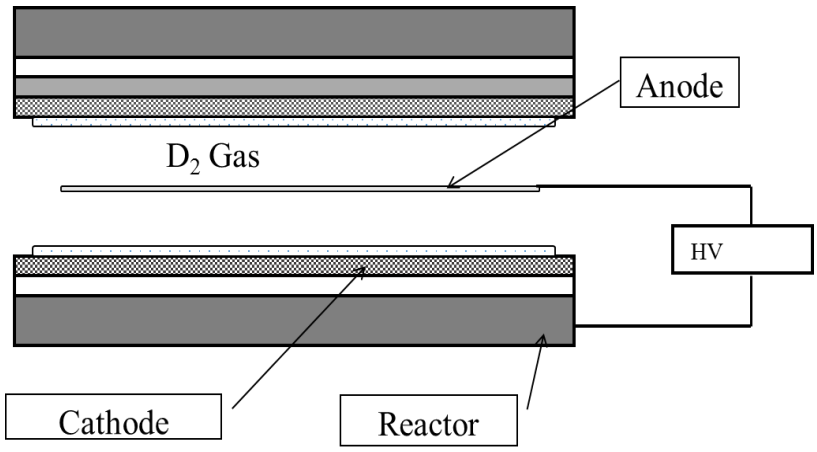

Schematic drawing of the cut section of the reactor/furnace.

From the top to center:

Reactor wall (SUS 316) — thick part

Multilayered reactant

Electric discharge rod (center)

Figure 2

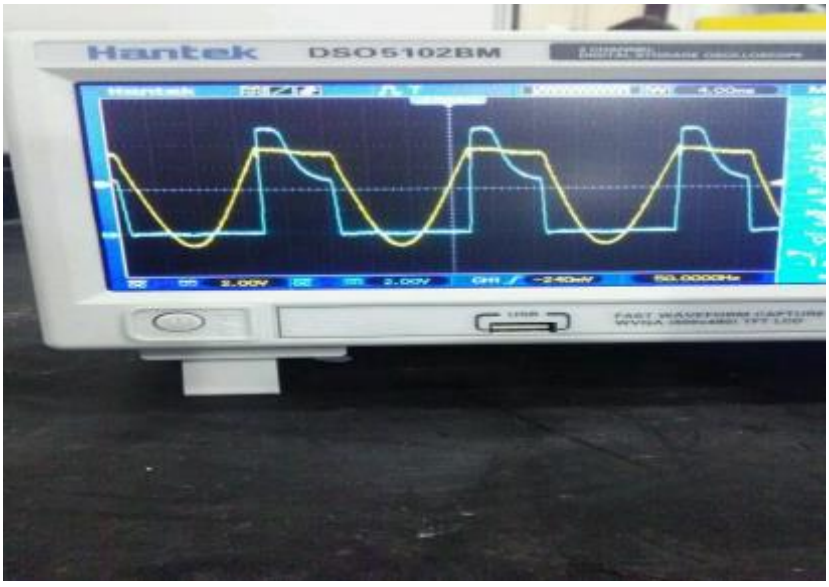

Changes in voltage and current during discharge processing

Figure 3

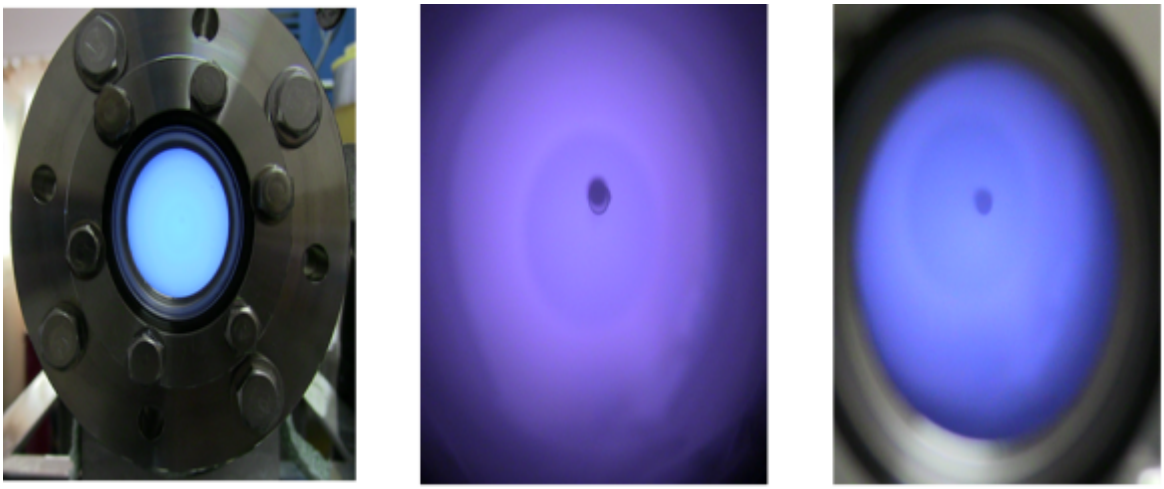

Figure 4 (left) – Inside view at the start of discharge processing

Figure 5 (center) – View at the time of discharge treatment with D_2 gas introduction

Figure 6 (right) – View at the completion of discharge treatment

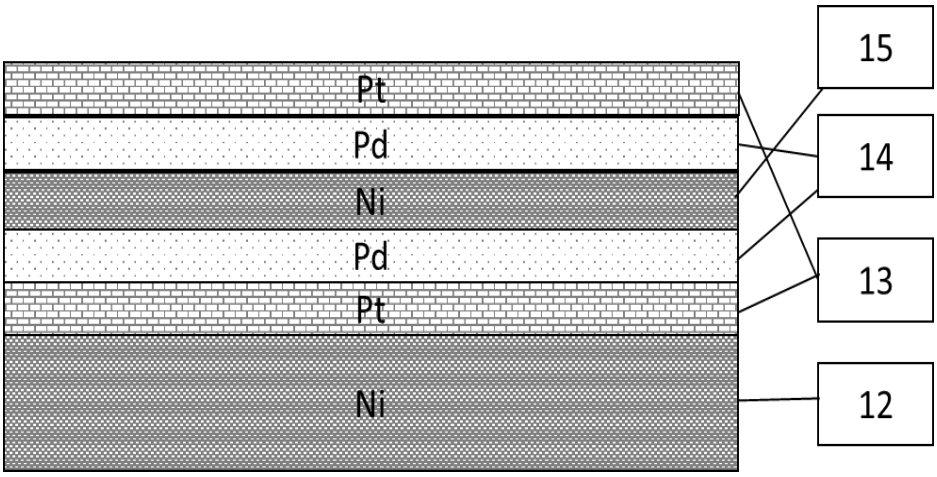

Multilayer film structure

12 is a nickel substrate ; 13 is platinum ; 14 is palladium ; and 15 is nickel.

Figure 7

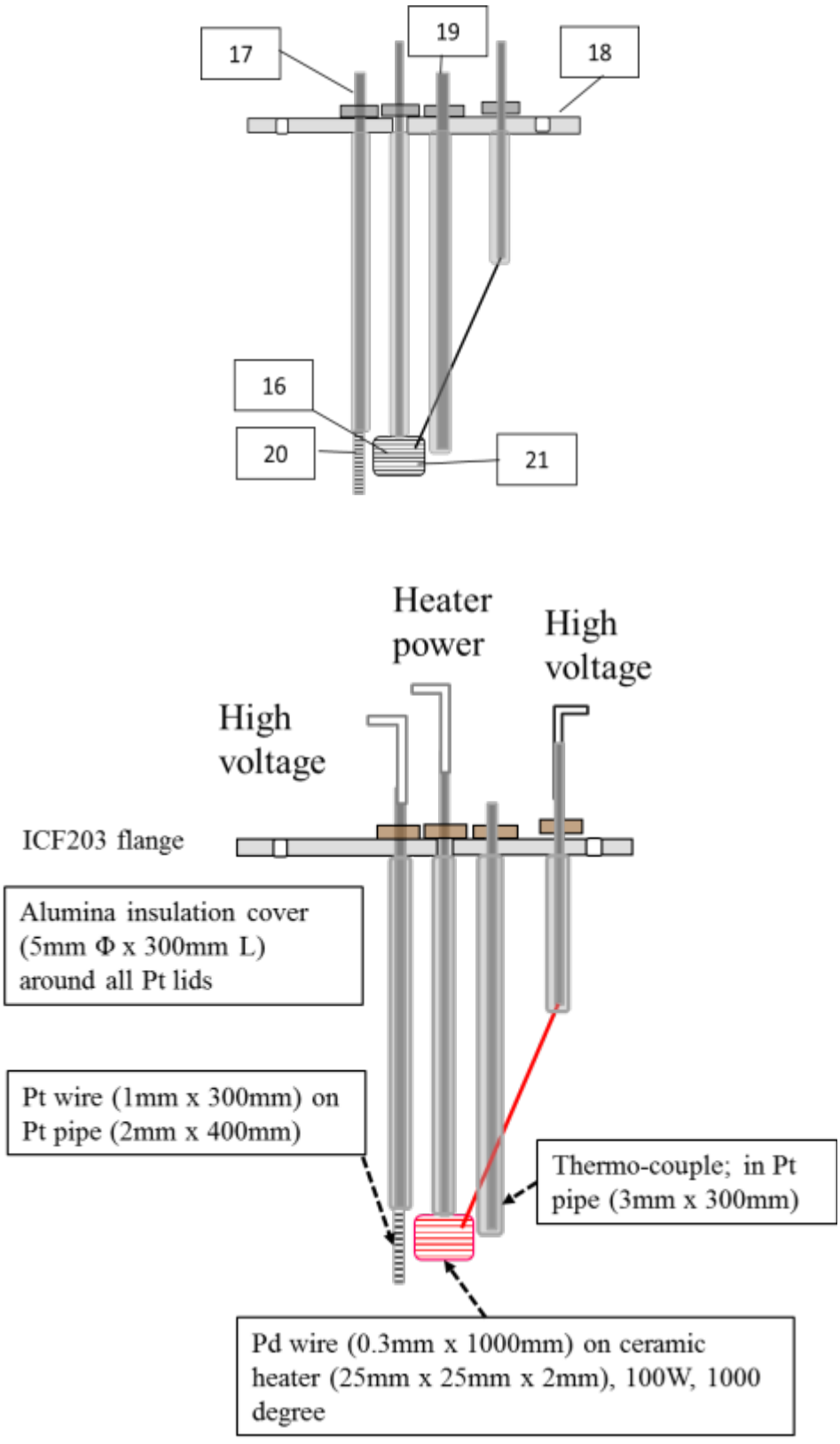

Thin surface generation electrodes

Figure 8

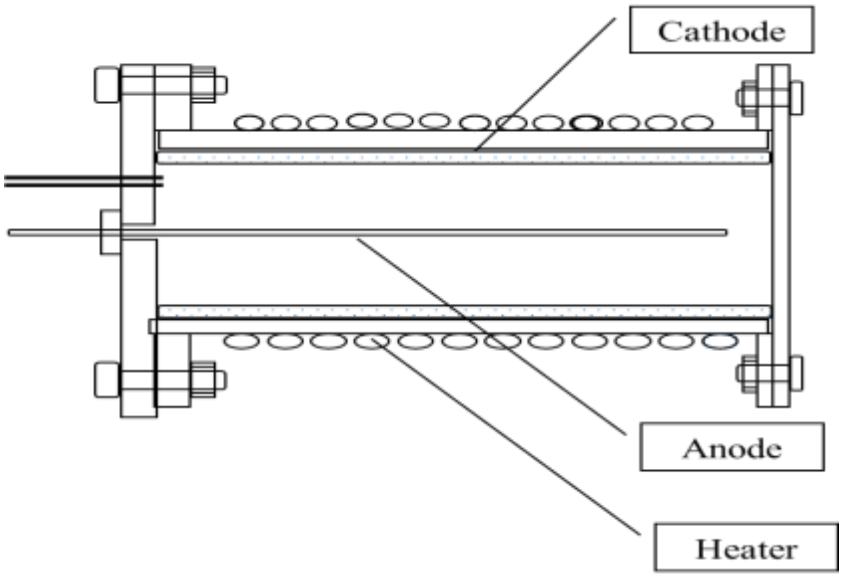

Cross section view of the main reactor/furnace body
Center rod is the discharge electrode (multilayered metal (reactant metal))

Figure 9

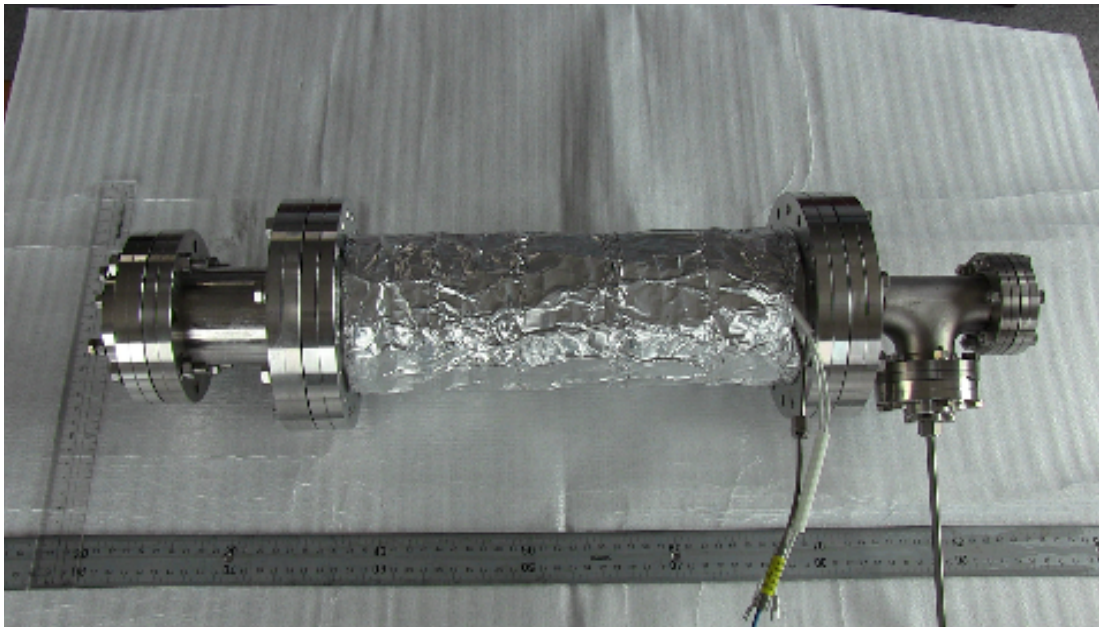

Outer view of reactor/furnace (aluminium foil covers the wrapped wire heater)

Figure 10

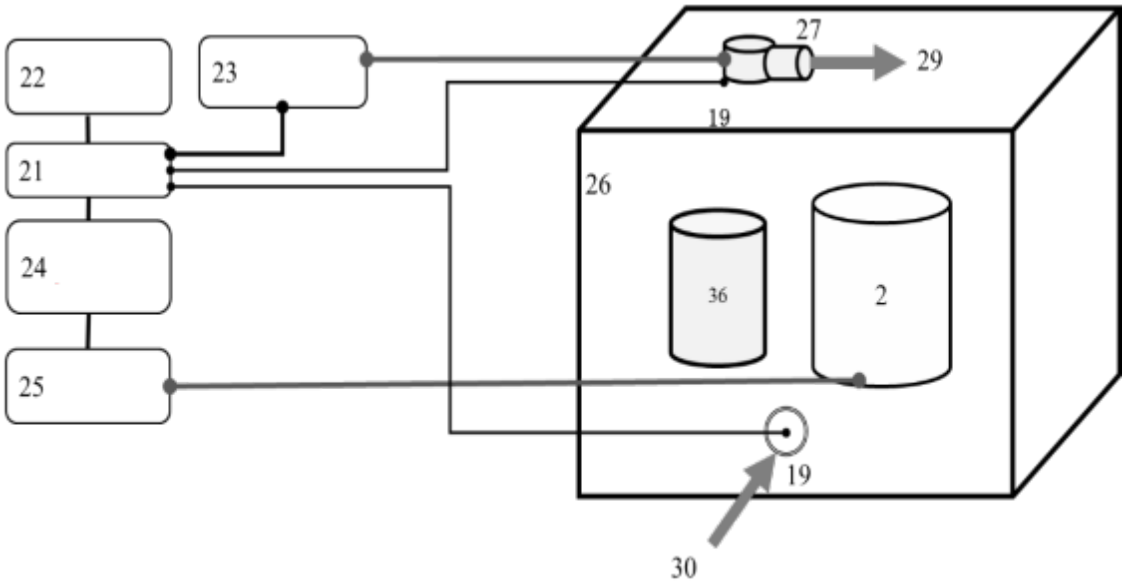

Schematic diagram of a measurement configuration

Figure 11

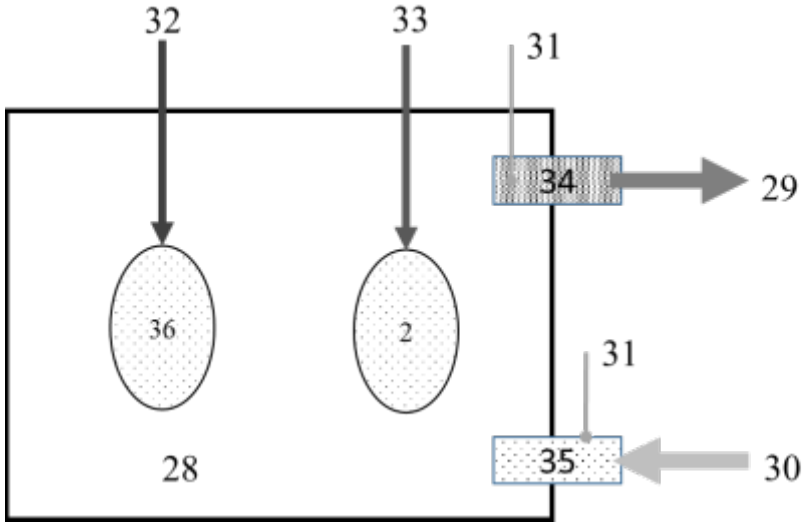

Conceptual and schematic view of thermal calibration method

Figure 12

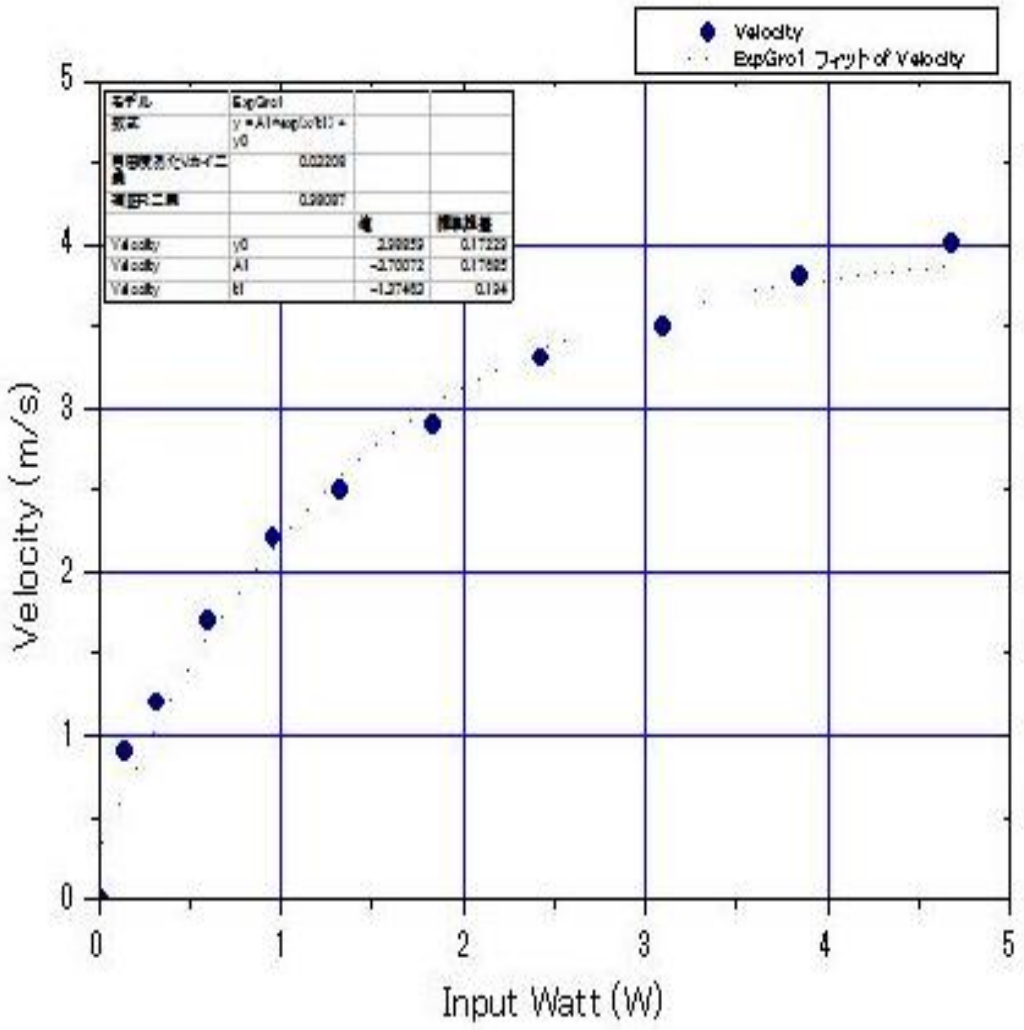

Graph showing the relationship between the input of the DC fan and the wind speed

Figure 13

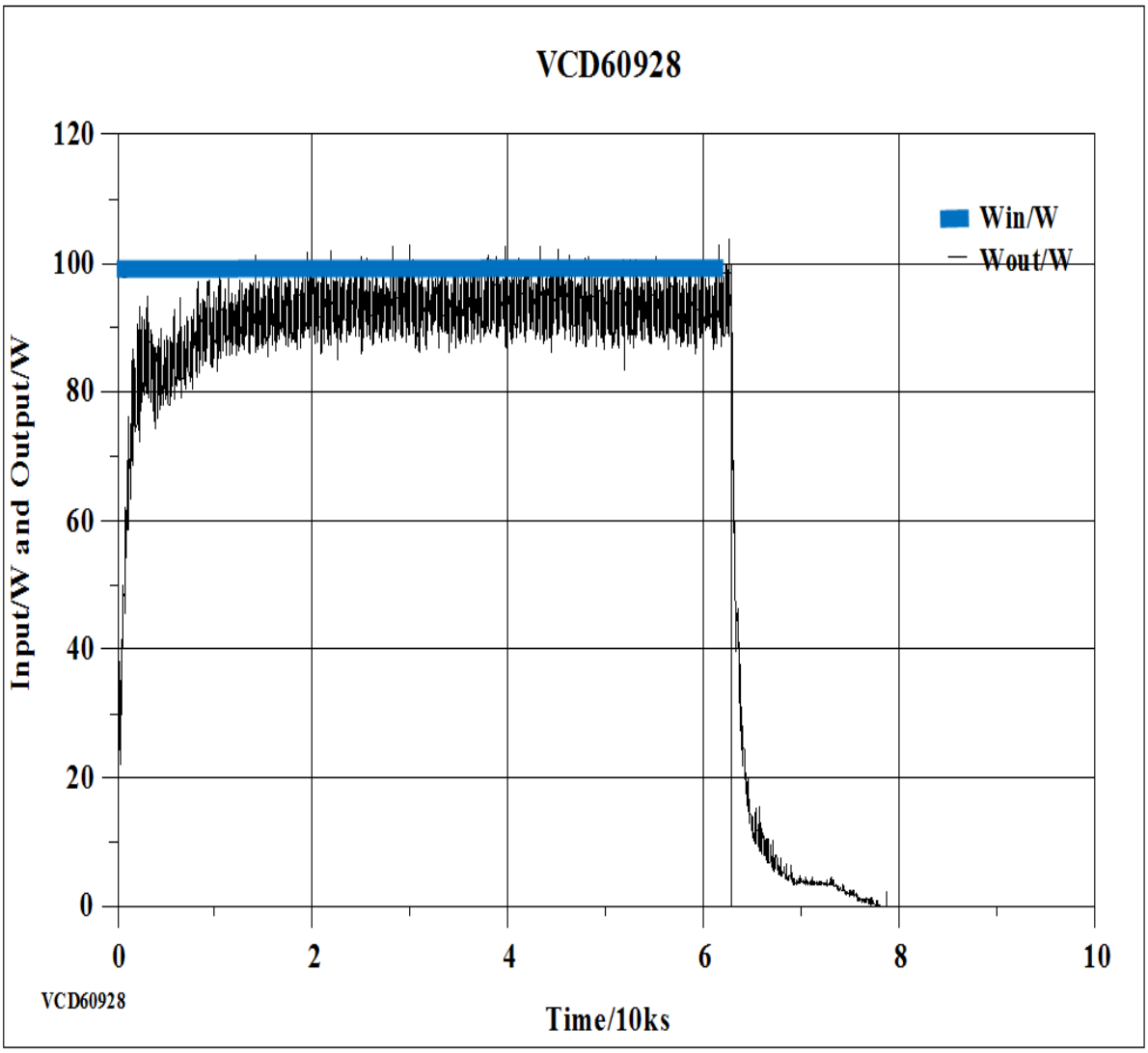

Test result drawing by a calibration heater

Figure 14

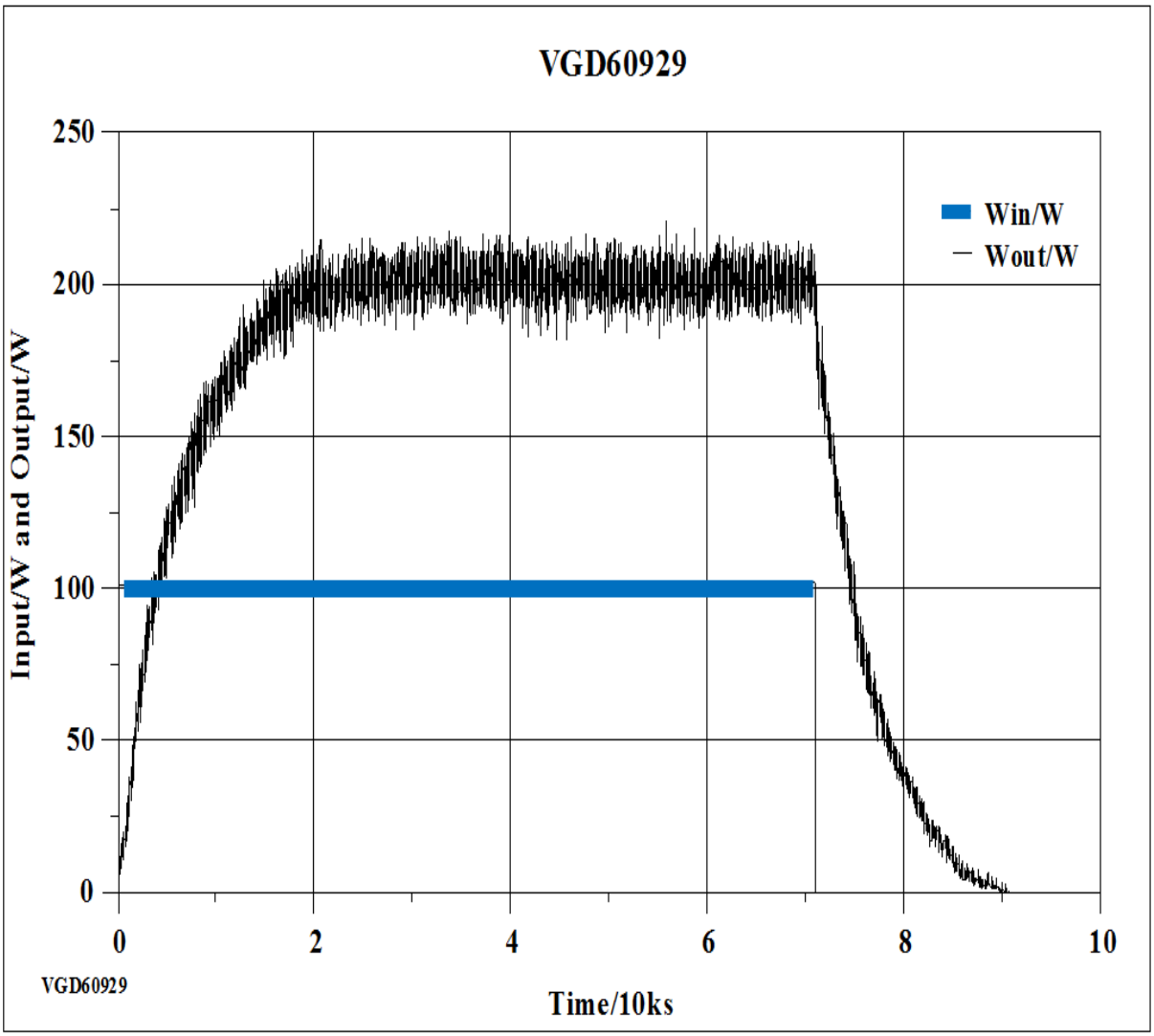

Thermal output diagram for the case of a reactor/furnace input of 100 W

Figure 15

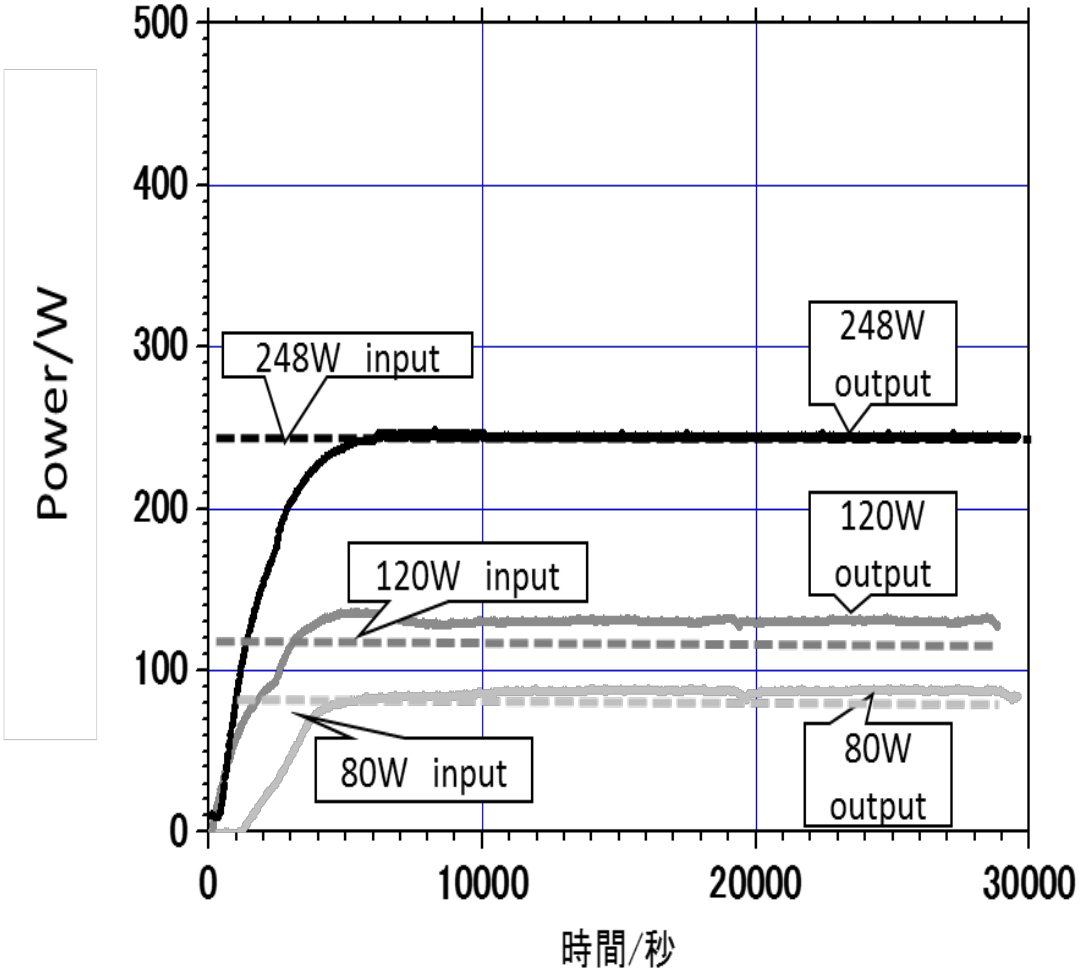

Change in output time when a calibration test is performed with various input powers

Figure 16

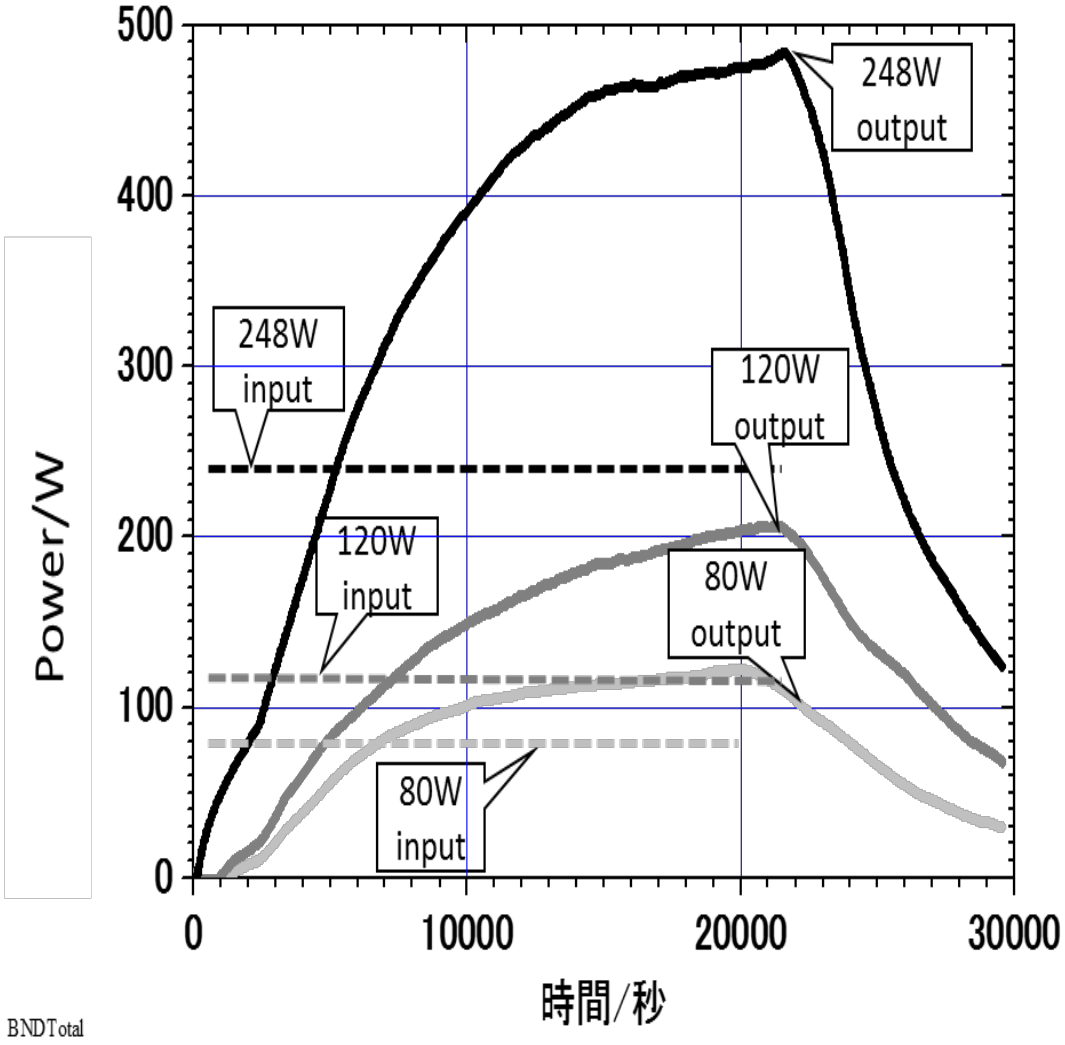

Change in output when the input to the reactor is changed

Figure 17

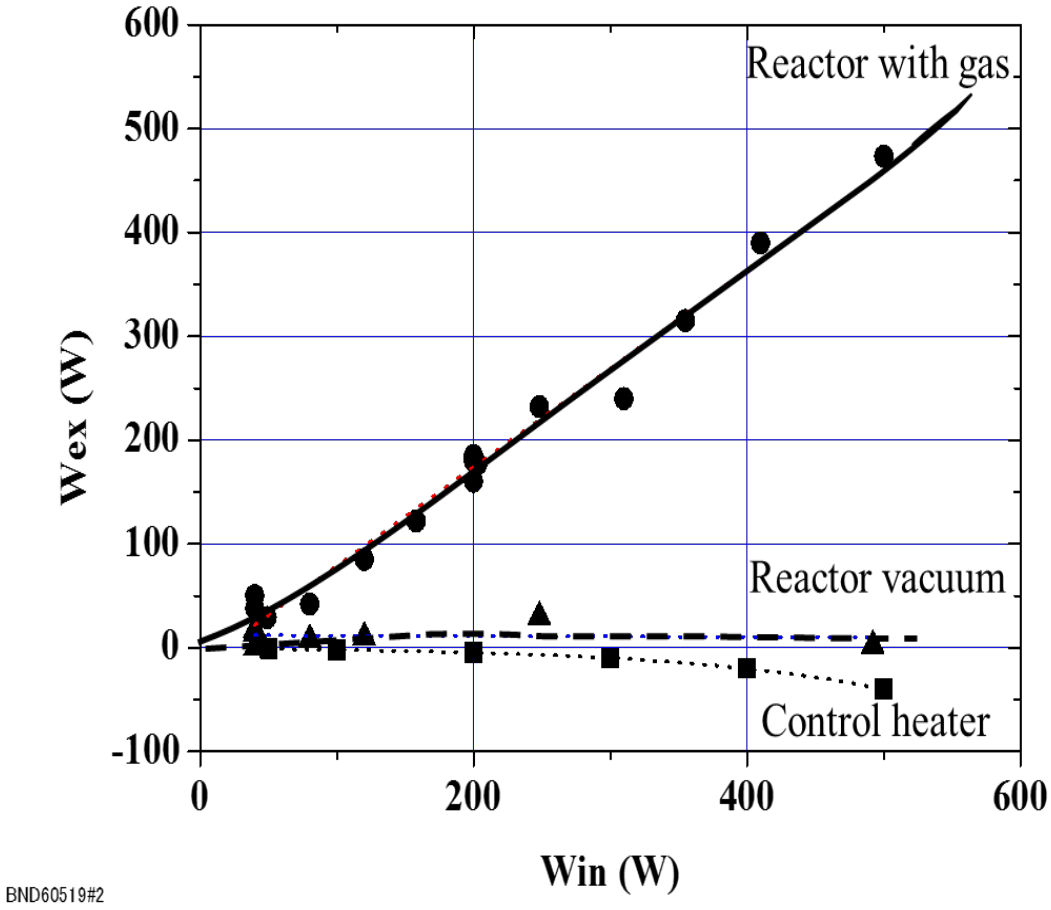

Example in which the test was conducted under various conditions

Figure 18

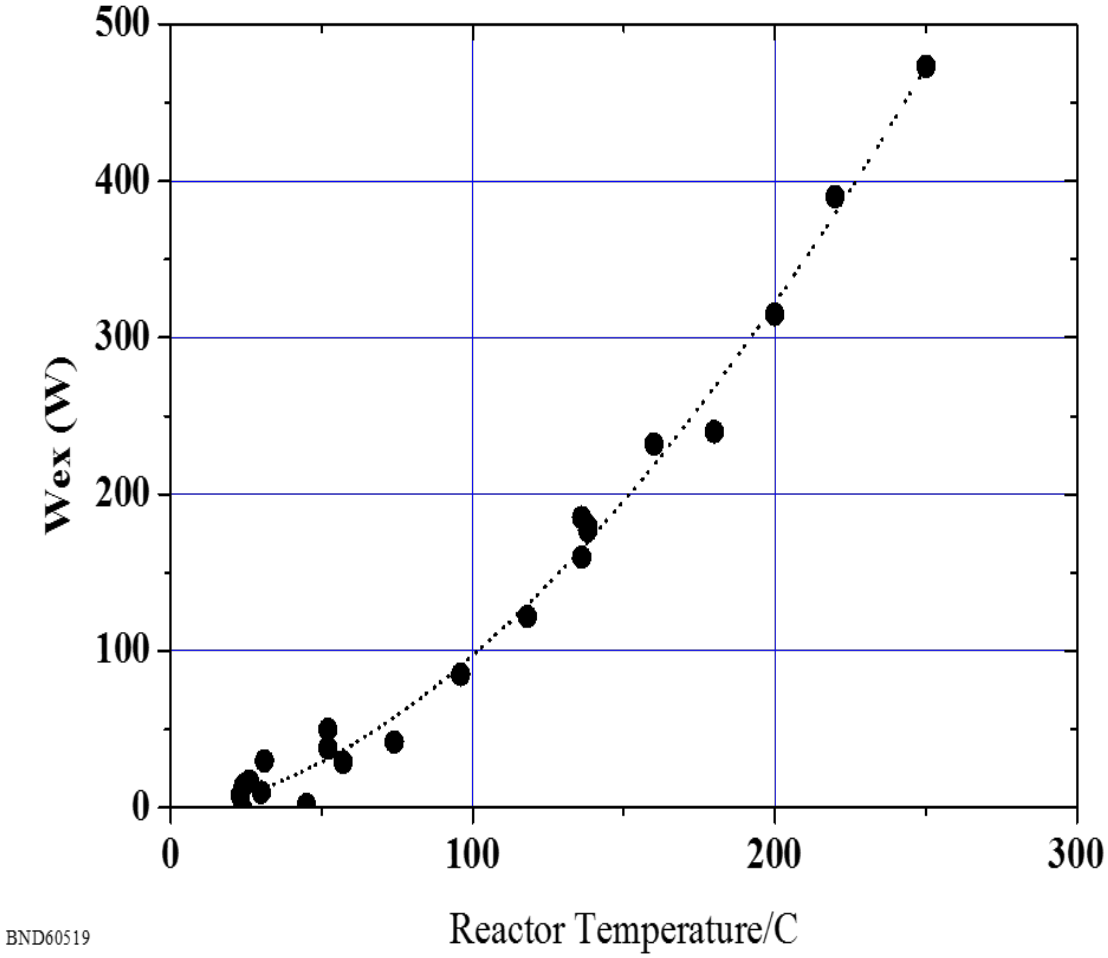

Graph showing the relationship between excess energy generation and reactor/ furnace body temperature

Figure 19

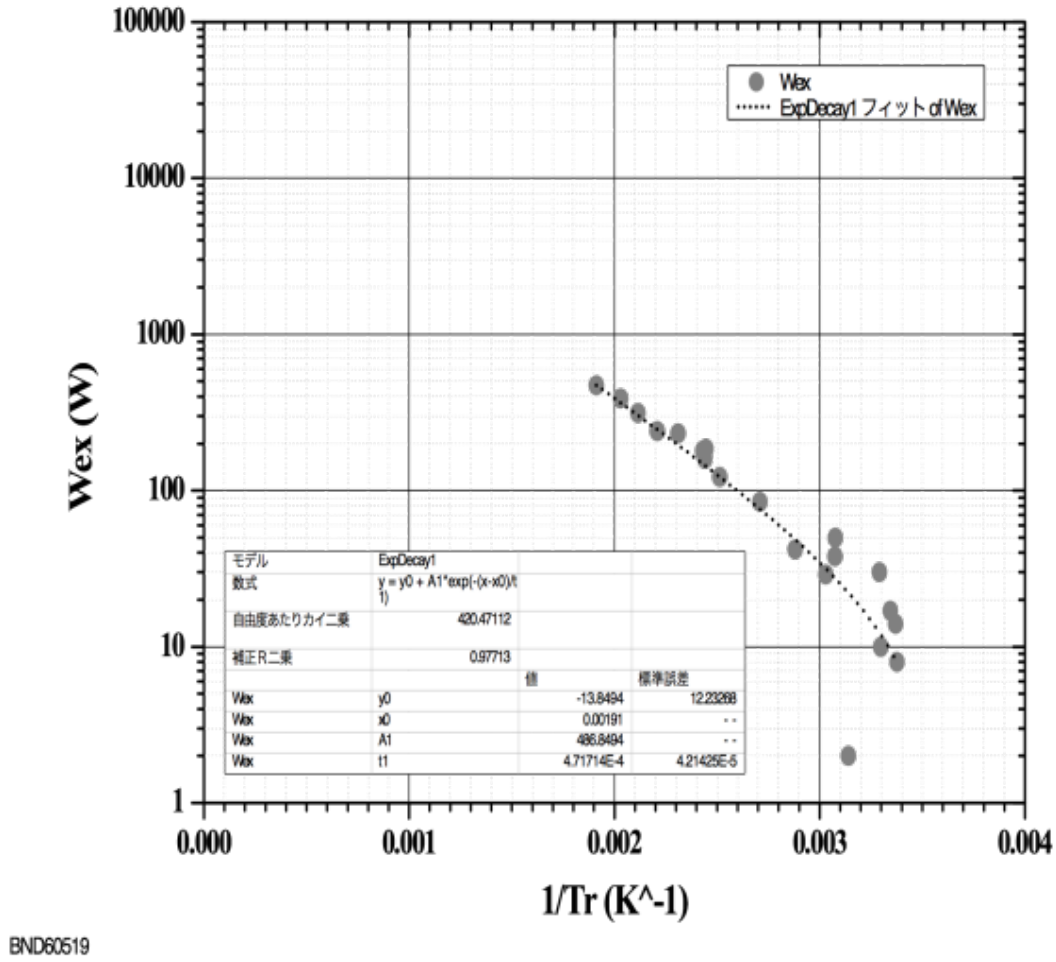

BND60519

Graph showing the relationship between generation of excessive energy and absolute temperature

Figure 20

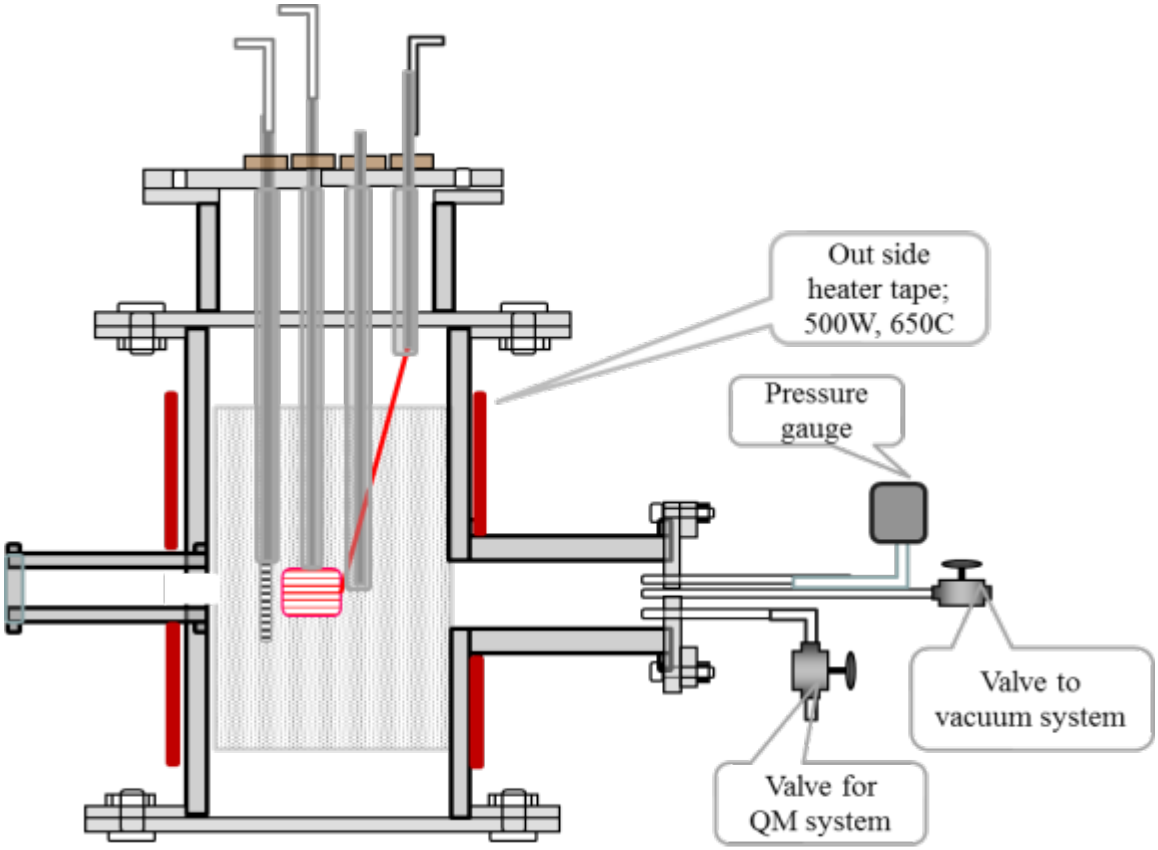
Out side
heater tape;
500W, 650C
Pressure
gauge
Valve to
vacuum system
Valve for
QM system

Figure 21A

Figure 21B

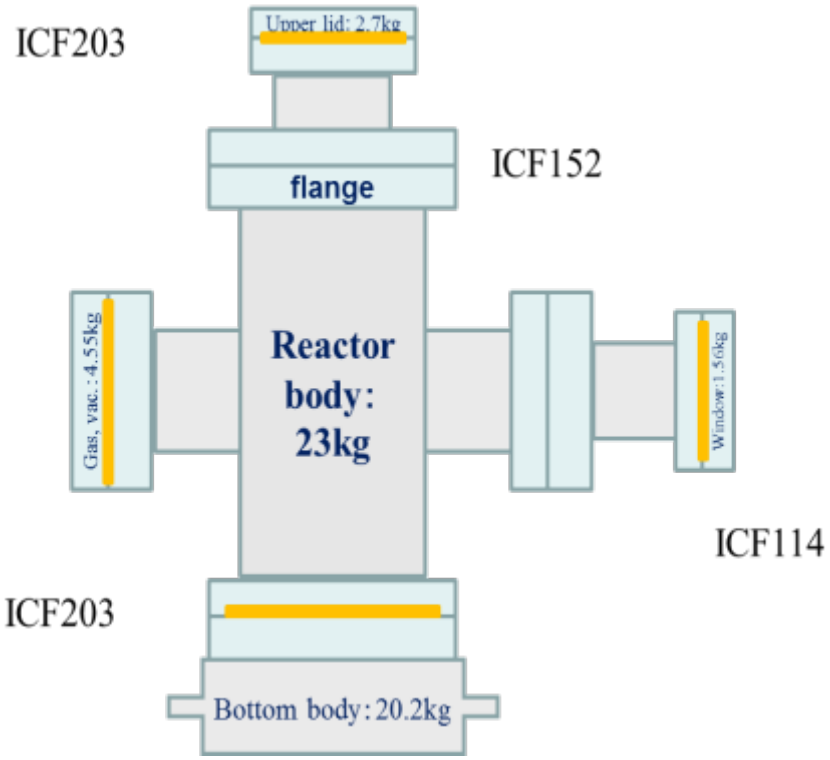

Figure 21C

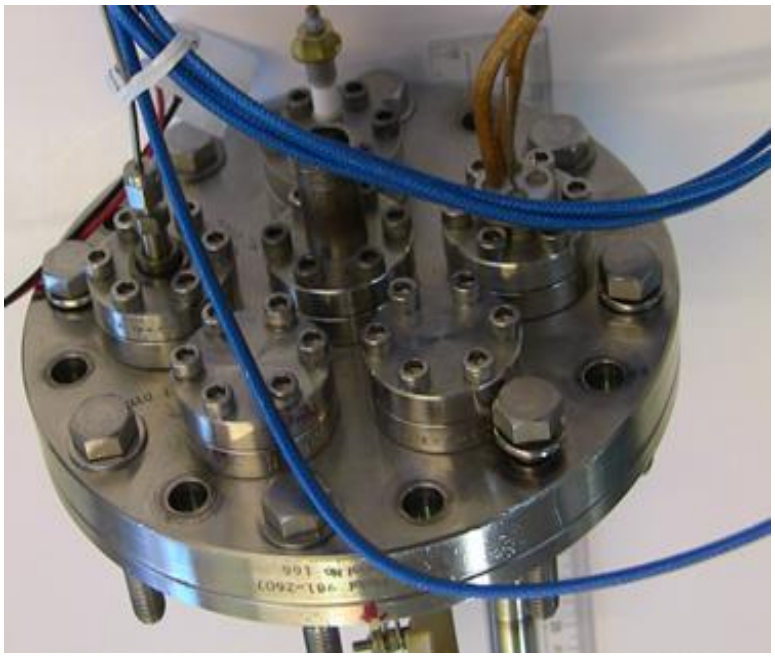

Figure 21D

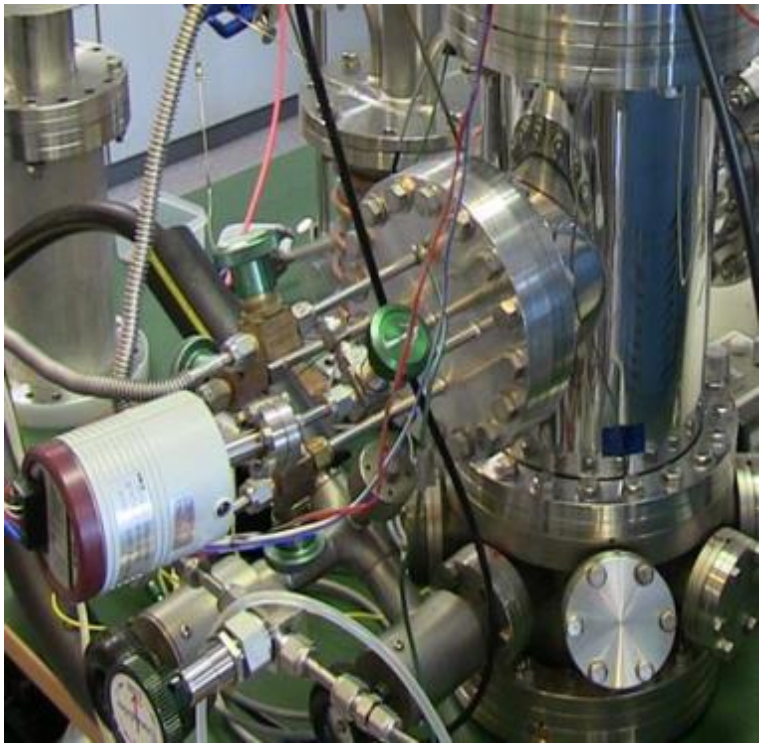

Figure 21E

Figure 21F

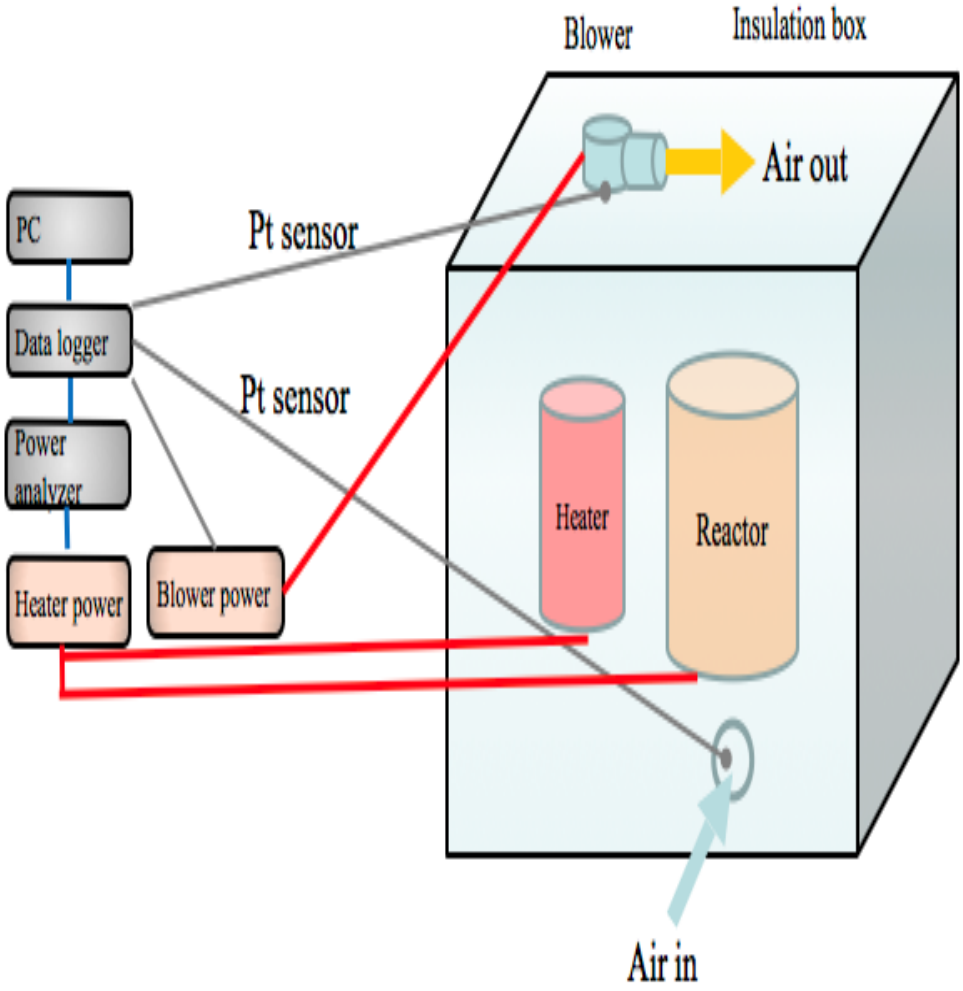

Schematic drawing of measurement system

Figure 22

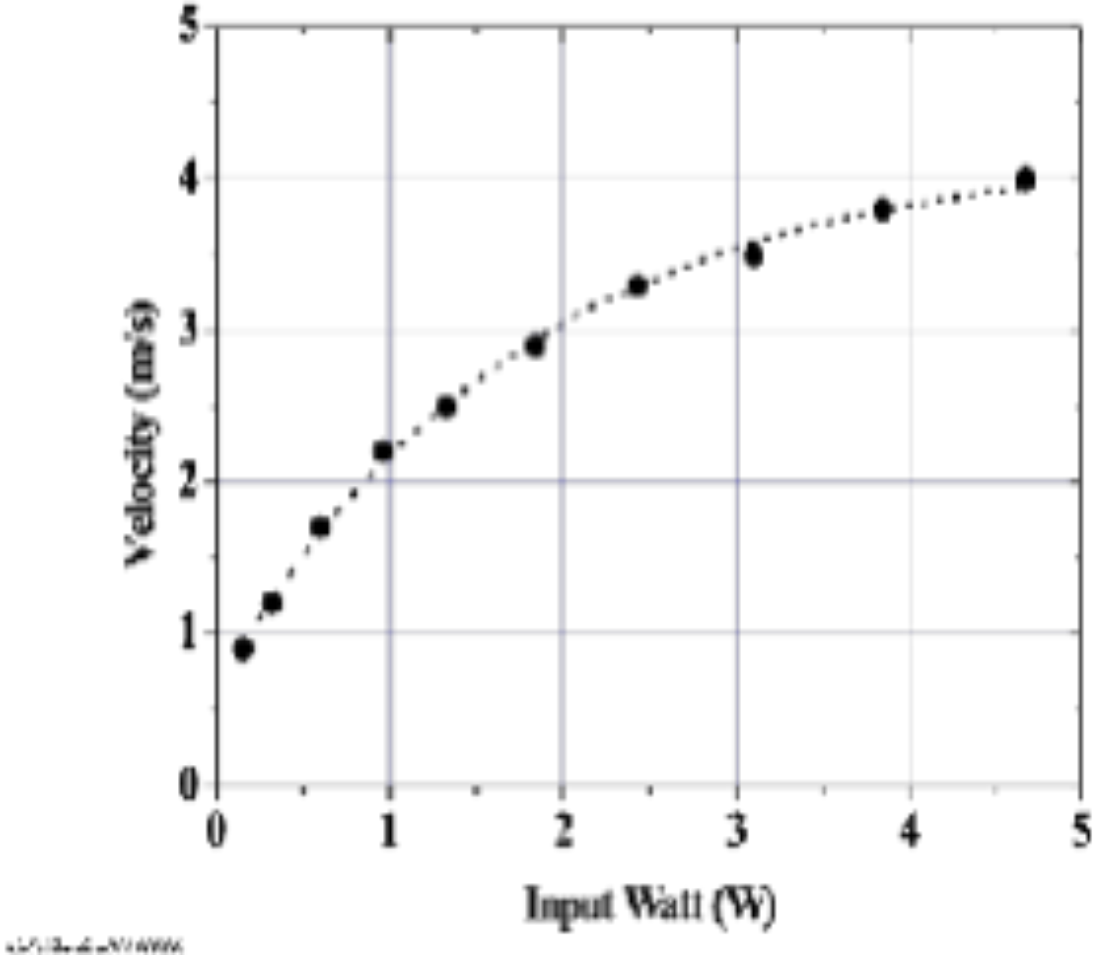

Relationship between the input power and the wind velocity of the fan

Figure 23

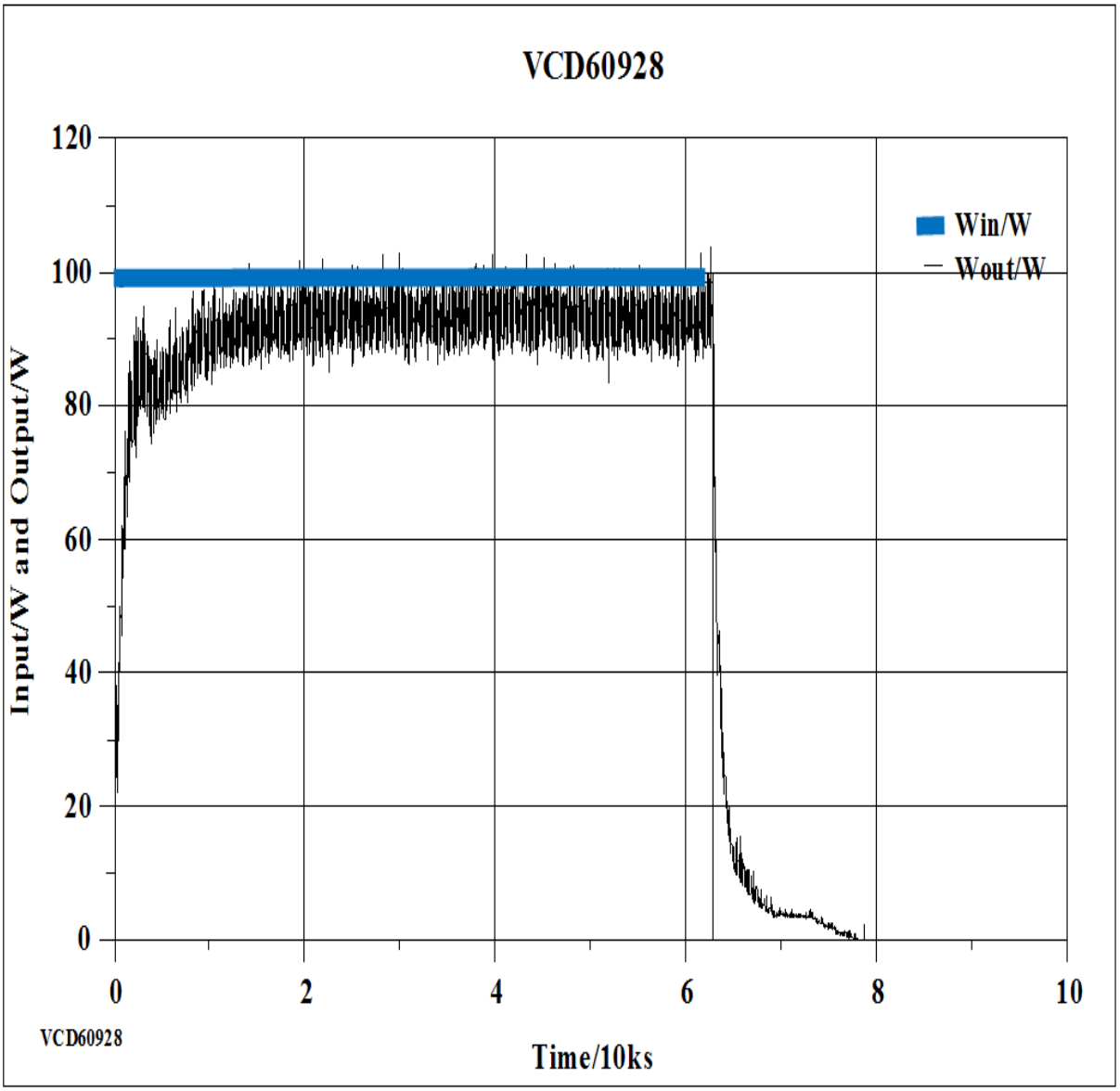

Test results obtained using a calibration heater with an input power of 100 W

Figure 24

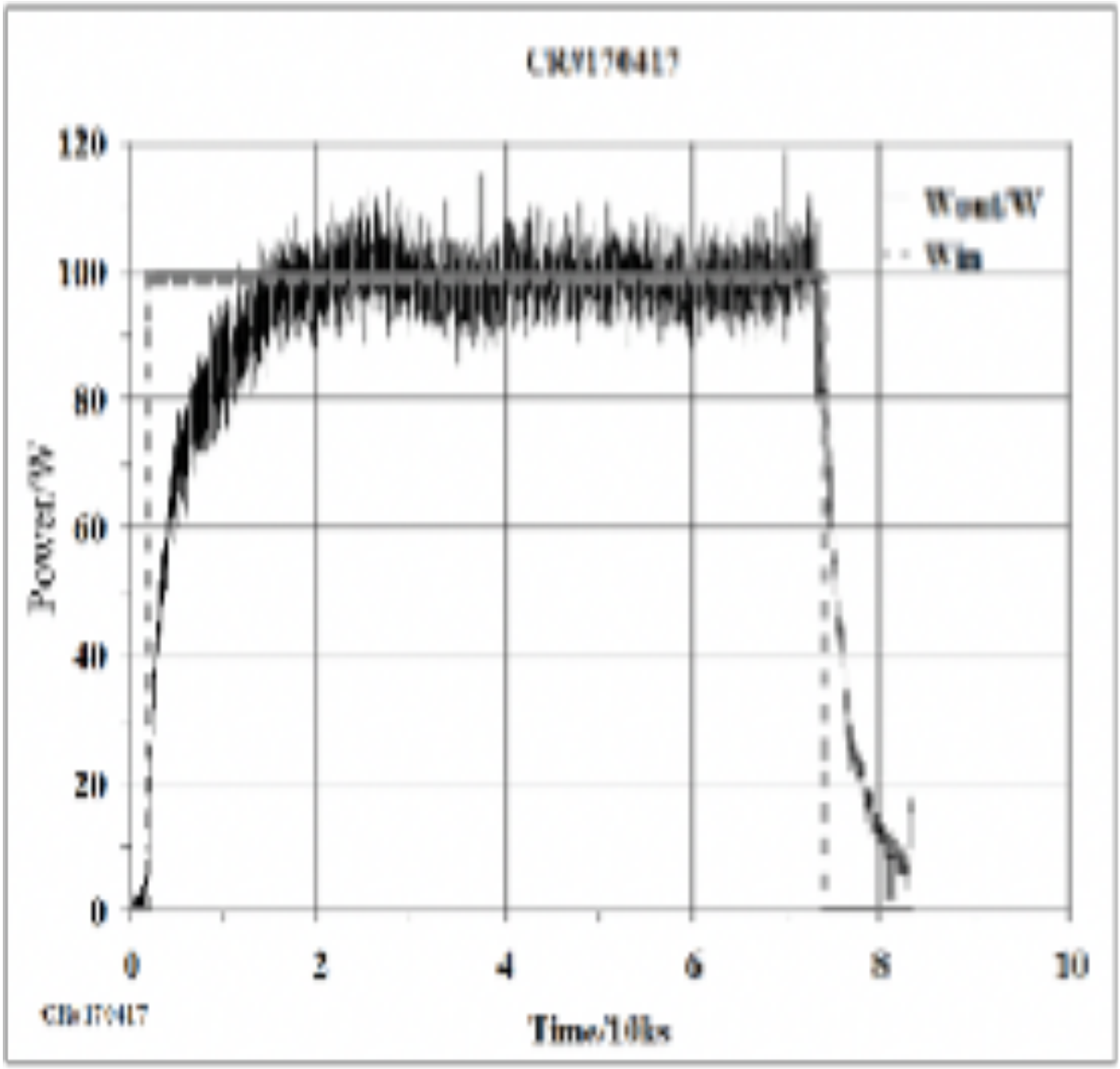

Test results obtained from reactor before activation at 100 W of input power

Figure 25

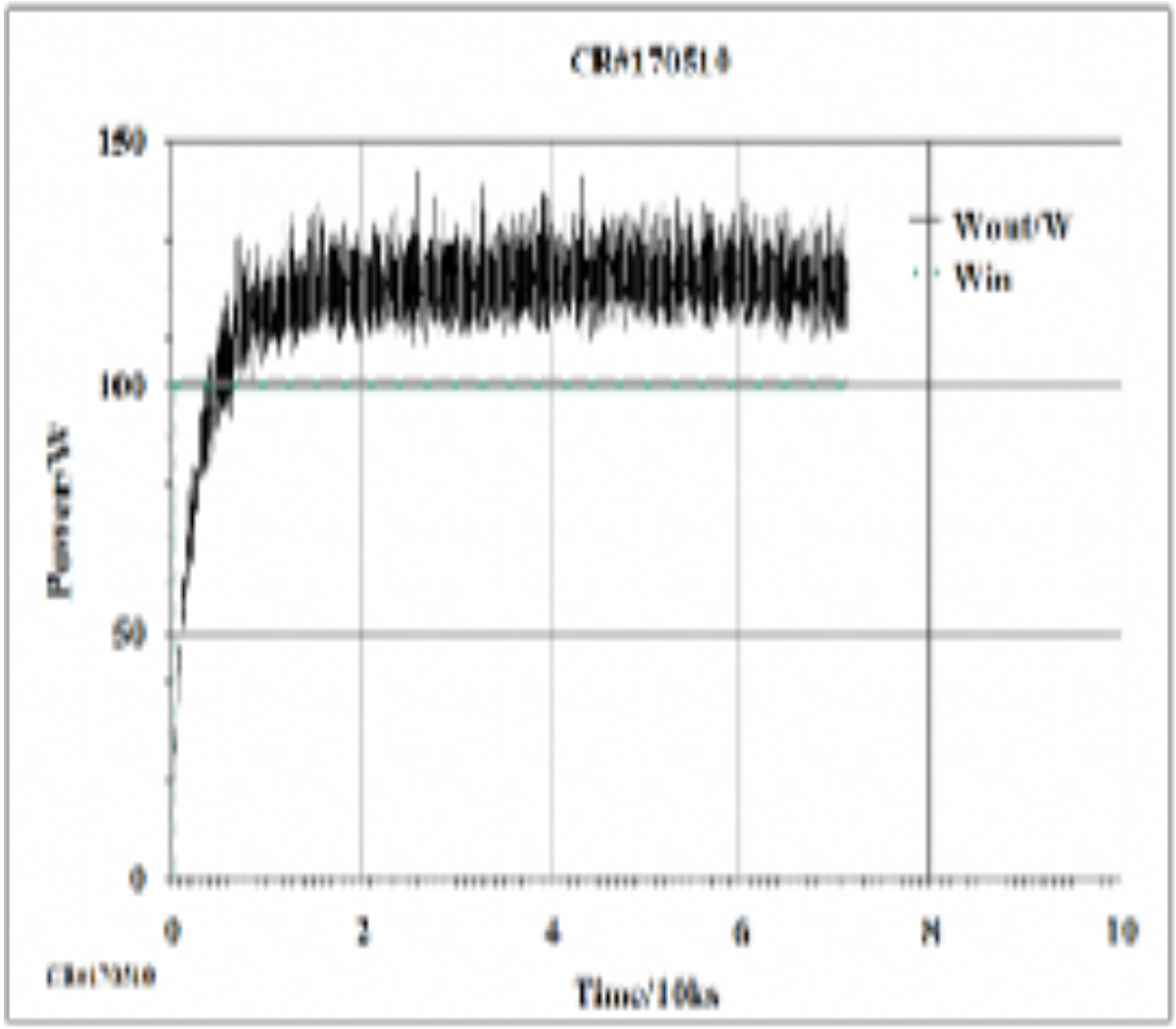

Test results obtained reactor during activation at 100 W of input power

Figure 26

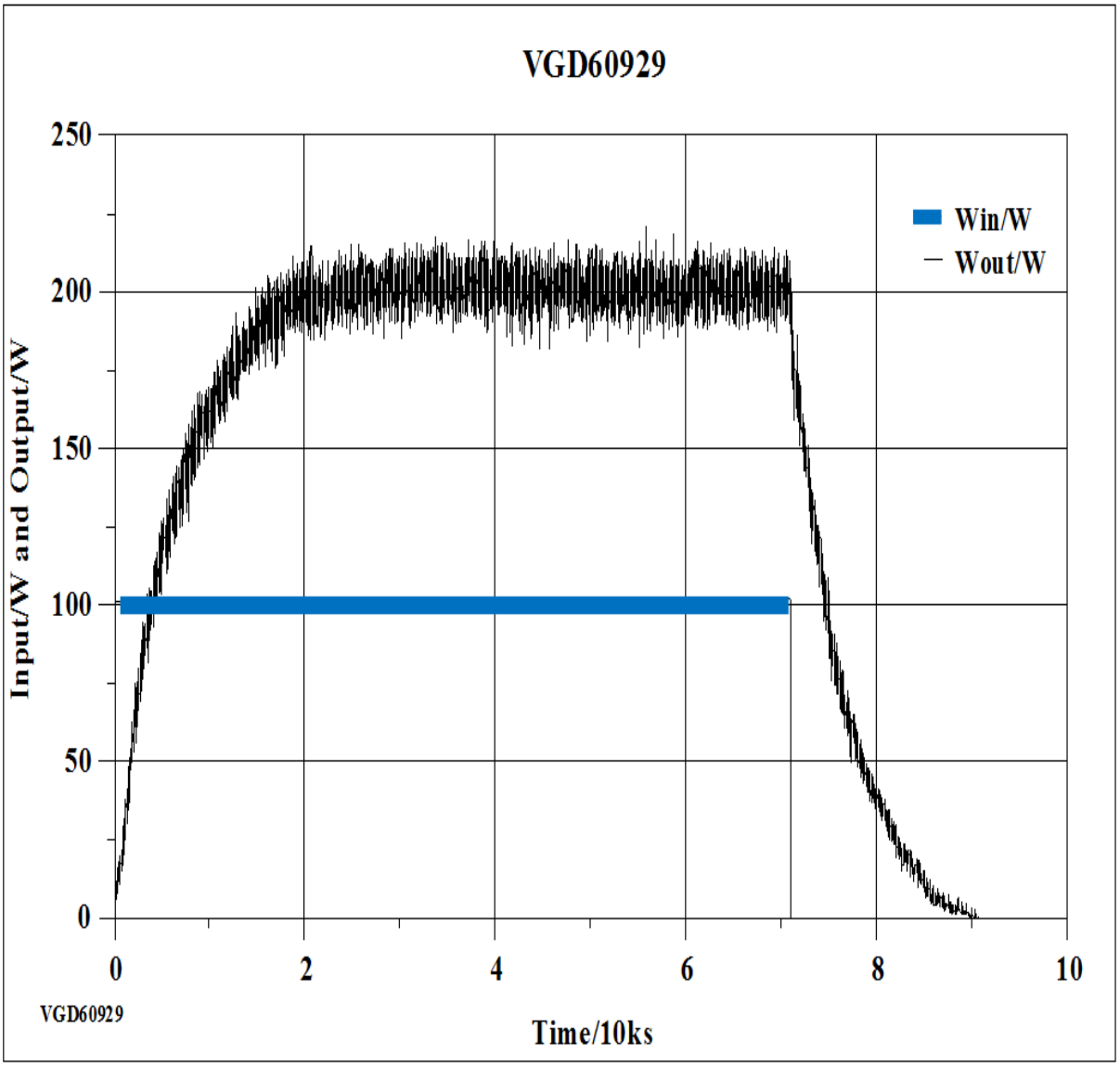

Heat output from a reactor with input of 100 W

Figure 27

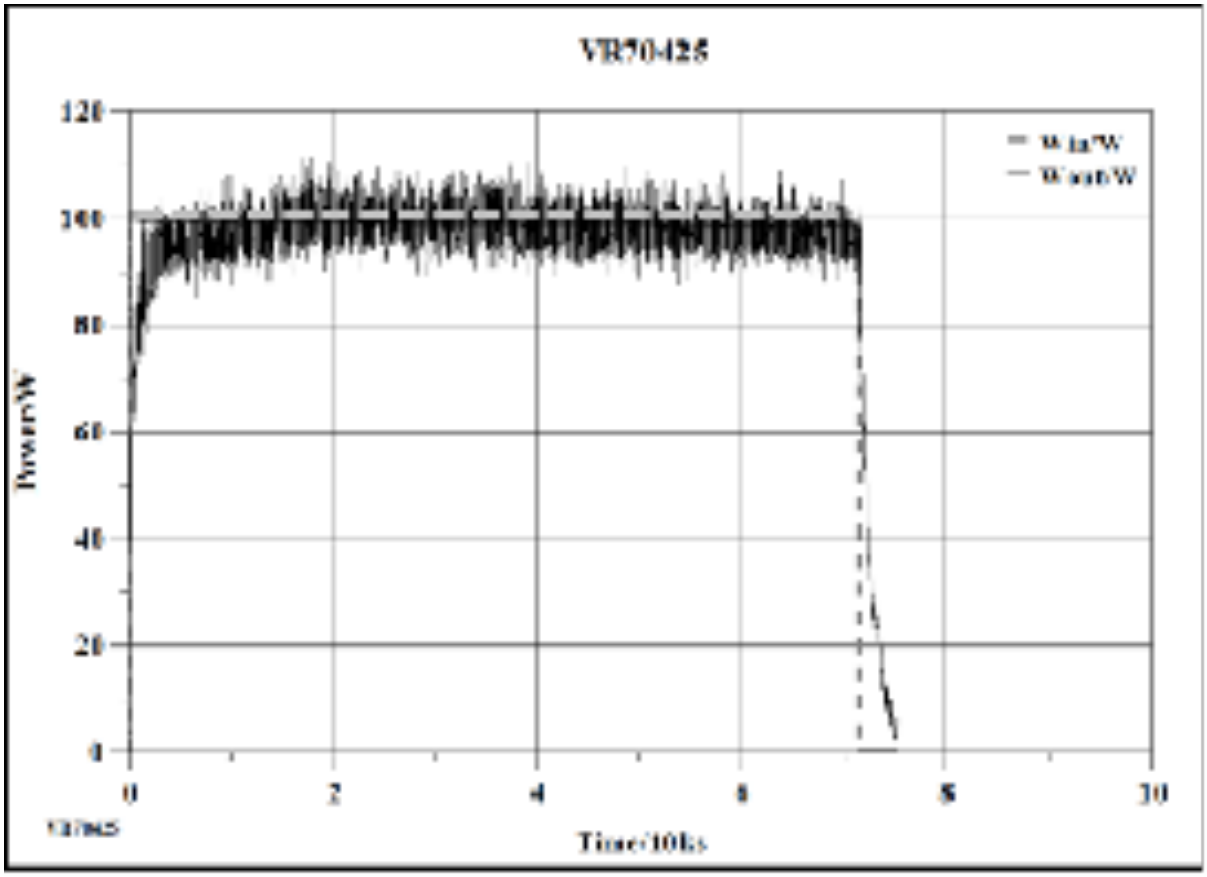

Heat output for a reactor input of 100 W when interior gas was replaced from D_2 to Helium of 760 Pa

Figure 28

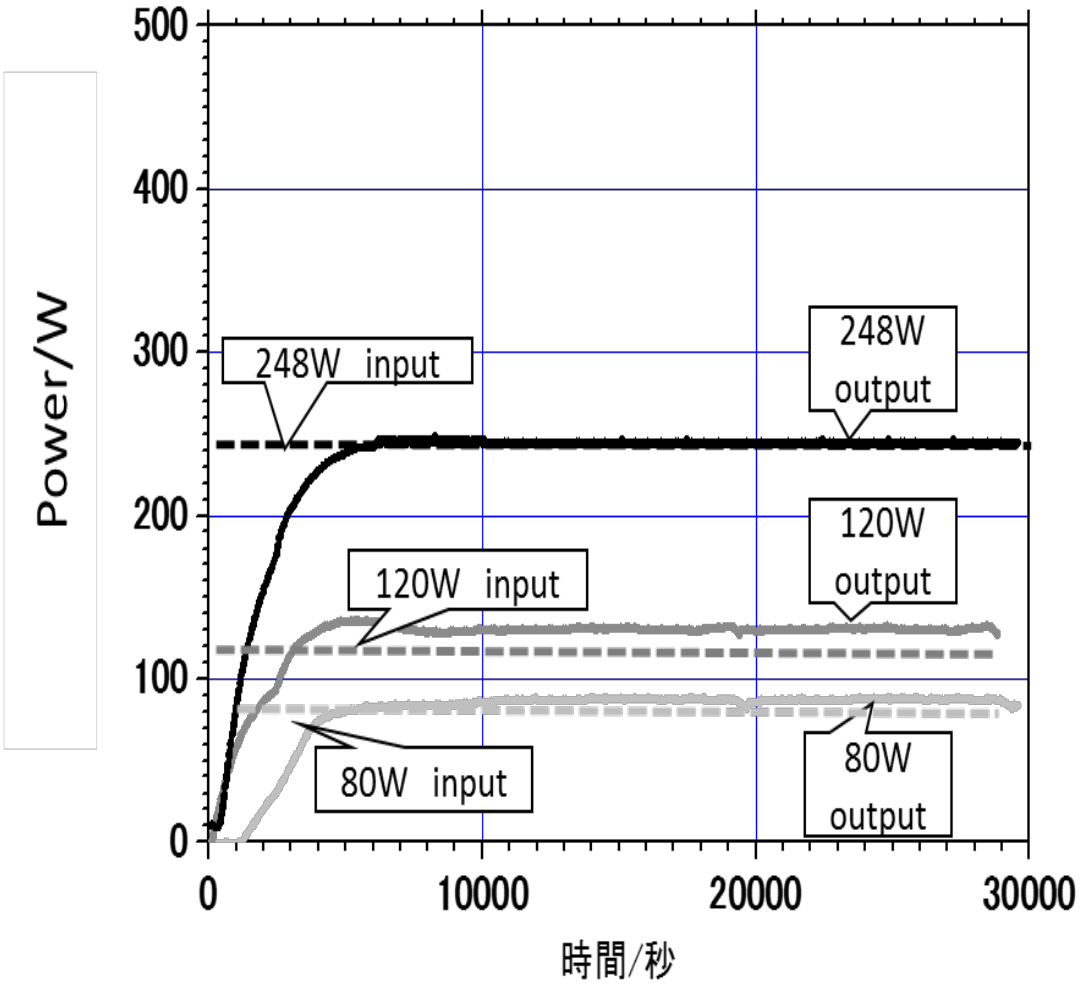

Change in output for calibration test with control heater

Figure 29

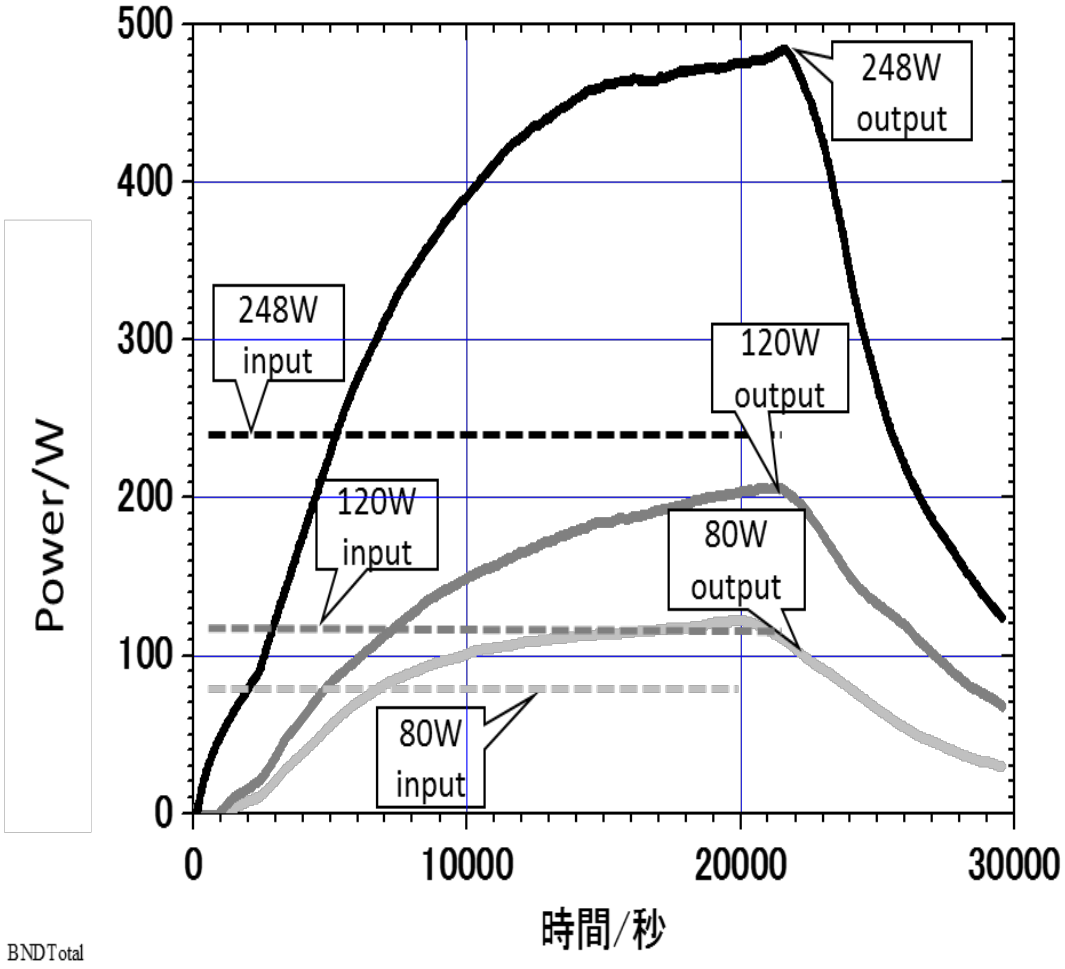

Change in output when input is changed to reactor

Figure 30

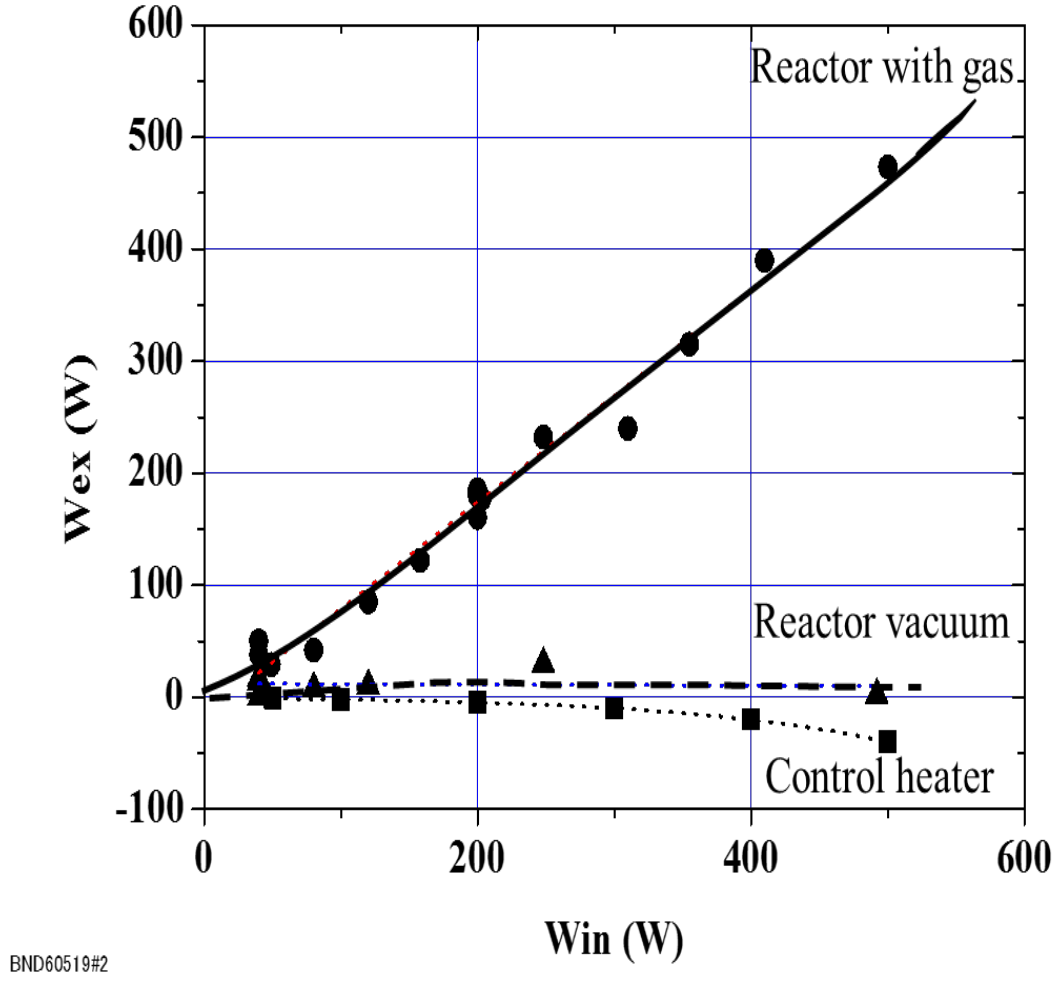

Excess heat results under various interior reactor conditions

Figure 31

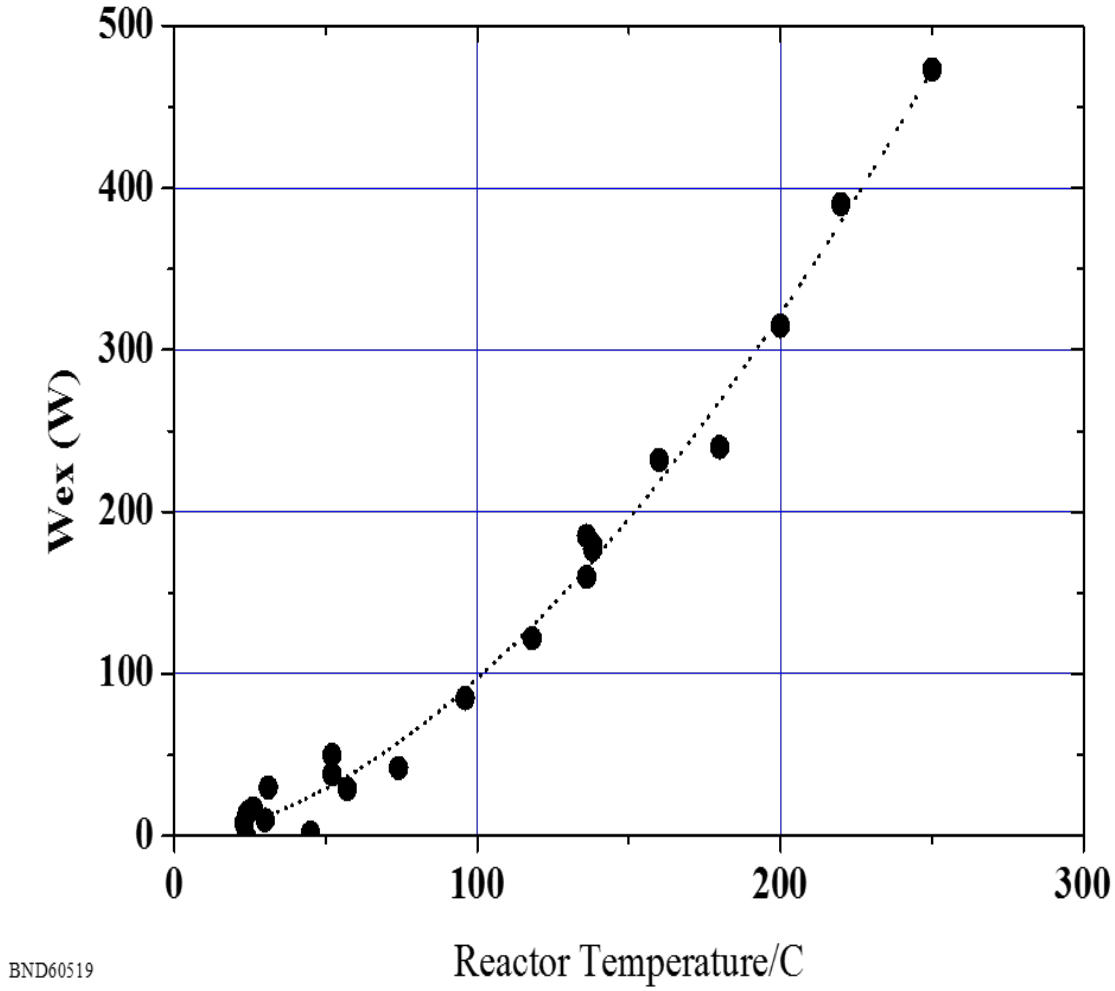

Relationship between excess heat and reactor temperature

Figure 32

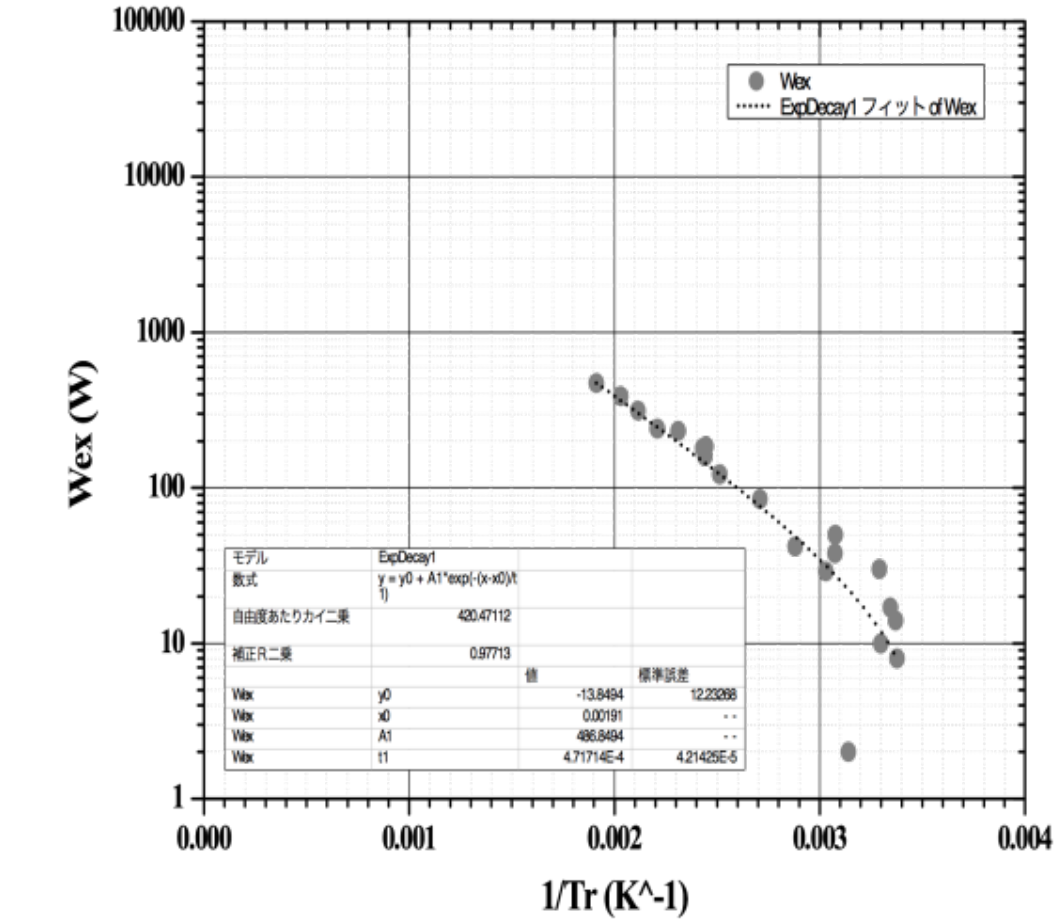

BND60519

Relationship between excess heat and the inverse of the absolute temperature Tr of the reactor

Figure 33

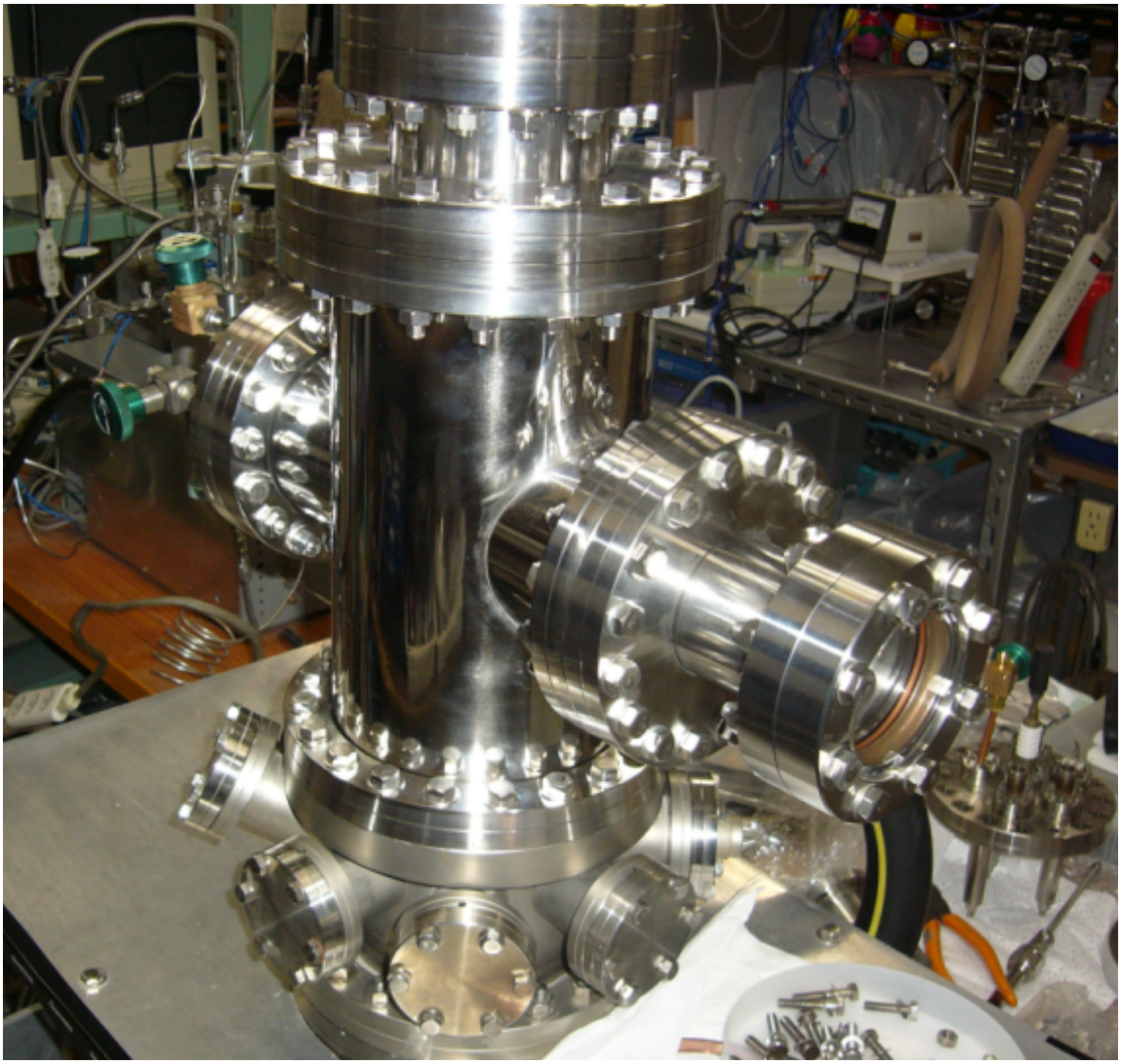

Figure 34

Figure 35

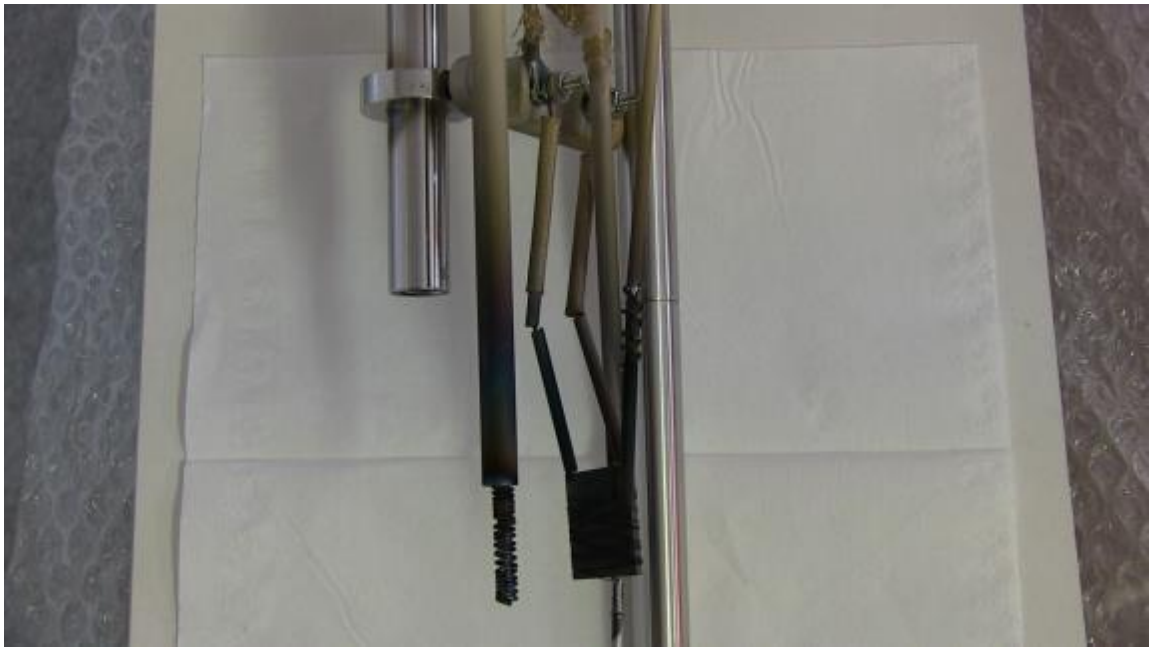

Figure 36

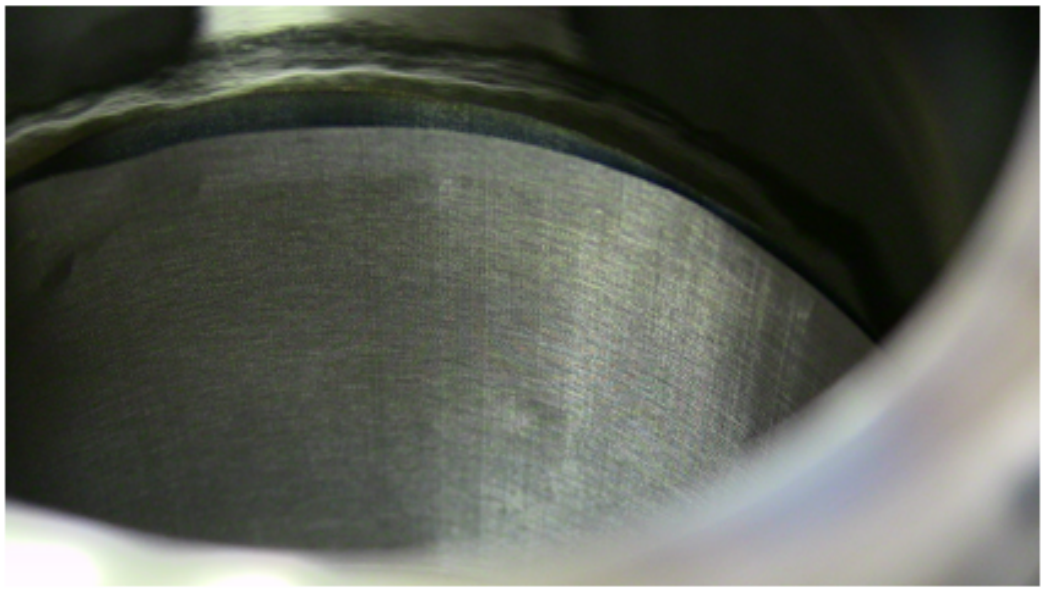

Figure 37

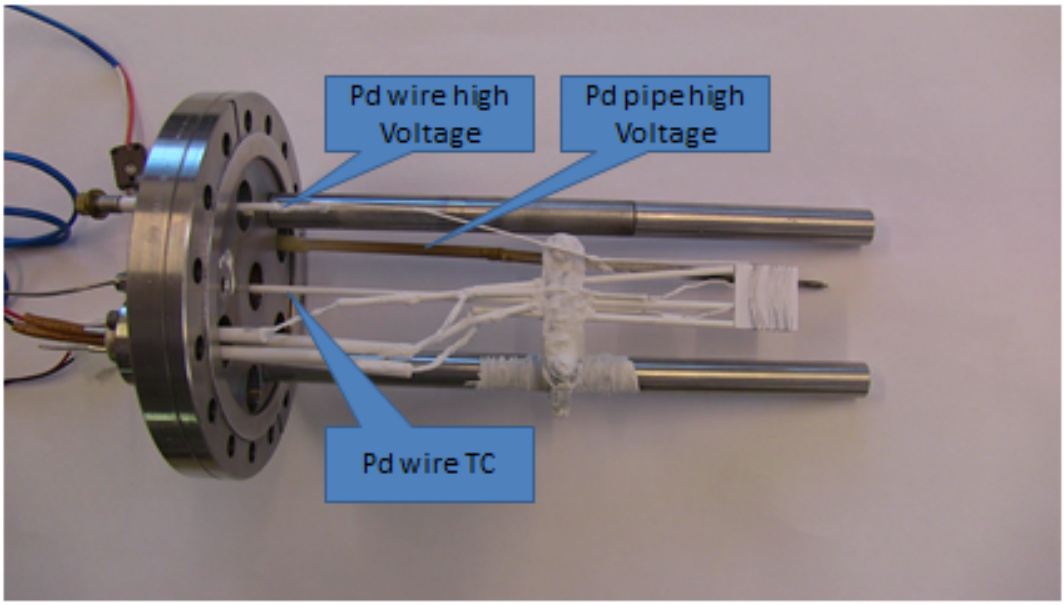

Figure 38

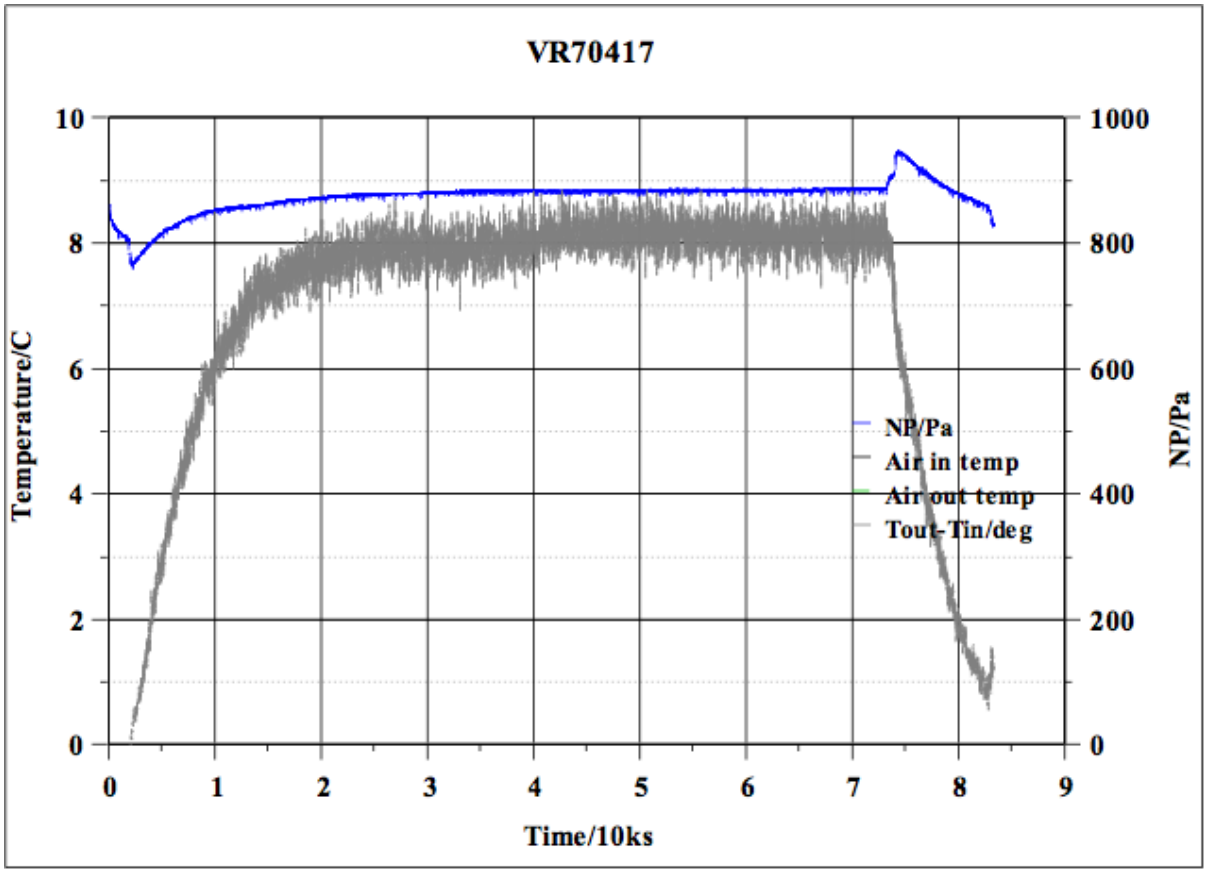
VR70417
Temperature/C
NP/Pa
Time/10ks
NP/Pa
Air in temp
Air out temp
Tout-Tin/deg
0
2
4
6
8
10
0
200
400
600
800
1000
0
1
2
3
4
5
6
7
8
9

Figure 39

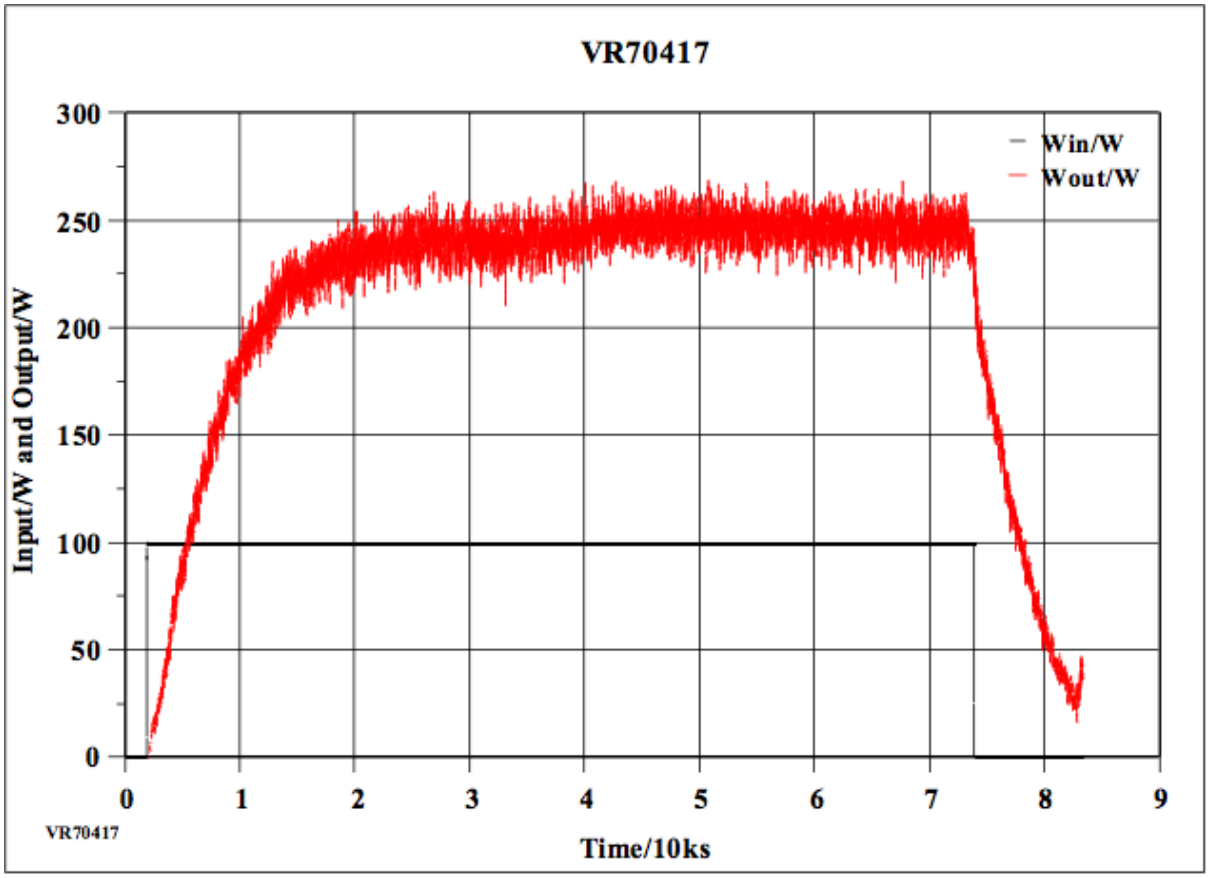
VR70417
Win/W
Wout/W
Input/W and Output/W
300
250
200
150
100
50
0
0
1
2
3
4
5
6
7
8
9
VR70417
Time/10ks

Figure 40

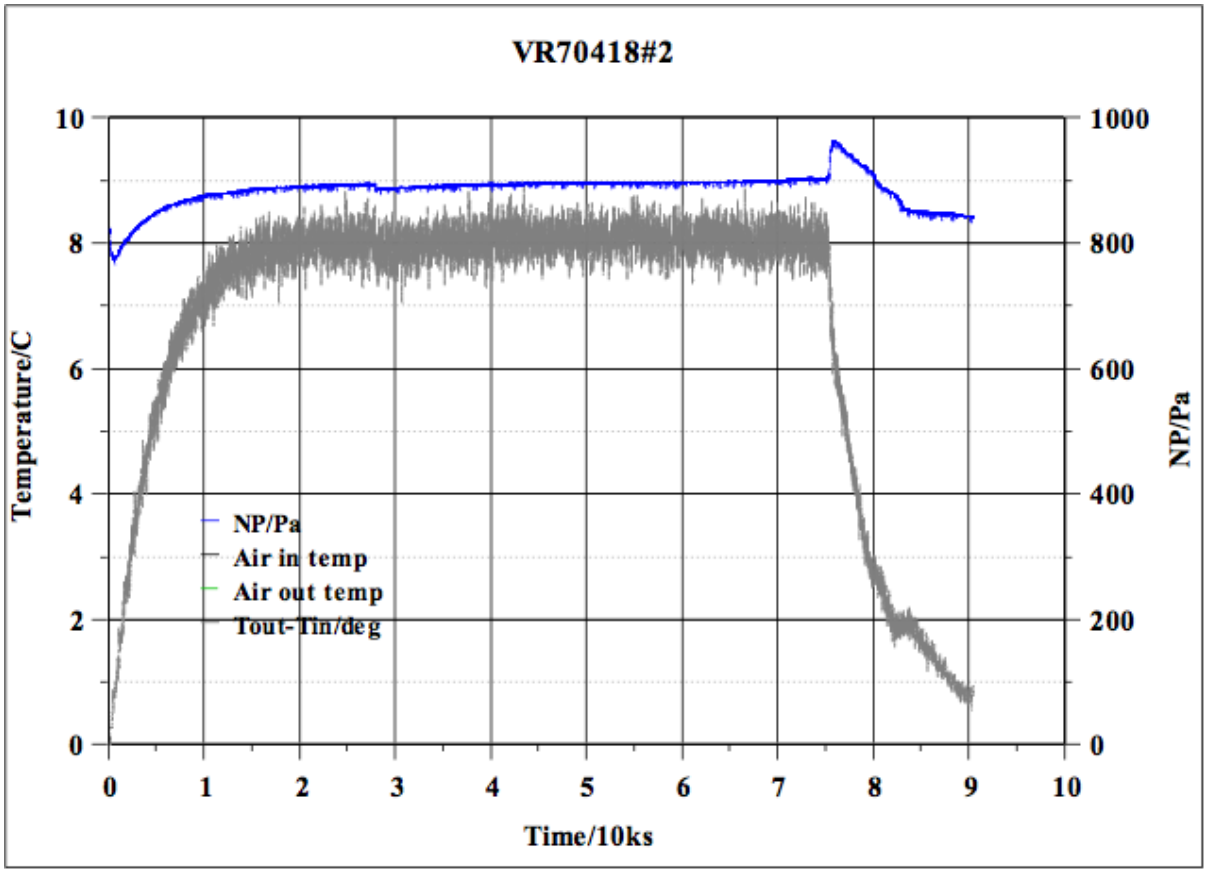
VR70418#2
Temperature/C
NP/Pa
Time/10ks
NP/Pa
Air in temp
Air out temp
Tout-Tin/deg
0
2
4
6
8
10
0
200
400
600
800
1000
0
1
2
3
4
5
6
7
8
9
10

Figure 41

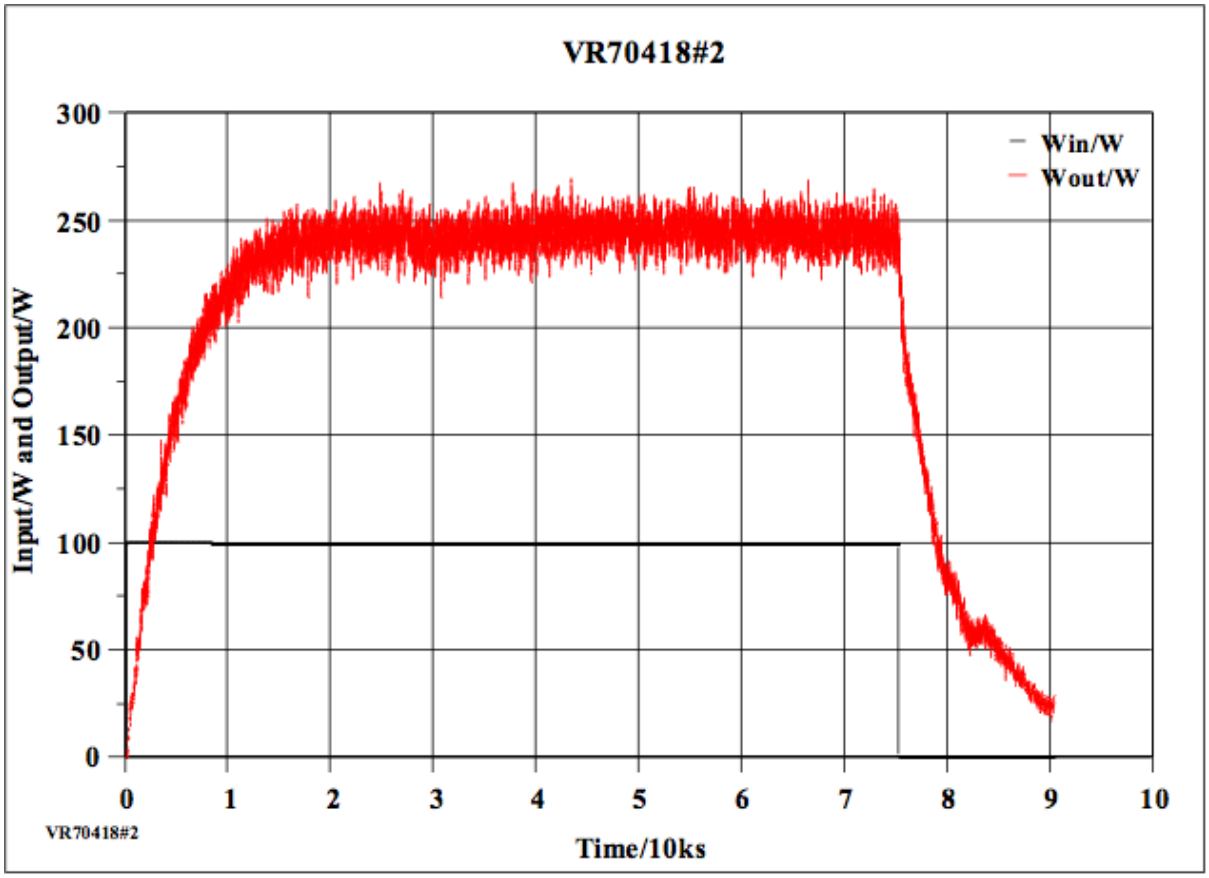
VR70418#2
Win/W
Wout/W
Input/W and Output/W
300
250
200
150
100
50
0
0
1
2
3
4
5
6
7
8
9
10
VR70418#2
Time/10ks

Figure 42

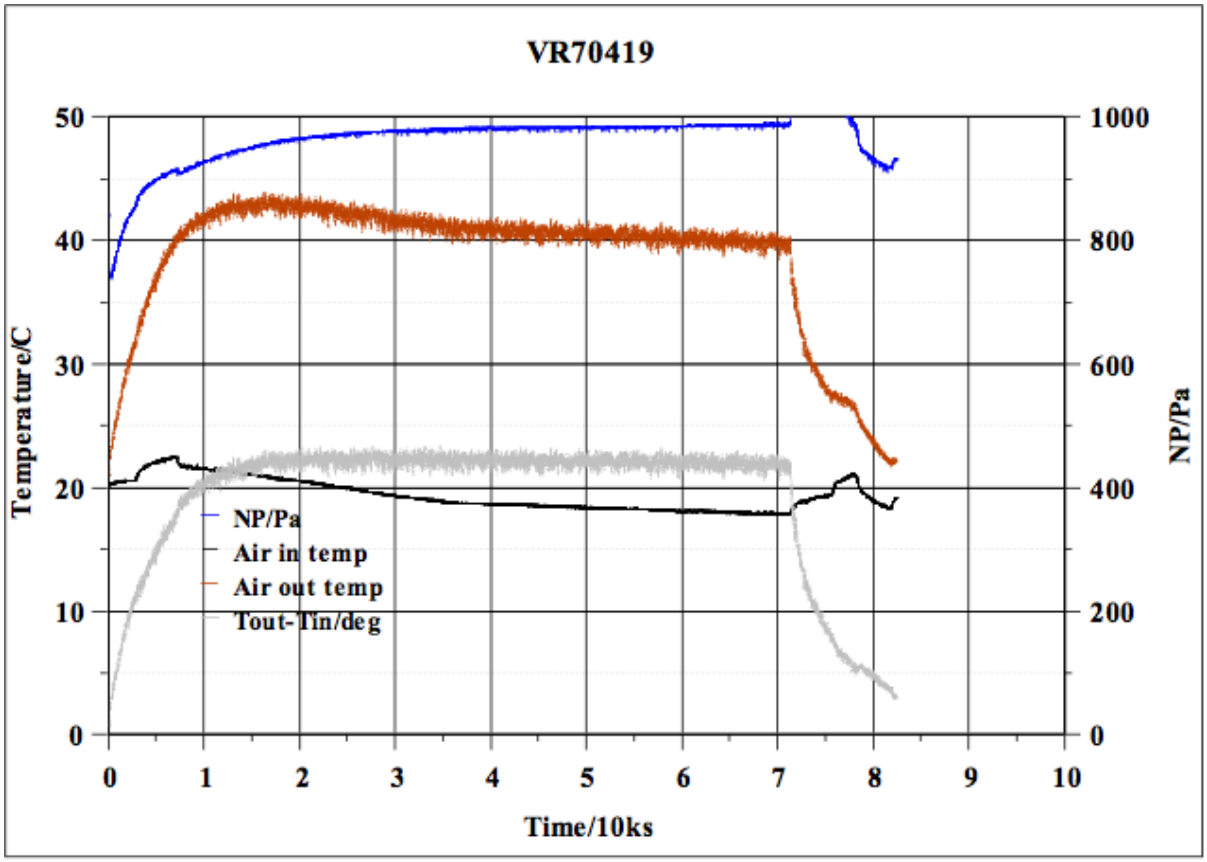
VR70419
Temperature/C
NP/Pa
Time/10ks
NP/Pa
Air in temp
Air out temp
Tout-Tin/deg
0
10
20
30
40
50
0
200
400
600
800
1000
0
1
2
3
4
5
6
7
8
9
10

Figure 43

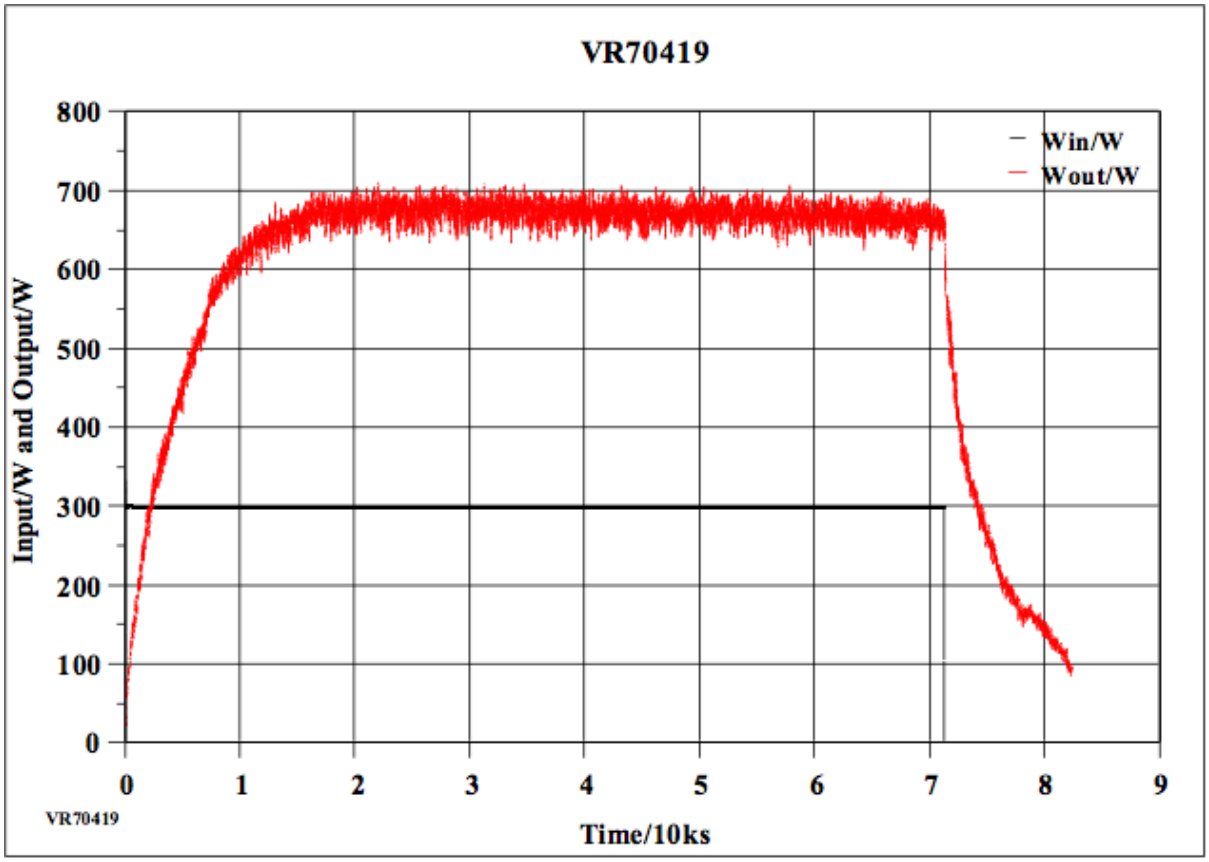
VR70419
Win/W
Wout/W
Input/W and Output/W
800
700
600
500
400
300
200
100
0
0
1
2
3
4
5
6
7
8
9
VR70419
Time/10ks

Figure 44

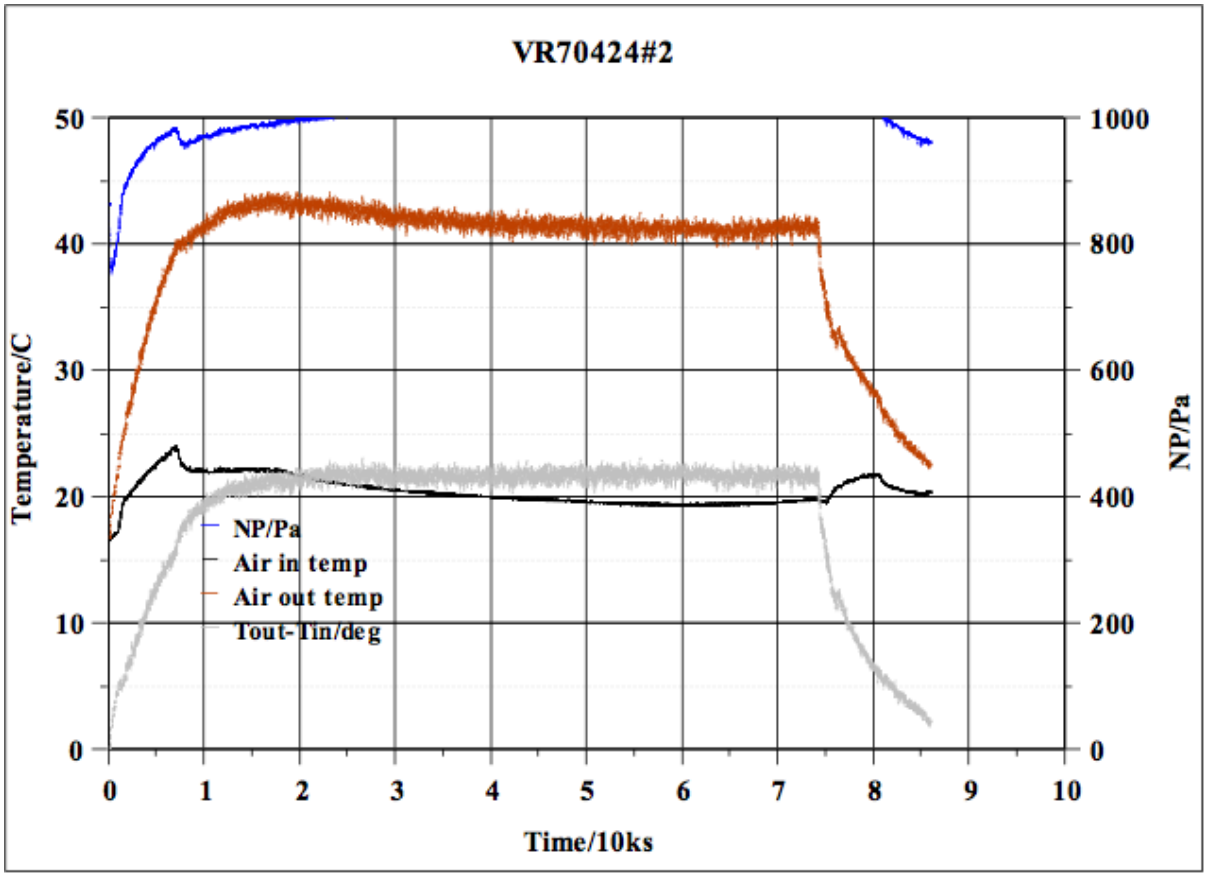
VR70424#2
Temperature/C
NP/Pa
Time/10ks
NP/Pa
Air in temp
Air out temp
Tout-Tin/deg
0
10
20
30
40
50
0
200
400
600
800
1000
0
1
2
3
4
5
6
7
8
9
10

Figure 45

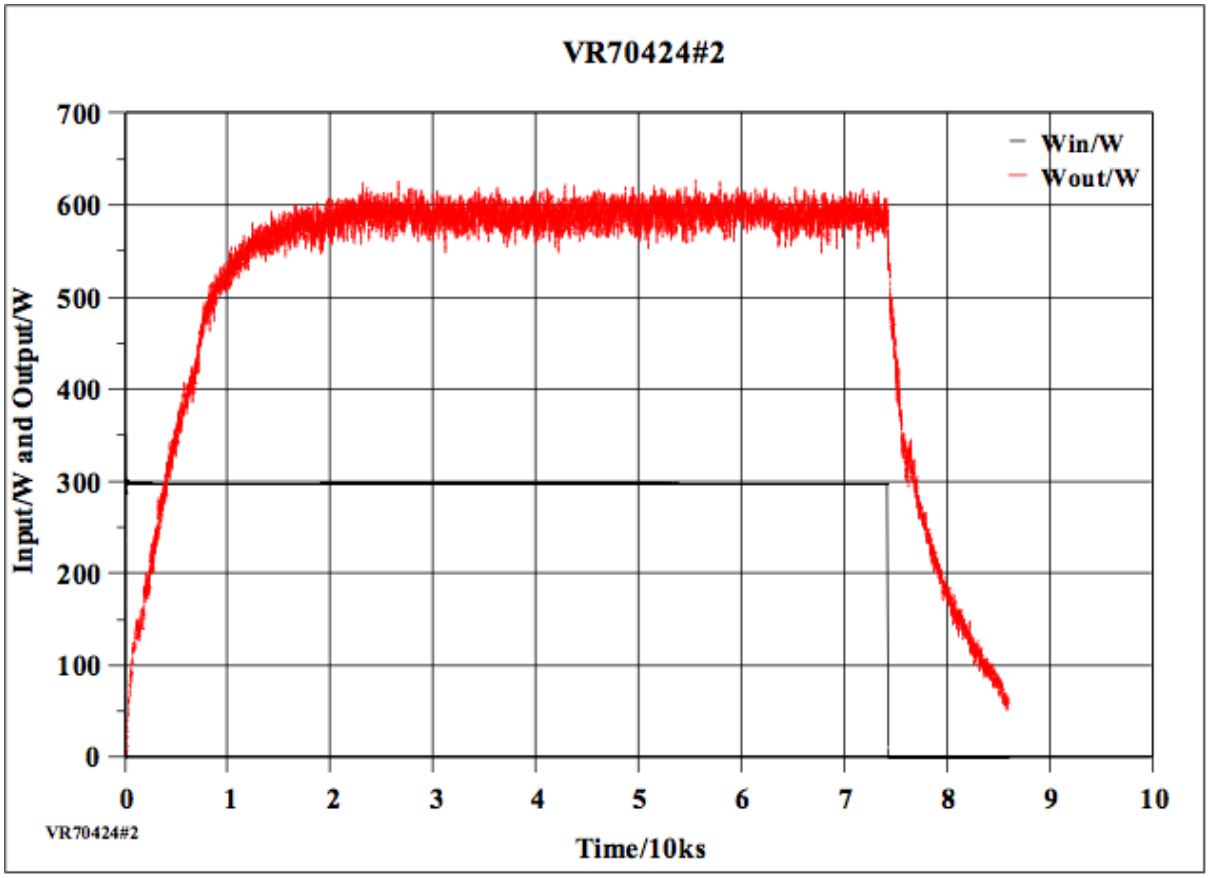
VR70424#2
Win/W
Wout/W
Input/W and Output/W
700
600
500
400
300
200
100
0
0
1
2
3
4
5
6
7
8
9
10
VR70424#2
Time/10ks

Figure 46

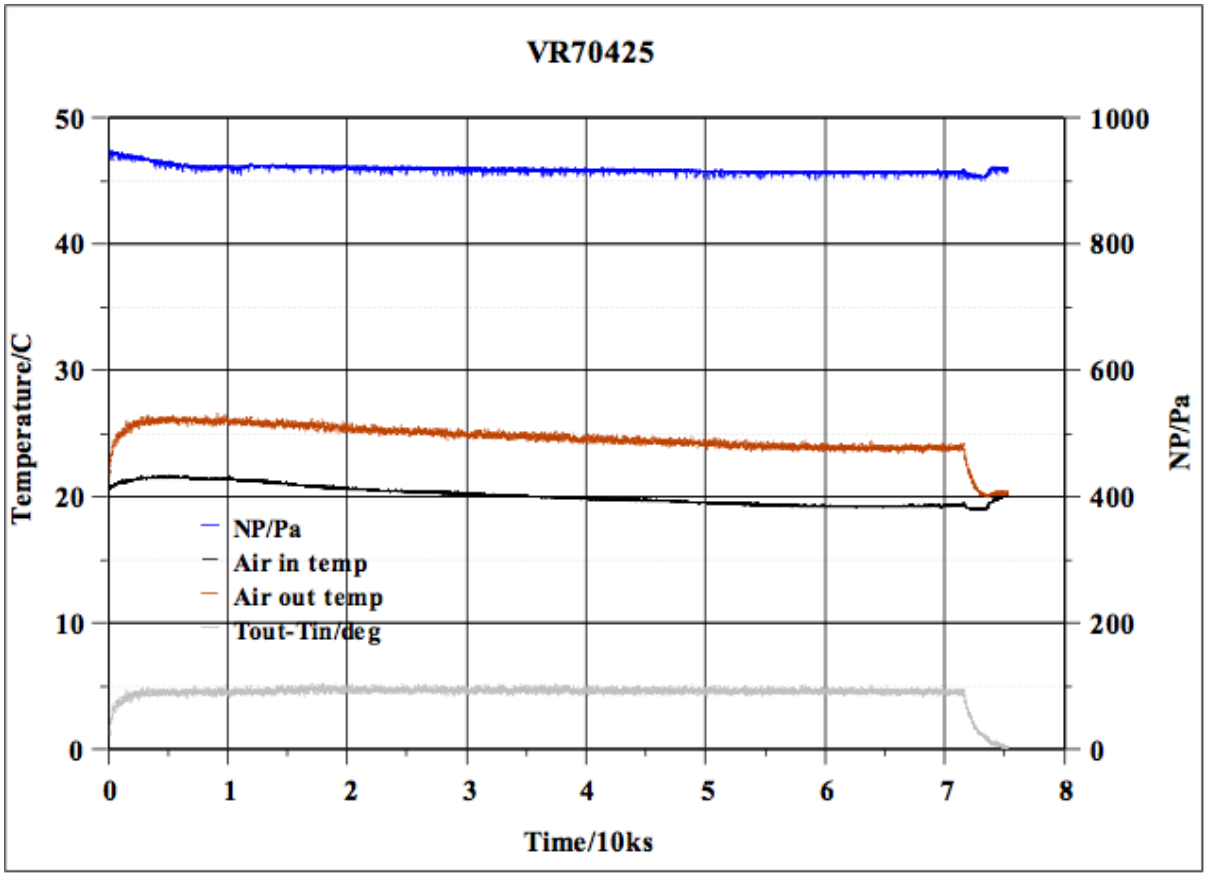
VR70425
Temperature/C
NP/Pa
Time/10ks
NP/Pa
Air in temp
Air out temp
Tout-Tin/deg
50
40
30
20
10
0
1000
800
600
400
200
0
0
1
2
3
4
5
6
7
8

Figure 47

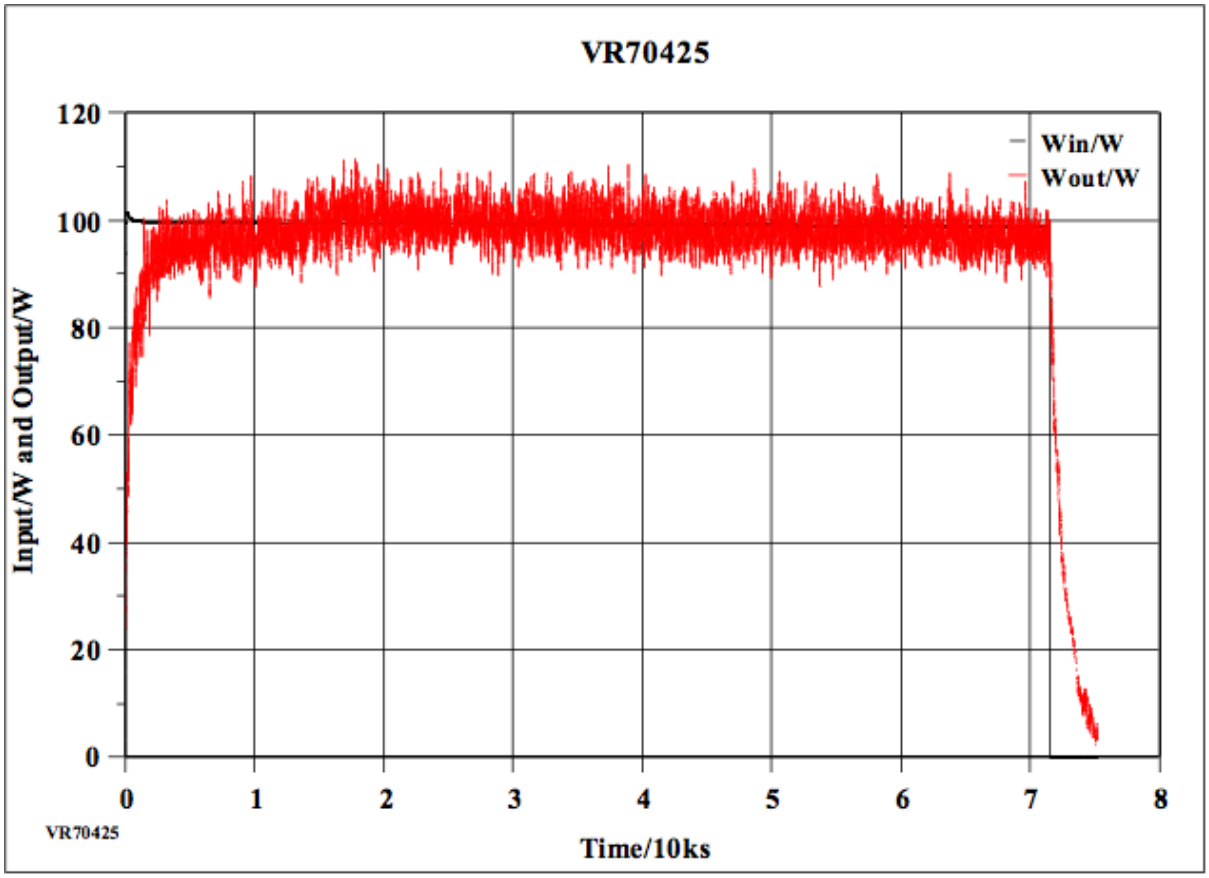
VR70425
Win/W
Wout/W
Input/W and Output/W
120
100
80
60
40
20
0
0
1
2
3
4
5
6
7
8
VR70425
Time/10ks

Figure 48

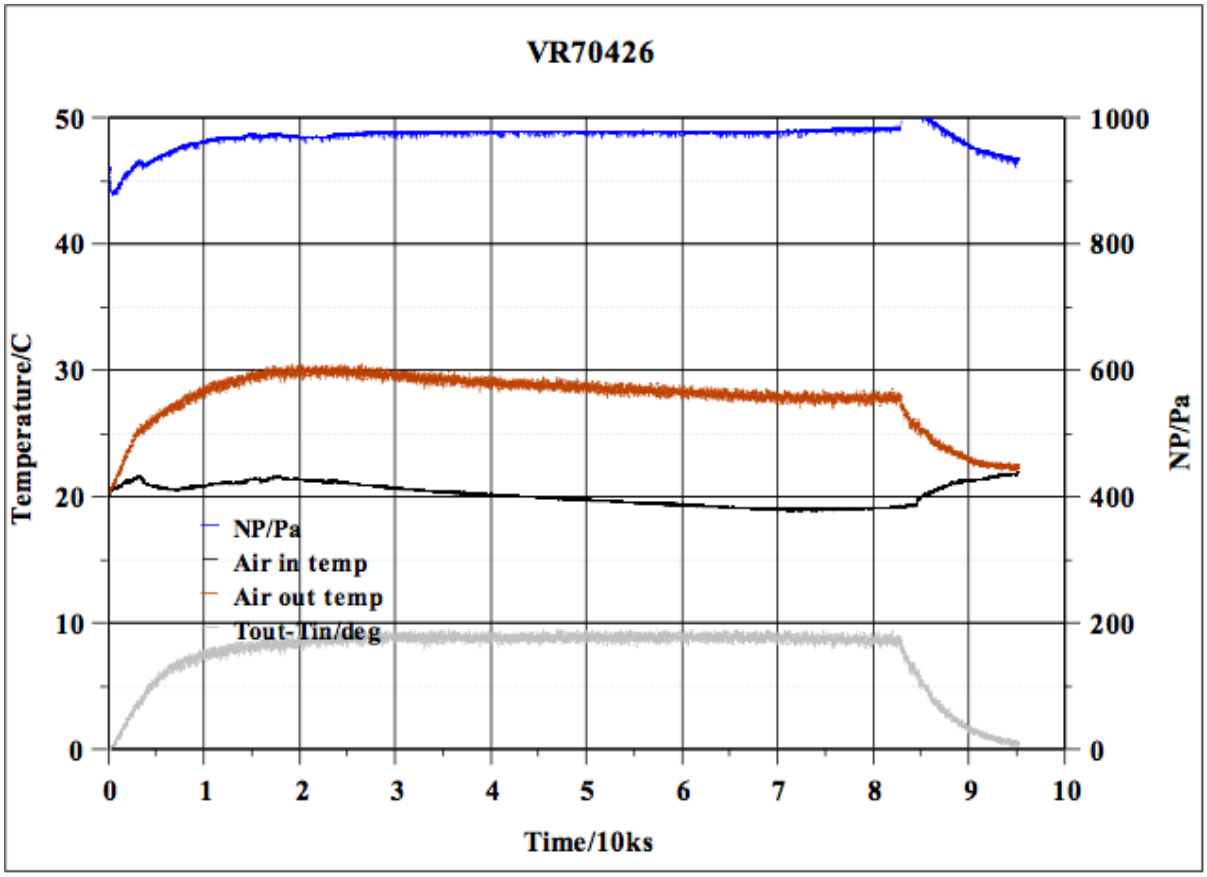
VR70426
Temperature/C
NP/Pa
Time/10ks
NP/Pa
Air in temp
Air out temp
Tout-Tin/deg
50
40
30
20
10
0
1000
800
600
400
200
0
0
1
2
3
4
5
6
7
8
9
10

Figure 49

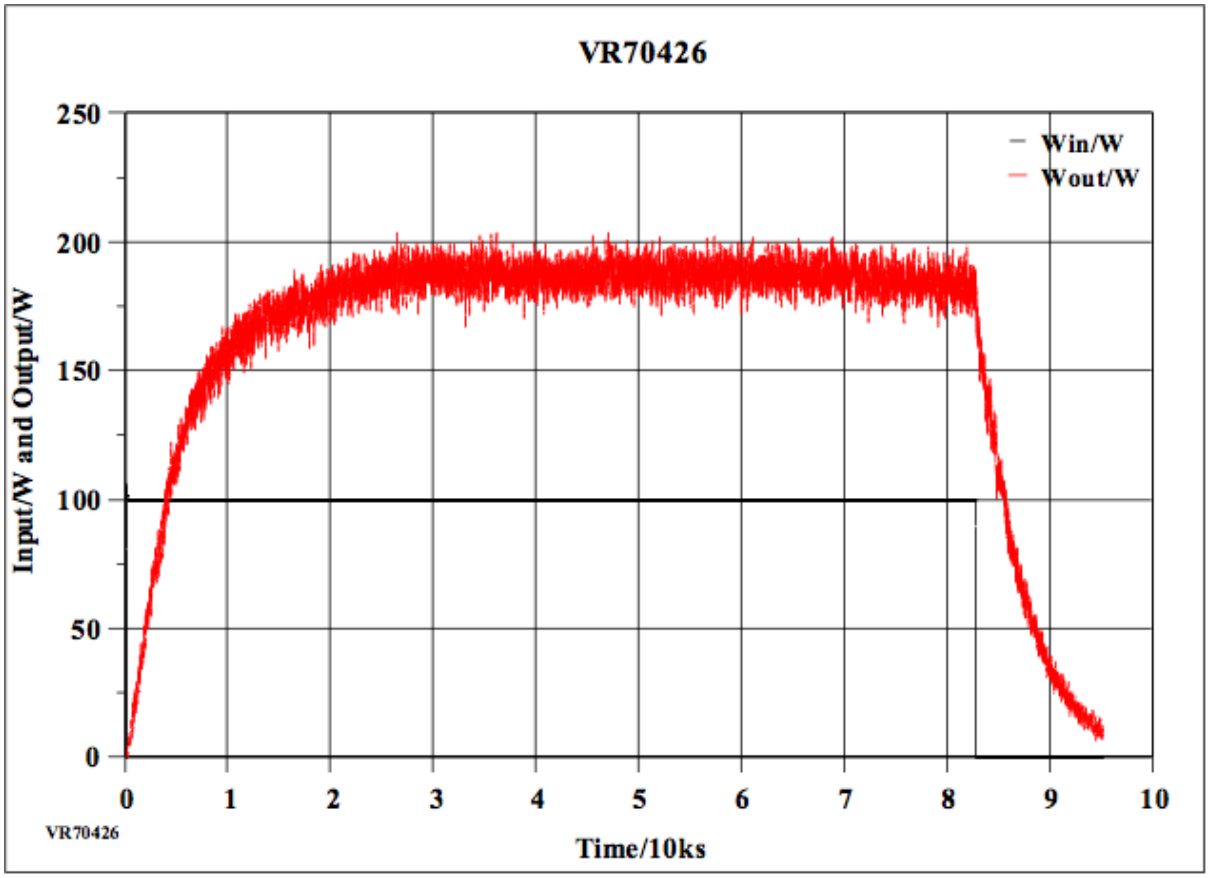
VR70426
250
200
150
100
50
0
Input/W and Output/W
Win/W
Wout/W
0
1
2
3
4
5
6
7
8
9
10
VR70426
Time/10ks

Figure 50

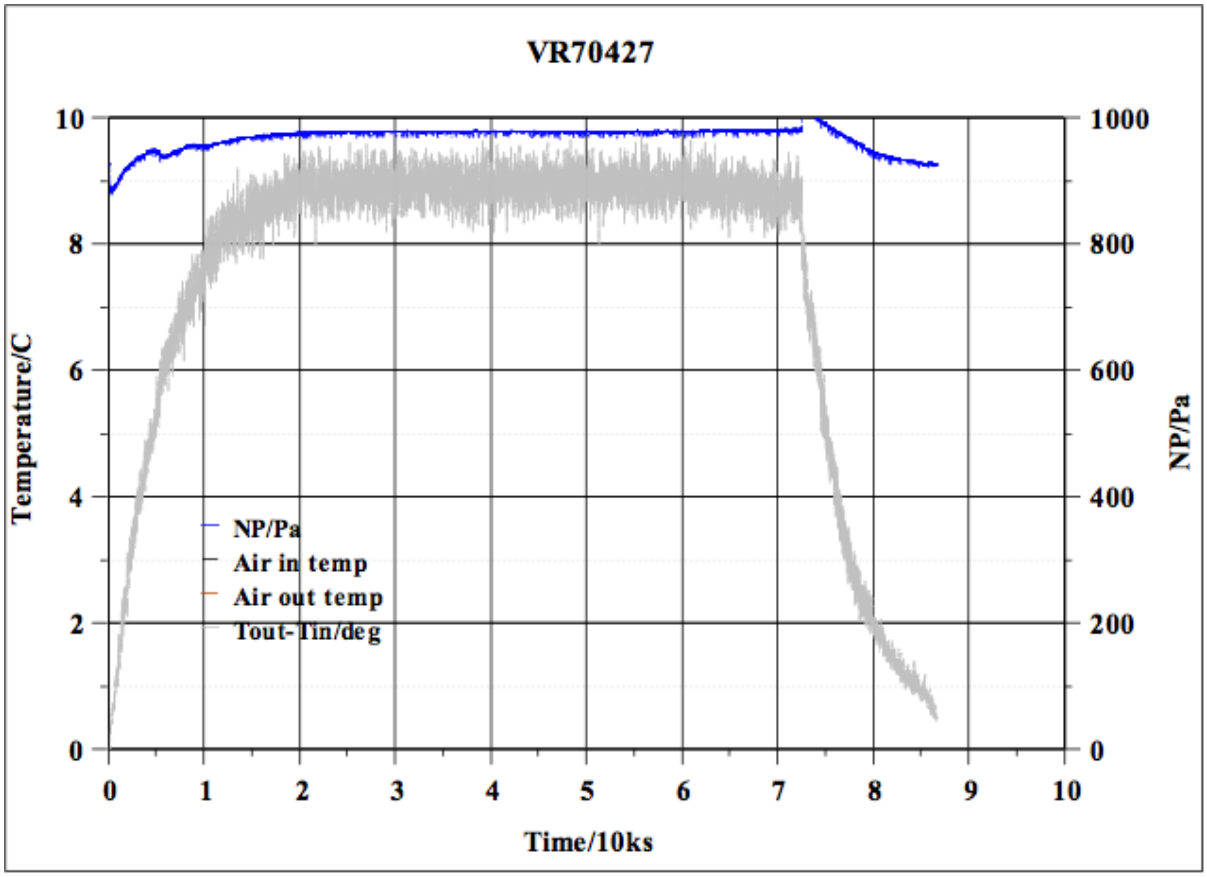
VR70427
Temperature/C
NP/Pa
Time/10ks
NP/Pa
Air in temp
Air out temp
Tout-Tin/deg
0
2
4
6
8
10
0
200
400
600
800
1000
0
1
2
3
4
5
6
7
8
9
10

Figure 51

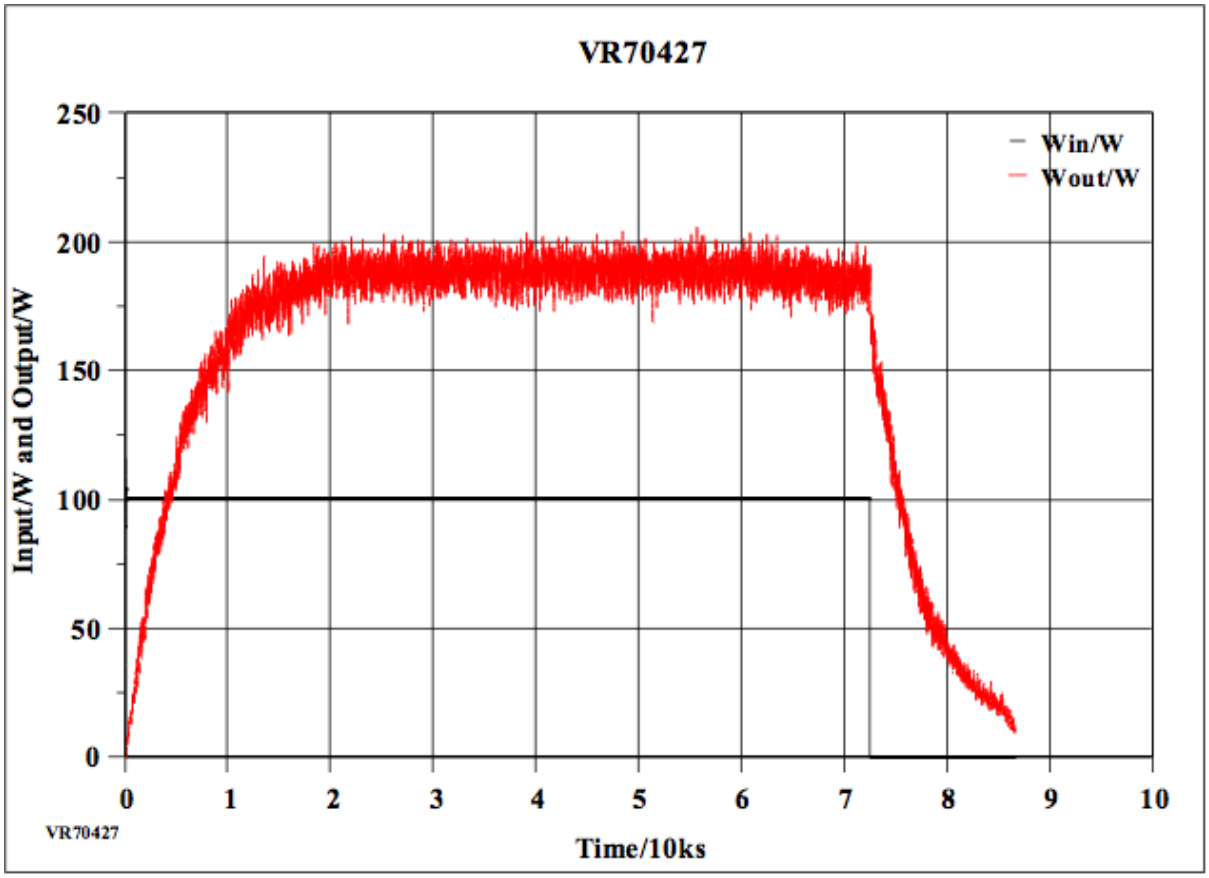
VR70427
250
200
150
100
50
0
Input/W and Output/W
0
1
2
3
4
5
6
7
8
9
10
Time/10ks
Win/W
Wout/W
VR70427

Figure 52

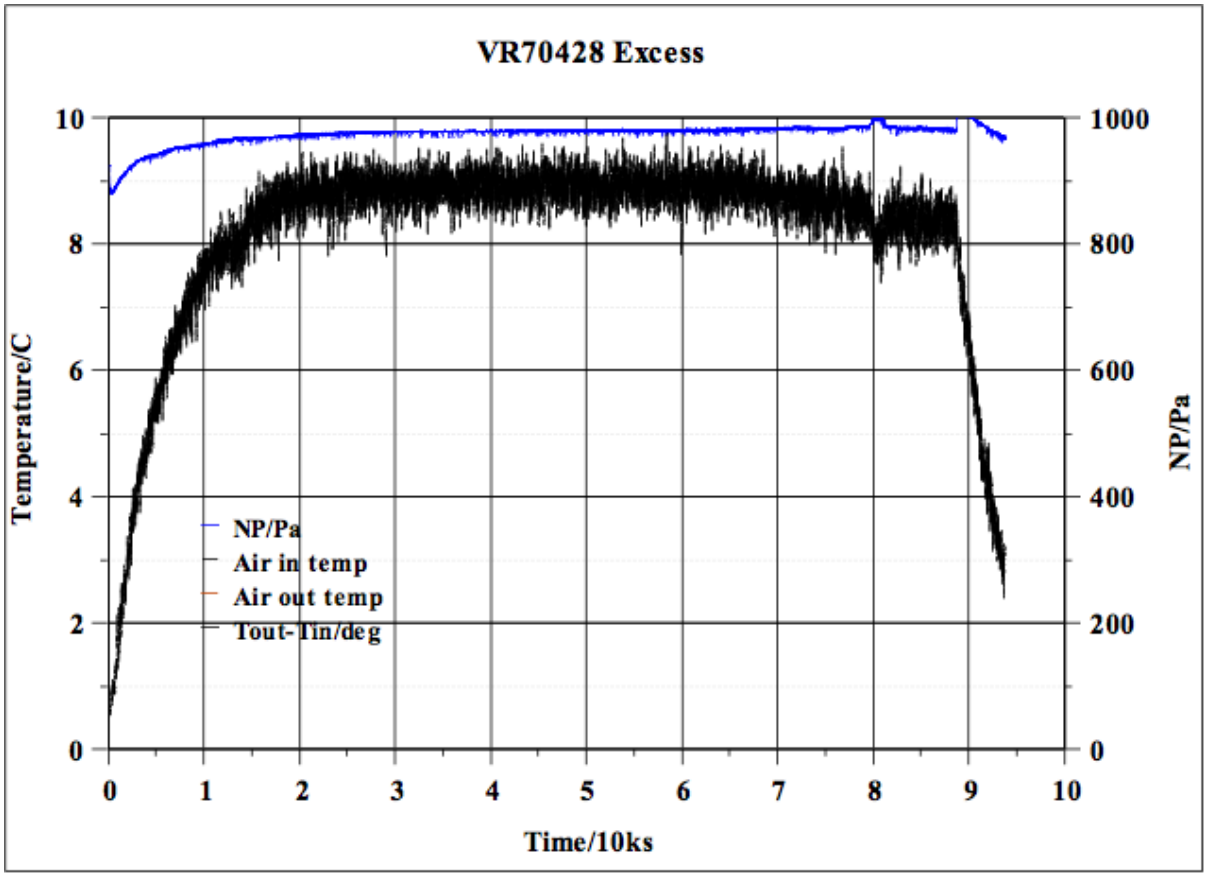
VR70428 Excess
Temperature/C
NP/Pa
Time/10ks
NP/Pa
Air in temp
Air out temp
Tout-Tin/deg
0
2
4
6
8
10
0
200
400
600
800
1000
0
1
2
3
4
5
6
7
8
9
10

Figure 53

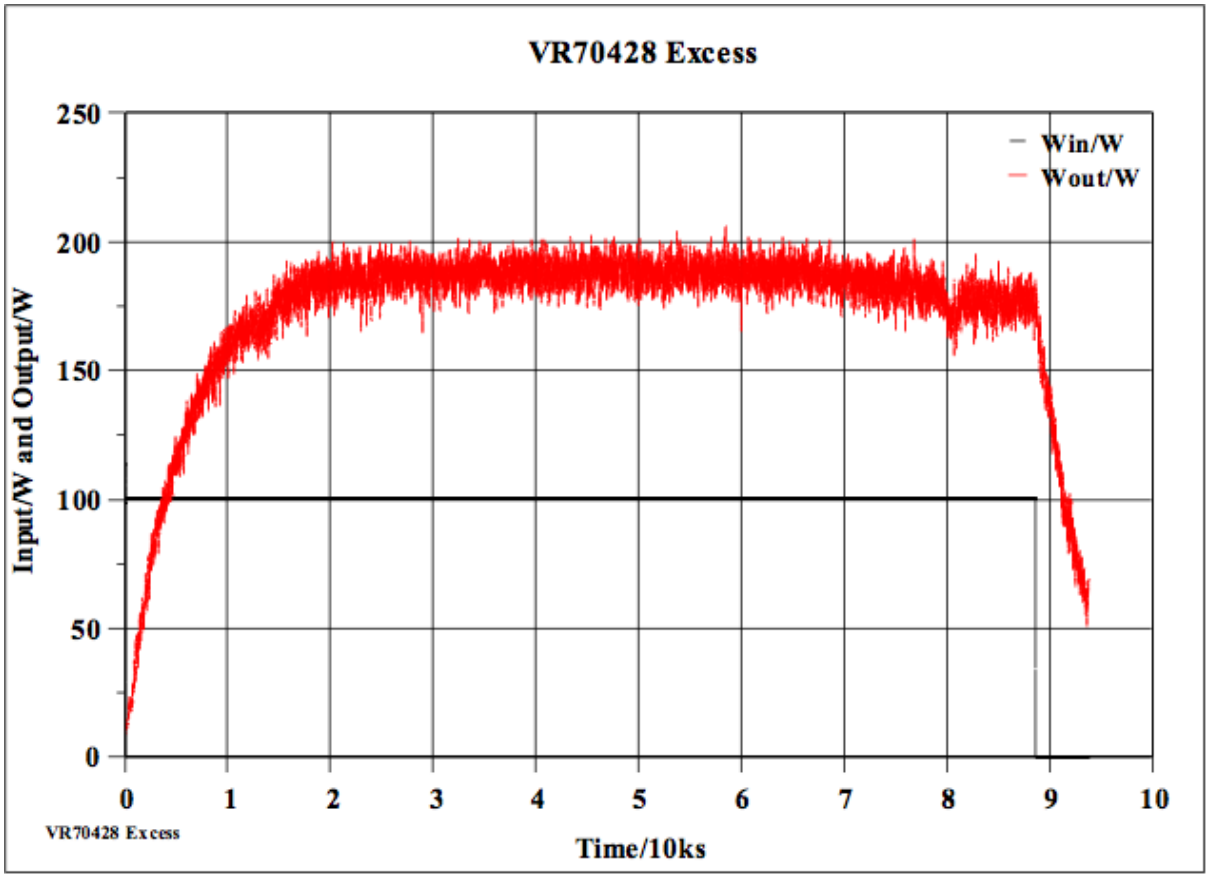
VR70428 Excess
Win/W
Wout/W
Input/W and Output/W
250
200
150
100
50
0
0
1
2
3
4
5
6
7
8
9
10
VR70428 Excess
Time/10ks

Figure 54